Probabilistic Graphical Models for Data Reconciliation and Causal Inference in Process Data Analytics

by

Arun Senthil Sundaramoorthy

A thesis submitted in partial fulfillment of the requirements for the degree of

Master of Science

in

Process Control

Department of Chemical and Materials Engineering

University of Alberta

Abstract

Data reconciliation methods play an important role in minimizing the measurement error and gross error that are present in the process data with respect to the process model. On the other hand, causal analysis helps in determining the relationship among the process variables from the data. It is important to note that these aforementioned methods help in understanding the process data better, provide valuable insights of the process and contribute to improving the decision making strategies in the day to day process operation. In this thesis, we develop approaches based on probabilistic graphical models to address the problems in data reconciliation and causal inference.

In the first part of the thesis, the problem of data reconciliation with state uncertainties is addressed in the framework of probabilistic graphical models. In many existing formulations for data reconciliation, process models are assumed to be error free. However, while operating the process in real time, process models can suffer from model inaccuracies, leading to uncertainties in states. This work introduces a new method for data reconciliation developed in the framework of Bayesian network, accounting for the state uncertainties. A novel method to construct acyclic Bayesian networks for process networks with recycle streams is proposed in this work. This method is also extended for data reconciliation of partially measured systems. The solution is obtained by utilising a Bayesian network model translated from the process model and using statistical inference techniques to estimate the reconciled values of the states. The efficacy of the proposed data reconciliation schemes is demonstrated on three case studies namely Simple Flow Network, Mineral Processing Unit (without Recycle) and Mineral Beneficiation Process (with Recycle).

In the second part of the thesis, novel methods are proposed for causal network modelling. First, a framework for causality analysis based abnormal event prediction is proposed. Also, a methodology to construct causal network of the process systems using finite impulse response model with sparsity constraints and process knowledge is developed. Using causal network reconstructed from data and the process knowledge, we develop and test process monitoring hypotheses. Efficacy of the proposed approach is illustrated using a real industrial process case study of flooding and weeping in a distillation column. Further, we discuss the outcomes and the findings from the field implementation of process monitoring framework.

Further, a methodology for causal analysis is developed that makes use of only the process data without any information about the process knowledge. In this method, the sparse inverse covariance estimation is coupled with dynamic likelihood score, and a two-step approach is proposed to address the problem of causal analysis. The estimation of sparse inverse covariance matrix for undirected sparse network reconstruction is performed with L_0 norm constraint in the framework of greedy sparse simplex (GSS) algorithm. Further, the GSS algorithm is suitably modified to incorporate the additional constraint of positive semi-definiteness of the inverse covariance matrix. To determine the causal direction among the variables, dynamic likelihood score is computed for the associated variables in the reconstructed network in the second step. The efficacy of the proposed approach for causal analysis is illustrated using a numerical example and an industrial application on prediction of flooding and weeping in a deethanizer column associated with a fluid catalytic cracking unit.

Preface

This thesis is an original work conducted by Arun Senthil Sundaramoorhty. The materials presented in this thesis are outcomes of the research projects conducted under the supervision of Dr. Biao Huang.

Chapter 2 of this thesis has been submitted as a research article to **AIChE Journal** and it is under review - Bayesian network approach to process data reconciliation with state uncertainties and recycle streams. **S. Arun Senthil**, J. Valluru and B. Huang. (2020).

A journal article is being prepared based on Chapter 3 of this thesis - Prediction of Flooding & Weeping in Process Operation using Causality Analysis. **S. Arun Senthil**, R. Raveendran, B. Huang, Y. Ma, H. Zhang and D. Wang.

A research article prepared based on Chapter 4 of this thesis has been submitted to **IEEE Transactions on Control System Technology** and it is under review - Sparse Inverse Covariance Estimation for Causal Inference in Process Data Analytics. **S. Arun Senthil**, S.K. Varanasi, B. Huang, Y. Ma, H. Zhang and D. Wang. (2020).

Arun Senthil Sundaramoorthy is responsible for the development of idea, algorithm derivation, performing simulation and manuscript preparation for all the publications listed above. Dr. Biao Huang have provided invaluable advice and critical feedback on the technical content and manuscript corrections for all the aforementioned publications. Dr. Jayaram Valluru, Dr. Rahul Raveendran and Dr. Santhosh Kumar Varanasi have provided valuable and critical feedbacks on the technical content and in the manuscript corrections of the journal articles prepared based on Chapter 2, Chapter 3 and Chapter 4 respectively. Dr. Yanjun Ma, Haitao Zhang and Dian Wang have played a pivotal role in technical discussions and in the industrial validation of results presented in Chapter 3 and Chapter 4.

You cannot answer a question that you cannot ask, and you cannot ask a question that you have no words for.

Prof. Judea Pearl

You are smarter than your data. Data do not understand causes and effects; humans do.

Prof. Judea Pearl

Yaadhum oore yaavarum kelir - Every commune on this Earth is where I belong and all people are my kin

Kaniyan Pungundranar

Never be a prisoner of your past. It was just a lesson, not a life sentence.

Dr. A.P.J. Abdul Kalam

Acknowledgments

First, I would like to take this moment to thank and express my gratitude towards my supervisor Prof. Biao Huang for his wonderful guidance, support, patience, motivation and for the freedom given to me to explore the research topics of my interest. Every discussion that I had with Prof. Biao helped me in realising my capabilities. I am really grateful to Prof. Biao for his kind and unfailing financial support without which this work wouldn't have been possible. I would like to acknowledge the financial support offered by Natural Sciences and Engineering Research Council (NSERC) of Canada. I take this opportunity to profusely thank Prof. Sirish Shah for a very inspiring and insightful discussion that I happened to have with him. I am thankful to Prof. Laksh (NUS) for encouraging me to go to the University of Alberta for my graduate studies. A special mention and thanks to my Mathematics teacher in undergrad Prof. Muthucumaraswamy for creating a passion in the subject. I am also thankful to my mentors at high school Mr. Viswakumar (*Chemistry*) and Mr. Vincent Raj (*Physics*) for their wonderful guidance and encouragement.

My special thanks to Dr. Jayaram Valluru, Dr. Rahul Raveendran and Dr. Santhosh Kumar Varanasi for their invaluable encouragement, support, constructive feedback and the time spent in reviewing my work and manuscripts. I would like to thank our industrial partners for introducing me to one of the challenging and interesting industrial problems. Further, I would like to acknowledge Department of Chemical & Materials Engineering, University of Alberta for giving me the opportunity to pursue my masters degree. During my graduate studies at the University of Alberta, I was very fortunate to have great teachers like Prof. Horacio Marquez, Prof. Jinfeng Liu, Prof. Vinay Prasad and my supervisor Prof. Biao Huang himself. I also take this opportunity to thank my defence committee members Prof. Vinay Prasad, Prof. Nilanjan Ray and Mr. Artin Afacan for their time and support.

This work would not have been complete without the support from my colleagues

of Computer Process Control group. I would like to thank and acknowledge Dr. Kirubakaran Velswamy, Dr. Nabil Magbool Jan (Now at IIT, Tirupati), Dr. Xunyuan Yin and other members for their invaluable support.

My journey in the graduate school was enjoyable because of my friends, Gokulakrishnan, Harish & Bharath from high school and undergrad, Rahul, Nabil, Kiru, Vishal, Shruti, Sushmitha, Brindhi, Arjun, Meenakshi, Santhosh, Nilesh, Faraz, Yashas, Arul, Sanjula, Ranjith, Anjana, Jayaram, Aswathi, Jingyi, Jim, Soumya, Anudari, Oguzhan, Sagar, Alireza, and many others from grad school. I would like to thank my friendly landlord Mrs. Jacqueline and my roommate Francis for making my stay in Edmonton as an enjoyable one. Trips to some of the beautiful places on earth such as Banff, Jasper and Waterton and the time spent with my friends are very memorable. Especially this lockdown period would have been really difficult without you people.

Last but not the least, I would like to express my gratitude towards my parents and my family for their love, encouragement and support throughout my graduate school.

Contents

List of Tables

List of Figures

Chapter 1

Introduction

1.1 Motivation

Process industries operate in a continuous and relentless manner to meet out the demand and also to maintain the quality of the products that are being manufactured. In chemical processes, due to the complexity in physical connections, operations and other types of external disturbances, process variables tend to fluctuate around the desired operating conditions causing an increase in material and energy consumption, process upsets, throughput reduction and at times drive the process to temporary shut down for maintenance. Therefore, to regulate the process in desired condition and to achieve hazard free operation, process variables are measured on-line and necessary decisions are made hierarchically. In order to achieve this objective, some of the commonly known approaches used are data reconciliation and causal inference. Due to the continuous measurement of process variables across the plant, large amount of data are generated over the time, which enables the industries to leverage analytics for deriving valuable insights from the process data and also to prune their decision making process. At the same time, it is important to account for the noise in process data, generated from the on-line measuring instruments and also due to the variability within the process. Since the analytics methods are sensitive to data quality, results obtained are subject to variations depending on the amount of noise present in the data. Therefore, to mitigate the effect of noise in the results and also to make them consistent with the actual process, as a pre-processing step, process data are subjected to data reconciliation [1]. In the actual problem, process model is

assumed to be deterministic. However, the model can be uncertain due to inaccuracies and using it might make the data reconciliation inaccurate. In the past decade, process data analytics gained enormous momentum than ever before due to various reasons and have been used extensively in the industries to address the problems in soft sensor design, estimation, fault detection & diagnosis etc [2, 3, 4]. In the course of development, various methods have been proposed in the literature [3, 5] to address the issues and improve the performance of the tools that fall under the scope of process data analytics. Inspite of the positive and promising outcomes achieved using the analytics, skepticism surrounds them due to the difficulty in interpretation of the results from physics perspective. In order to address this problem, the concept of probabilistic graphical models was integrated with statistical learning.

Probabilistic graphical models are considered to be one of the unique advances in the field of artificial intelligence and statistical learning theory. Given the set of random variables and their distribution, theory of probabilistic graphical models provides necessary conditions to illustrate the relationship among them as a graphical model and also as conditional probability distribution [6]. Due to its ability to decode the relationship among the random variables, probabilistic graphical models and the foundations of causal inference are considered to be pivotal for the development of interpretable statistical learning algorithms. Irrespective of its interpretation capabilities, probabilistic graphical model as an independent entity, are useful in illustrating the data-driven models in the graphical format for better understanding of the respective models [7] and also to model the uncertainties [6].

Therefore, in this thesis, novel methods are proposed to address the problems associated with data reconciliation and causal inference using the concept of probabilistic graphical models. In data reconciliation problem, Bayesian network based approach is proposed accounting for state uncertainties. In causal inference problem, a framework is proposed for the prediction of abnormal events in process operation such as flooding and weeping. Also, sparse inverse covariance estimation coupled with dynamic likelihood score is proposed for causal inference. Later in the thesis, efficacy of the proposed methods are demonstrated using intensive simulations and in an industrial application of flooding and weeping. In the forthcoming sections, contributions and outline of the thesis are detailed.

1.2 Thesis Contributions

The thesis contributes on the development of approaches for data reconciliation and causal inference in the framework of probabilistic graphical models. To be more specific, algorithms and techniques are proposed to address the problem of data reconciliation in uncertain systems and also to resolve the issue of flooding and weeping in distillation columns. Contributions of the thesis are listed in detail as follows.

1. A novel method for data reconciliation using Bayesian network, accounting for uncertainty in the state variables and probabilistic representation of process network model as a Bayesian network, with the preservation of process logic and Bayesian network properties, is proposed.

2. A novel row echelon reduction based approach is proposed to achieve acyclic construction of Bayesian network for process networks with recycle. This row echelon reduction method is also extended for data reconciliation of partially measured systems.

3. Algorithms are developed for statistical inference of measured and unmeasured state variables through Maximum Likelihood (MLE) estimation, Maximum-a-Posteriori (MAP) estimation and Particle Expectation Maximization (Particle-EM) estimation methods. Demonstrated the advantages of the proposed data reconciliation schemes through simulation studies covering three benchmark systems.

4. An approach integrating the findings of data-driven model with that of the process knowledge is proposed for the reconstruction of causal network. Finite impulse response model is identified with L_0 & L_1 constraint to extract the information of possible causal variables. In the course of addressing the problem, FIR model with L_0 constraint is identified using greedy sparse simplex algorithm and analytical expressions are derived to arrive at the solution.

5. Hypotheses driven approach is also proposed for early prediction of flooding and weeping in process operation. Efficacy of the proposed framework is demonstrated in an industrial case study, where causal network is constructed and monitoring rules are implemented for flooding and weeping detection in a deethanizer column associated with FCC unit. Findings are then implemented in the Industry to prevent the flooding and weeping events in real-time.

6. Sparse inverse covariance estimation approach is integrated with causality measures for causal inference in process data. The proposed problem, in the presence of L_0 constraint becomes non-convex optimization problem which is solved using greedy sparse simplex method [8] to achieve near global optimal solution. The algorithm is modified to account for the additional positive semi-definite constraint on the inverse covariance matrix.

7. Dynamic likelihood score is derived to determine the causal direction in the estimated undirected graph. The proposed approach for causal analysis is illustrated with a numerical and an industrial case study. In particular, the root cause and causal map for flooding and weeping in a deethanizer associated with Fluid catalytic cracking (FCC) is identified in the industrial case study.

1.3 Thesis Outline

The thesis is organized as follows

In Chapter 2, the problem of data reconciliation is introduced and a detailed discussion on Bayesian network types and their properties are provided. Then, the concept of degrees of freedom is introduced for linear system of equations along with the conditions for the consistency of linear system of equations. Following the preliminaries, the proposed Bayesian network approach for data reconciliation for the system with state uncertainties and recycle streams is discussed. A novel method to construct acyclic Bayesian networks for process networks with recycle streams is proposed in this work. This method is also extended for data reconciliation of partially measured systems. The solution is obtained by utilising a Bayesian network model translated from the process model and using statistical inference techniques to estimate the reconciled values of the states. The efficacy of the proposed data reconciliation schemes is demonstrated on three case studies namely Simple Flow Network, Mineral Processing Unit (without Recycle) and Mineral Beneficiation Process (with Recycle).

Chapter 3 describes the methodology for the prediction of flooding and weeping in process operations based on causal inference. Here, the method to reconstruct causal network using finite impulse response model with sparsity constraint and process knowledge is described in detail. Then, an approach proposed for the prediction of flooding and weeping using the causal information is discussed. Later, the proposed

methodology is demonstrated in an industrial case study of flooding and weeping prediction in a deethanizer column.

Chapter 4 proposes a novel approach for data-driven causal network reconstruction for process data analytics by integrating sparse inverse covariance estimation with causal score computation. The estimation of sparse inverse covariance matrix for undirected sparse network reconstruction is performed with L_0 norm constraint in the framework of greedy sparse simplex (GSS) algorithm. Further, the GSS algorithm is suitably modified to incorporate the additional constraint of positive semi-definiteness of the inverse covariance matrix. To determine the causal direction among the variables, dynamic likelihood score is computed for the associated variables in the reconstructed network in the second step. The efficacy of the proposed approach for causal analysis is illustrated using a numerical case study and an industrial application on prediction of flooding and weeping in a deethanizer column associated with a fluid catalytic cracking unit.

Chapter 5 provides conclusion for the thesis chapters along with future extensions of the present work.

Chapter 2

Bayesian Network approach for Data Reconciliation with State Uncertainties and Recycle Streams

2.1 Introduction

Process variables such as temperature, flow-rate and concentration, when measured online, are corrupted with random sensor noise. Using these noisy measurements directly for process control applications can lead to considerable deterioration of closed loop performance. To resolve this problem, the data reconciliation technique was introduced by David and Kuehn (1961), where the process data is corrected with the help of steady state material and energy balance models of the process (as shown in Figure 2.1). Data reconciliation is widely used in the industry as a pre-processing technique. The corrected estimates of the measurements obtained by data reconciliation will help in achieving effective monitoring of the process, closed loop control and real-time optimization.

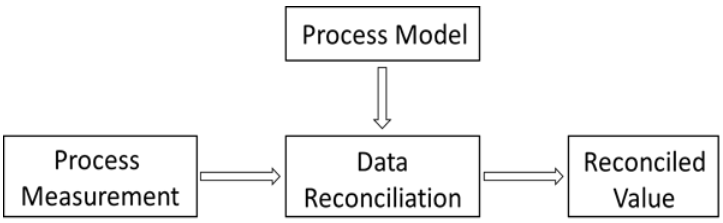

Figure 2.1: Outline of Data reconciliation

In general, data reconciliation is formulated as constrained optimization problem with available process models as constraints [9, 1]. From probabilistic perspective, data reconciliation can be addressed as Maximum Likelihood estimation (MLE) [10] or Maximum a Posteriori estimation problem (MAP). Data reconciliation problem formulated initially for the linear systems was later extended to nonlinear systems by linearizing the nonlinear model around the steady state [11, 12]. Nonlinear data reconciliation is also solved using nonlinear programming methods such as sequential quadratic programming (SQP). Some of the recent developments in data reconciliation are based on formulating the problem in statistical learning frameworks such as Principal Component Analysis [13, 14], Bayesian inference [15] and Expectation Maximization [16]. In principal components based method, process network is reconstructed from the data coupled with de-noising, which is later shown as the reconciled value [13]. This method is also extended to nonlinear data reconciliation using Kernel PCR [14]. In Bayesian method for data reconciliation [15], a statistical framework (Hierarchical Bayesian) is proposed for data reconciliation and gross error detection, with the inference of true state and corresponding parameters by Maximum–a–Posteriori (MAP) approach. In Expectation Maximization (EM) approach [16], the EM algorithm is utilized to carry out simultaneous data reconciliation and gross error detection. In general, data reconciliation accounts only for the error in measurement model and does not consider the error in process model. However, performing reconciliation without accounting for uncertainty in process model [17, 18] might lead to inaccurate reconciled value. Thus, accounting for process model uncertainty in solving data reconciliation is of utmost importance for obtaining accurate estimates. To overcome the issue of model inaccuracy in data reconciliation, methods are proposed in literature [19, 17], in which model parameters are assumed to be uncertain and the problem is reformulated as simultaneous data reconciliation and parameter estimation. Apart from uncertainty in parameters, uncertainties in the models can also arise due to uncertainties in the state. Here, the state refers to a process variable whose measurement is corrupted with noise. Under a Bayesian network framework

to be introduced next, this state is a hidden variable to be estimated. In this work, data reconciliation accounting for uncertainty in states is addressed in the Bayesian network framework.

Bayesian network, a member of probabilistic graphical model family [6], provides a framework to effectively address problems involving uncertainty. Bayesian network is represented as directed acyclic graph (G) with nodes (N) and edges (V), in which each node represents a random variable, following certain distribution, and edges between the nodes represent the logical relationship among them. The main advantage of Bayesian network lies in its compact representation of joint density of several random variables by the use of conditional independence relation among them. From the application perspective, Bayesian network has been utilised in the domain of fault detection and diagnosis. Here, the cause and effect relation of the process variables is built based on the process knowledge provided by process flow diagram and process data. Bayesian network developed, through inference and identification rules, is used to identify the location of fault [20, 21, 22]. In addition, Bayesian network plays an important role in the field of expert systems by helping the users in making key decisions at the right instant [23]. The ability of Bayesian networks in handling uncertainty is the main motivation for this work to use them as a tool to reformulate the data reconciliation problem accounting for uncertainties in the state. So far in the literature of process systems engineering, data reconciliation and Bayesian networks (knowledge based models) have been considered as two separate topics.

This work aims at addressing the data reconciliation problem from Bayesian Network perspective, with state uncertainties taken into account in order to achieve better estimates of true states. At first, a process network model is considered and interpreted probabilistically, which is then translated into a Bayesian network with preservation of process logic and network properties. With the help of available measurements and the Bayesian network constructed from the process model, algorithms are developed in this work to make estimates of the states using three different statistical inference methods, namely i). Maximum Likelihood Estimation (MLE), ii). Maximum–a-Posteriori (MAP) estimation and iii). Particle Expectation Maximization (Particle-EM). The directed acyclic property of the Bayesian network requires that the Bayesian network constructed from the process network model should be free from any recycle loop. However, in practice, process networks do have multiple recycle streams; hence, direct translation of process model will violate the directed acyclic property of Bayesian network. In order to construct Bayesian networks with acyclic structure for process networks with recycle streams, a novel row echelon reduction

approach is proposed and demonstrated in this work. For systems with partial measurement of states, data reconciliation is another challenging problem. In this work, the row reduction approach developed for systems with recycle streams is extended to address Bayesian network based data reconciliation for partially measured systems. The efficacy of the proposed Bayesian network based data reconciliation schemes is demonstrated on three benchmark case studies namely (a). Simple Flow network [9]; (b). Mineral Processing Unit [24] and (c). Mineral Beneficiation Process [25]. The performance of the proposed Bayesian network schemes for data reconciliation compares well with some of the existing schemes from the literature and their advantages over the existing methods are demonstrated in this work.

2.2 Data Reconciliation

Consider a linear steady state model represented by

$$Ax = 0 \tag{2.1}$$

where, A corresponds to incident matrix of process network with dimension $\mathbb{R}^{M_p \times N}$, M_p is the number of process units and N is the number of process streams connecting the process units. x is the vector of true state with dimension $\mathbb{R}^{N \times 1}$. The measurement model is given as

$$y = x + \epsilon \tag{2.2}$$

where, y is the vector of measurements with dimension $\mathbb{R}^{N \times 1}$. The measurement corrupted with random error ϵ is modelled as zero mean white noise following Gaussian distribution with covariance (Σ_y) i.e. $\epsilon \sim \mathcal{N}(0, \Sigma_y)$.

By considering the steady state model in Eq. 2.1 and measurement model in Eq. 2.2, the conventional data reconciliation problem is formulated as constrained weighted least squares problem and is represented as follows

$$\hat{x} = \min_{x} (y - x)^T (\Sigma_y)^{-1} (y - x) \tag{2.3}$$

$$s.t.\ Ax = 0$$

Optimal value of the state obtained by solving the aforementioned optimization problem is taken as the reconciled value of the process variable. By solving the constrained least squares problem given in Eq. 2.3, following analytical expression is obtained.

$$\hat{x} = [I - \Sigma_y A^T (A \Sigma_y A^T)^{-1} A] y \tag{2.4}$$

From the assumptions that the measurements are independent, the reconciliation problem can be posed in probabilistic framework as maximum likelihood estimation (MLE) problem, where the reconciled estimates are obtained by maximizing the probability of measurements, which is given as

$$\hat{x} = arg\max_{x} P(y|x) \tag{2.5}$$
$$s.t\ Ax = 0$$

In the scenario where the prior information about the probability distribution of the true state variable is available, maximum likelihood estimation (MLE) problem given in Eq. 2.5 can be reformulated as maximum a posteriori (MAP) estimation problem, which is given as

$$\hat{x} = arg\max_{x} P(y|x)P(x) \tag{2.6}$$
$$s.t\ Ax = 0$$

The conventional formulations given by Eq. 2.3, 2.5 and 2.6 are proposed in the literature [9] under the assumption that the process is in perfect steady state and the constraints represent the process behaviour exactly. However, possible uncertainties in the state can result from model – plant mismatch, reduction of the large scale model, and unaccounted retrofit of the existing process [17]. Thus, under such uncertain conditions, reconciling or estimating process variables through conventional approaches may yield inaccurate estimates of the state variables. To the best of our knowledge, formulations proposed so far to address the uncertainty in process model account only for the uncertainty in model parameter and the problem is solved as simultaneous data reconciliation and parameter estimation [19, 18]. In the present work, a data reconciliation scheme accounting for the state uncertainty is proposed and the problem is solved under Bayesian network framework.

Following assumptions are made in developing the proposed data reconciliation schemes.

Assumption. 1

Process variables, also defined as states (x) in this work, tend to be uncertain, with uncertainty following Gaussian distribution with zero mean and variance (σ_x^2). The magnitude of uncertainty in the process model is reflected as the variance (σ_x^2) in the state variable.

Assumption. 2

Measurements of the process variables are unbiased and free of gross errors. Further,

it is assumed that process variables have some redundancy and they are observable unless stated otherwise.

2.3 Bayesian Network

Bayesian network, a member of probabilistic graphical model family, represents the random variables and relationship among these variables by means of conditional dependence via directed acyclic graph (DAG) structure (G) [6]. In this graphical representation of the system, variables are the nodes (N) and vertices (V) connecting the nodes represent the relationship among these variables. From the graph theory perspective, a graph G is represented as follows

$$G = (N, V)$$

In Bayesian network, the source node is defined as a parent node and the terminal node is defined as a child node. Let $Z = (Z_1, Z_2, \ldots Z_M)$ be a set of random variables. Depending upon the type of relationship between these variables, a Bayesian network representing this relationship is classified as one of the three fundamental directed acyclic graph (DAG) structures (Figure 2.2) namely Chain, Common Cause and Common Effect.

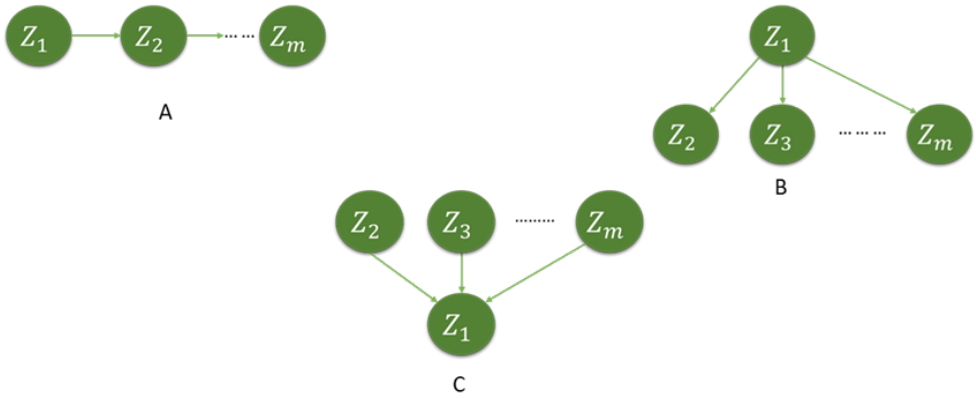

Figure 2.2: Directed acyclic Graph structure of Bayesian networks(A. Chain, B. Common Cause, C. Common effect)

2.3.1 Chain

Among the three Bayesian network structures, chain is assumed to be simplest in structure as shown in Figure 2.2(A). Here, the random variables are connected to one another in the form of chain with the single child (Z_2) for a parent (Z_1) or single parent (Z_{M-1}) for a child (Z_M), source node (Z_1) stays without any parent and terminal node (Z_M) stays without any children. The joint probability distribution of the variables in chain structure given in Figure 2.2(A) can be represented as the product of independent conditional distribution given in Eq. 2.7.

$$P(Z_1, Z_2, ...Z_{M-1}, Z_M) = P(Z_M \mid Z_{M-1})...P(Z_2 \mid Z_1)P(Z_1) \tag{2.7}$$

2.3.2 Common Cause

Common cause network is a type of Bayesian network structure where a parent is expected to have two or more children as shown in Figure 2.2(B). In general, this can be stated as variable with confounders. Joint probability distribution and conditional independence of the variables representing common cause Bayesian network can be represented as Eq. 2.8.

$$P(Z_1, Z_2, ...Z_{M-1}, Z_M) = P(Z_2 \mid Z_1)P(Z_3 \mid Z_1)...P(Z_M \mid Z_1)P(Z_1) \tag{2.8}$$

2.3.3 Common Effect

Common effect network is another important Bayesian network structure where two or more parents share a common children as shown in Figure 2.2(C). Similar to chain and common cause Bayesian networks, the joint distribution of the variables in common effect Bayesian network can be represented as product of conditional distribution as given in Eq. 2.9.

$$P(Z_1, Z_2, ...Z_{M-1}, Z_M) = P(Z_1 \mid Z_2, Z_3, ...Z_M)P(Z_2)P(Z_3)...P(Z_M) \tag{2.9}$$

The probabilistic model corresponding to the aforementioned three fundamental network structures given in Figure 2.2 can be generalized and presented as,

$$P(Z_1, ..., Z_M) = \prod_{i=1}^{M} P(Z_i|Pa_{Z_i})P(Pa_{Z_i})$$

$$Z_i \notin Pa_{Z_i}, Z_i \in Pa_{Z_i}^C \& Pa_{Z_i} \in Z_i^C.$$

where, $P(Z_1, ..Z_M)$ is the joint probability distribution, $P(Z_i \mid Pa_{Z_i})$ is the conditional probability distribution and Pa_Z corresponds to parent of the variable Z. Z and Pa_Z are considered to be a tuple of variables (finite sequence) with Z being a complement of Pa_Z and Pa_Z being complement of Z. In Bayesian networks, probability distribution is chosen usually from an exponential family of distributions and it can be a continuous or a discrete type.

2.3.4 D-Separation

D – Separation, also known as directional separation, helps in deciding the independence among the given set of variables and its corresponding Bayesian network. For a better understanding of the concept, let us consider a set of three random variables X,Y,Z, whose joint distribution and conditional independence are represented as the following

$$P(X, Y, Z) = P(X \mid Y)P(Y \mid Z)P(Z)$$

Then, D - Separation for the mentioned set of variables, with the assumption of Y to be known, can be represented as $(Z \perp\!\!\!\perp X \mid Y)$. Now, with the assumption of Z to be known, D - Separation can be stated as $(X \not\perp\!\!\!\perp Y \mid Z)$.

2.3.5 Markov Blanket

An important property of a Bayesian network is Markov blanket, which is a boundary around an arbitrary node with its parents, children and co-parents of the children in the boundary. This concept can be understood from the arbitrary network provided in Figure 2.3. From the given arbitrary network, Markov blanket can be constructed around the node Z_6 using the variables Z_5, Z_8 (Parent), Z_1, Z_7 (Children) and Z_2 (Co-parent). Markov blanket provides the knowledge that is essential to build joint distribution around a node in the Bayesian network. This principle also holds for the undirected graphical models like Markov random field. Details about the properties of Bayesian network and general graphical models can be found in [6].

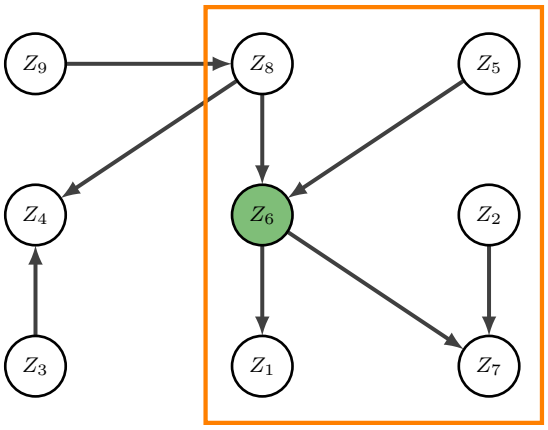

Figure 2.3: Markov Blanket in Graphical Model

2.3.6 Degrees of Freedom

Degrees of freedom indicates the minimum number of variables that are required to uniquely determine the solution for a system of equations. Degrees of freedom N_d is defined as

$$N_d = N_{uk} - N_{eq} \tag{2.10}$$

where, N_{uk} is the number of unknowns and N_{eq} is the number of independent equations representing the mathematical model of a system. In other words, the degrees of freedom can be interpreted as the information requirement for defining a system, where the information refers to the number of known and unknown variables that are essential to determine the unique solution. Using the degrees of freedom as the basis, Bayesian network structure is constructed from the process network.

Rouche-Capelli Theorem

For the linear system $Ax = b$ with dimension $x \in \mathbb{R}^M$, there exists a solution set x_s in the subspace of $\mathbb{R}^M$ with dimension $M - rank(A)$, if and only if $rank(A) = rank([A \mid b])$, where $[A \mid b]$ is the augmented matrix. Further, the linear system of equation is expected to be consistent if $N_d = (M - rank(A))$, where N_d is degrees of freedom.

2.4 Data Reconciliation based on Process Bayesian Network

The ability of Bayesian network to deal with uncertainties modelled in a probabilistic framework is the main motivation for the present work. The objective is to develop a data reconciliation scheme for a process with state uncertainties using Bayesian network representation of the process. With the knowledge of process flow network such as flow direction and degrees of freedom, process variables are represented as joint distribution and decomposed into a set of conditional probability distributions, as illustrated in the flowchart in Figure 2.4.

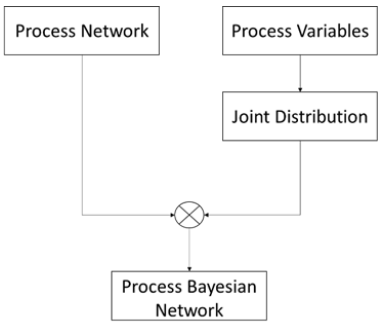

Figure 2.4: Converting Process network to Bayesian network

In converting the process network into a Bayesian network, it is important to ensure that the basic properties of the Bayesian network are preserved. In Bayesian network based data reconciliation proposed in this work, the conventional data reconciliation scheme represented in Figure 2.1 is modified by replacing the process model with a process Bayesian network model as shown in Figure 2.5.

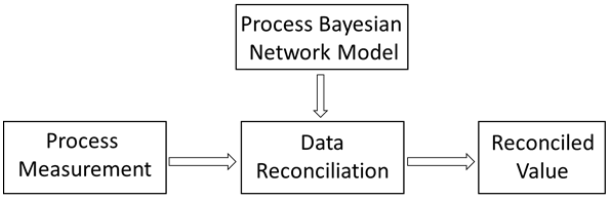

Figure 2.5: Data reconciliation with Process Bayesian network

The proposed scheme can be understood better from an illustrative example of a simple process flow network. This process flow network [9] with 4 process units and

6 streams (Figure 2.6), has been reported widely in the literature as a case study problem for demonstrating various data reconciliation schemes. Eq. 2.11 represents the underlying steady state process model and its conditional probability distribution, utilised for obtaining the Bayesian network representation of the process network.

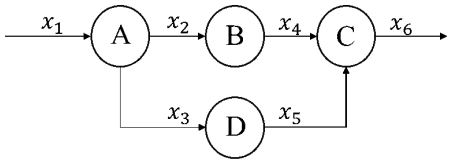

Figure 2.6: Simple Flow network

Process Unit	Mass Balance	Probabilistic Model
A	$X_1 = X_2 + X_3$	$P(X_2 \mid X_1, X_3)P(X_1)P(X_3)$
B	$X_2 = X_4$	$P(X_4 \mid X_2)$
C	$X_3 = X_5$	$P(X_5 \mid X_3)$
D	$X_6 = X_4 + X_5$	$P(X_6 \mid X_4, X_5)$

(2.11)

Here, the key is to interpret the process model as a conditional probability distribution model such that the Bayesian network properties of D-separation and acyclicity are satisfied. In any process flow-sheet, process units with different input/output configurations can be observed. For instance, in the process flow-sheet presented in Figure 2.6, A is a process unit with one input and two outputs configuration, C is a process unit with two inputs and one output configuration, and B and D are process units with one input and one output configuration. For the process network presented here with different configuration of process units, uniqueness of solution to the system of mass balance equations can be interpreted from degrees of freedom. Consider the model equation $x_1 = x_2 + x_3$ for the process unit A. Common cause Bayesian network may be constructed for the given process model by simply taking the inputs as parent nodes and outputs as children nodes. Physically, one can interpret the network corresponding to this model as 'change in x_1 leads to change in x_2 and x_3'. But, such an interpretation gives rise to infinite number of solutions to this model equation as it means that there is no one unique set of values that x_2 and x_3 can take given the value of x_1. To handle this problem, degree of freedom is utilized in construction of the Bayesian network. For the given process model, degree of freedom is computed

to be 2, which means, two process variables must be specified for the solution to be unique. Therefore in the process model, x_1 and x_3 may be specified first and the conditional probability distribution describing these three variables is interpreted as $P(x_2 \mid x_1, x_3)P(x_1)P(x_3)$. In $P(x_2 \mid x_1, x_3)P(x_1)P(x_3)$, it can be interpreted as that given the information of $(x_1 \& x_3), x_2$ is independent of $(x_1 \& x_3)$. Similarly, using the degrees of freedom analysis explained here, Bayesian networks can be constructed for the configuration of various process units in the process flow network. Upon analysis of different process network configurations, it is found that the degrees of freedom condition should be utilized and a generalized condition for constructing the Bayesian network is given as $card(Pa_X) = N_d$ i.e. number of primary parents for the variable X must be equal to the degrees of freedom. If this condition is not satisfied then the solution becomes inconsistent (From Rouche-Capelli theorem). Therefore, using this condition, the process model in Eq. 2.11 is interpreted probabilistically and process Bayesian network is constructed, taking process variables as the Nodes (N) and relationship among these variables as the edges (E). The process Bayesian network, thus constructed from the process model, is shown in Figure 2.7.

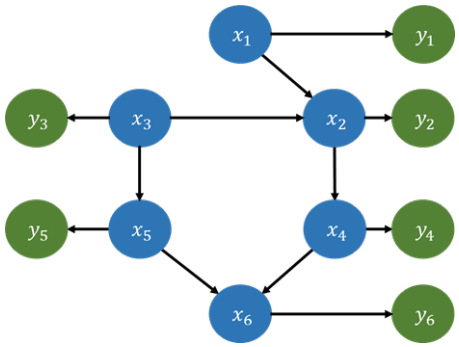

Figure 2.7: Process Bayesian Network of Simple Flow network

In Figure 2.7, the nodes in green represent measurements that are available and the nodes in blue represent true states of the process variables to be estimated. Based on the aforementioned discussion on probabilistic interpretation of the process model and the construction of Bayesian network, it can be stated that this sort of interpretation can be made for any process network. The discussion provided to construct the Bayesian network from the process network can be summarized as follows.

1. Compute degrees of freedom (N_d) using Eq. 2.10 for the given system A.
2. Fix the parents according to the degrees of freedom for each node. The number of parents of each node equals to the degrees of freedom, and the configuration

is not unique. To avoid the structural complexity, whenever possible physical input variables to the process node are selected as the parents of the node, namely flow direction of the process variable in the given process network is generally considered as of the arcs directions in the Bayesian network to be constructed.

3. Condition 2 is valid for the process network without recycle. In the presence of recycle, method to be introduced in Section 2.4.1 should be used.

Thus, for any process network with process variables $X = (x_1, x_2, ..., x_M)$ and its corresponding measurements $Y = (y_1, y_2, ..., y_M)$, process Bayesian network similar to Figure 2.7 can be constructed. The joint distribution of X and Y for a generic process Bayesian network can be expressed as a product of measurement model and process model as follows

$$P(y_1, .., y_M, x_1, .., x_M \mid \sigma^2_{y_j}, \sigma^2_{x_j}) = \prod_{j=1}^{M} P(y_j \mid x_j, \sigma^2_{y_j}) P(x_j \mid Pa_{x_j}, \sigma^2_{x_j}) \tag{2.12}$$

For computational convenience, the joint distribution in Eq. 2.12 can be expressed in logarithmic form, given as,

$$\log P(y_1, .., y_M, x_1, .., x_M \mid \sigma^2_{y_j}, \sigma^2_{x_j}) = \sum_{j=1}^{M} \log P(y_j \mid x_j, \sigma^2_{y_j}) + \log P(x_j \mid Pa_{x_j}, \sigma^2_{x_j}) \tag{2.13}$$

where, $\sigma^2_{y_j}$ and $\sigma^2_{x_j}$ represent variances of the measurement and state variable respectively.

Further, considering a batch of N independent and identically distributed measurements of M process variables (Y) and their corresponding true state variables (X) i.e.

$$Y = \begin{bmatrix} y_{1,1} & .... & y_{1,M} \\ . & .... & . \\ y_{N,1} & .... & y_{N,M} \end{bmatrix} X = \begin{bmatrix} x_{1,1} & .... & x_{1,M} \\ . & .... & . \\ x_{N,1} & .... & x_{N,M} \end{bmatrix}$$

The joint probability density function in Eq. 2.13 can be expanded to include this batch of data and is given as follows.

$$\log P(X, Y \mid \sigma^2_y, \sigma^2_x) = \sum_{i=1}^{N} \sum_{j=1}^{M} \log P(y_{i,j} \mid x_{i,j}, \sigma^2_{y_{j,j}}) + \log P(x_{i,j} \mid Pa_{x_{i,j}}, \sigma^2_{x_{j,j}}) \tag{2.14}$$

2.4.1 Handling Cycles in Process Bayesian Network

In some practical scenarios, process networks (A) have recycles streams. When a process network with recycle is considered directly to develop the Bayesian network model, cycles will be introduced to the Bayesian network, thereby violating the acyclicity condition. Thus, in the construction of Bayesian network from the process model, it is a challenge to avoid the effect of recycles introduced by the process model. In order to overcome this problem, a row echelon reduction method is developed in this work. In this method, the process network (A) with recycle is reduced to a row echelon form (A_R) by Gauss elimination. Reduced row echelon form of linear system (A_R) divides the system of linear equations into (A_D) and (A_I), corresponding to dependent and independent variables respectively.

$$\left(A \xrightarrow{GaussElim.} A_R\right) \rightarrow [A_D \ (-A_I)] \tag{2.15}$$

Row echelon reduced process network A_R results in an acyclic Bayesian network structure due to the possibility of representing dependent process variables as a function of independent process variables. Aforementioned approach is demonstrated using a simple network with recycle loop (Figure 2.8). From Figure 2.8, it can be seen that direct probabilistic interpretation of process network with recycle introduces cycle in the probabilistic network as well.

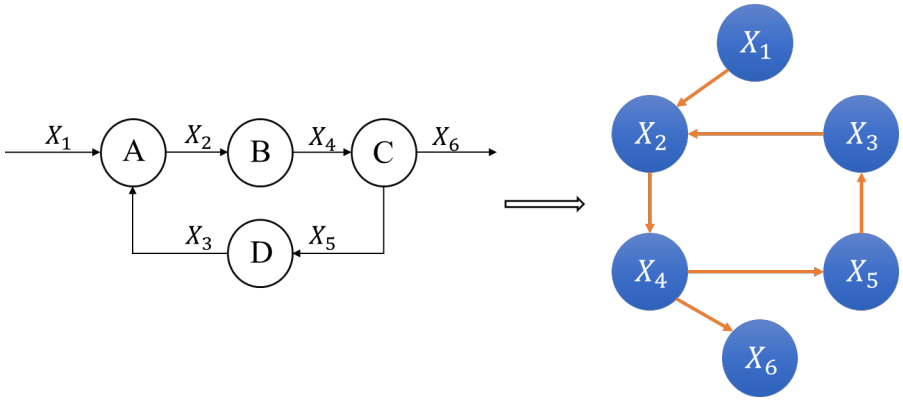

Figure 2.8: Probabilistic interpretation of network with recycle (Left: Actual network Right: Probabilistic interpretation)

Now, reducing the process network matrix (A) to row echelon form (A_R) by Gauss

elimination, we obtain the following

$$A = \begin{bmatrix} 1 & -1 & 1 & 0 & 0 & 0 \\ 0 & 1 & 0 & -1 & 0 & 0 \\ 0 & 0 & 0 & 1 & -1 & -1 \\ 0 & 0 & -1 & 0 & 1 & 0 \end{bmatrix} \rightarrow A_R = \begin{bmatrix} 1 & 0 & 0 & 0 & 0 & -1 \\ 0 & 1 & 0 & 0 & -1 & -1 \\ 0 & 0 & 1 & 0 & -1 & 0 \\ 0 & 0 & 0 & 1 & -1 & -1 \end{bmatrix}$$

In this reduction, X_5, X_6 are independent variables and $X_1, X_2, X_3 \& X_4$ are dependent variables respectively. Thus, probabilistic interpretation of reduced process network (A_R) yields a Bayesian network that is acyclic in structure as shown in Figure 2.9. Thus, using this row echelon reduction approach, Bayesian network with acyclic structure can be obtained for process network with recycle.

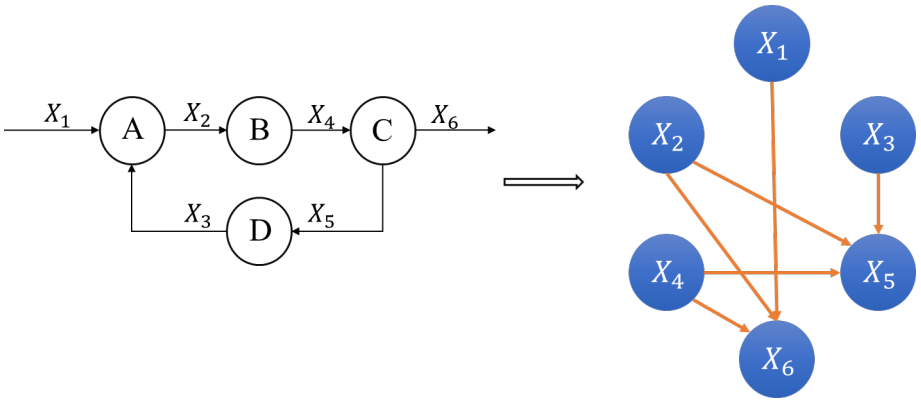

Figure 2.9: Probabilistic interpretation of network with recycle (Left: Actual network Right: Probabilistic interpretation (After obtaining Echelon form))

Upon overcoming the issue of recycle in constructing the Bayesian network, uniqueness of the solution may be questioned due to the change in process network structure resulting from the reduced row echelon matrix A_R. We justify the uniqueness of the solution using the theoretical foundations of linear algebra and data reconciliation. In data reconciliation, the constraint equation corresponding to the process model is given as $Ax = 0$ with $A \in \mathbb{R}^{M \times N}$ and $x \in \mathbb{R}^{N \times 1}$. From the linear algebra perspective, the solution to the constraint equation can be interpreted as, the solution vector $x \in \mathbb{R}^{N \times 1}$ spanning the Null space of A.

Proposition 2.4.1

If $Ax = 0$ and $A_R \in \mathbb{R}^{M \times N}$ is the row echelon reduced form of A, then solution for $A_R x = b$ exits if and only if $b \in \mathbb{R}^{M \times 1}$ is zero [26].

Therefore, based on the linear algebraic interpretation of $Ax = 0$ and Proposition 2.4.1, one can state that the basis vector (solution vector) x must span the same null space of both A and A_R, such that, $Ax = A_R x = 0$. This implies that A and A_R are row equivalent for a unique value of $x \neq 0$. Although the new balance equation resulting from row echelon transformation is no longer same as the original one physically, the new equation is equivalent to the original one in the sense that the same process data have to satisfy both the original and the new equation namely the equality constraint. This justifies the use of the new set of reduced form of equations for data reconciliation of systems with recycle streams. Further, the row echelon transformation results in the altered state uncertainties. However, in theory, this will not affect the reconciled values of the state estimates obtained using the proposed Particle-EM technique presented in the subsequent Section 2.5.3, since the transferred state uncertainties themselves are estimated parameters in the proposed Particle-EM algorithm. Application of this method developed for handling cycles in process network will be demonstrated in a case study of Mineral Beneficiation Process in Section 2.6.3. The flowchart in Figure 2.10 illustrates the sequence of Bayesian network construction.

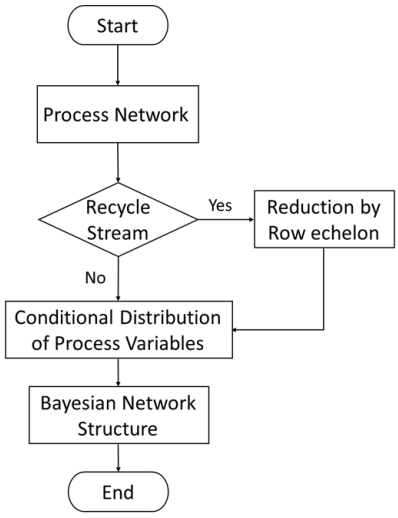

Figure 2.10: Flowchart describing the method for handling recycle in Process network for Bayesian network construction

2.4.2 Data Reconciliation for Partially Measured Systems

One of the challenges in performing data reconciliation is handling the process network, when not all the process variables are measured. From the literature, some of

the widely used methods for handing partially measured systems are matrix projection approach [27] and method of orthogonal transformation [28]. In the aforementioned methods, process network matrix is segmented into measured and unmeasured portion from which unmeasured section of process network is projected into the null space to decouple the unmeasured process network from the measured process system. Once the decoupling is complete, measured portion is reconciled first, followed by reconstruction of unmeasured region with measured process variables. With respect to Bayesian network approach for data reconciliation, due to the direct utilization of process network knowledge, estimating unmeasured process variables by orthogonal projection may not be possible, as the structural information of unmeasured region is hidden in projection matrix. In order to preserve the structural information during decoupling, row echelon reduction method, introduced in Section 2.4.1, is extended for data reconciliation of partially measured systems. Here, row echelon form is obtained through row reduction by simple initial rearrangement of process variables in the network.

Consider a process network matrix, A, which has both measured and unmeasured process variables. With the initial knowledge on available measurements, process network matrix A can be split into measured and unmeasured variables as shown in Eq. 2.16, followed by rearrangement mentioned in the same.

$$A_1 X_M + A_2 X_{UM} = 0 \rightarrow \begin{bmatrix} A_2 & A_1 \end{bmatrix} \begin{bmatrix} X_{UM} \\ X_M \end{bmatrix} = 0 \rightarrow N_{PM} \tilde{X} = 0 \tag{2.16}$$

where, A_1 is the measured component of process network and A_2 is the unmeasured component of process network with X_M and X_{UM} being variables corresponding to measured and unmeasured components of the process network respectively. N_{PM} is rearranged process matrix and $\tilde{X}$ is the vector of rearranged process variables. With rearranged process matrix, echelon form is obtained through row reduction which provides dependent variable coefficient matrix (D_M) and free variable coefficient matrix (F_M) as the following.

$$\begin{bmatrix} D_M & F_M \end{bmatrix} \begin{bmatrix} X_{UM} \\ X_M \end{bmatrix} = 0 \tag{2.17}$$

Here, the structure of augmented $\begin{bmatrix} D_M & F_M \end{bmatrix}$ is similar to the structure of A_R presented in section 2.4.1. In particular, after the row echelon reduction, non - zero entries of dependent variable coefficient matrix (D_M) can be written as a function of free variable coefficient matrix (F_M). As the row-reduction is performed after

rearrangement, dependent variable coefficient matrix (D_M) has the information of unmeasured variables and free variable coefficient matrix (F_M) has the information of measured variables. From the new reduced model in Eq. 2.17, Bayesian network is constructed in order to perform data reconciliation. In order to solve the data reconciliation problem with unmeasured variables in the proposed approach, rank of the unmeasured variable matrix (A_2) must be less than or equal to the row rank of the process matrix A ($rank(A_2) \leq rowrank(A)$). If this rank criterion is not satisfied, then the system will be under-determined and unique solution cannot be obtained [29]. The generic Bayesian network representation for partially measured system can be represented as the following.

$$\log P(X, Y \mid \sigma_Y^2, \sigma_X^2)) = \sum_{i=1}^{N} \sum_{j=1}^{M-U_M} \log P(y_{i,j} \mid x_{i,j}, \sigma_{y_{j,j}}^2) + \log P(x_{i,j} \mid Pa_{x_{i,j}}, \sigma_{x_{j,j}}^2) \tag{2.18}$$

where, U_M is the number of unmeasured process variables and $(M - U_M)$ is the size of measured variable set, with which unmeasured variables are estimated. Application of this method developed for handling partially measured processes will be demonstrated in a case study of Mineral Processing Unit in Section 2.6.4.

2.5 Statistical Inference in Bayesian Network for Data Reconciliation

The joint probability distribution function (Eq. 2.14) obtained for the process Bayesian network is used in the estimation of reconciled states through different statistical inference techniques. In this work, three different statistical inference techniques are considered namely i) maximum likelihood estimation (BN-MLE), ii) maximum-a-priori estimation (BN-MAP) and iii) Particle Expectation Maximization (Particle-EM) based approximate estimation. In the data reconciliation schemes using maximum likelihood estimation (BN-MLE) and maximum-a-priori Estimation (BN-MAP), uncertainties in the state and measurements (σ_x^2, σ_y^2) are assumed to be known. Whereas, in the absence of any knowledge about the uncertainties in state and measurements, the Particle Expectation Maximization (Particle-EM) based estimation algorithm will be able to simultaneously estimate both the reconciled states and the uncertainty parameters in iterative steps.

The assumption made in the BN-MLE and BN-MAP schemes that the availability of

information about state and measurement uncertainty (σ_x^2, σ_y^2) is essential for estimation of reconciled states is a purely hypothetical one, as in no practical situation these uncertainties will be known. In spite of this unrealistic assumption, the BN-MLE and BN-MAP schemes developed in this work are crucial, as the simulated results generated using these schemes can serve as a benchmark for comparing and evaluating the performance of particle-EM algorithm, which is a more realistic one when it comes to practical application. Detailed derivations of these statistical inference algorithms for estimation of reconciled states are presented in the following sections.

2.5.1 Maximum Likelihood Estimation

In this sub-section, maximum likelihood estimation approach for Bayesian network based data reconciliation scheme is developed for obtaining the reconciled estimates. Using maximum likelihood principle, the reconciled estimates are obtained by minimizing the negative log likelihood of joint density function given in Eq. 2.14,

$$\hat{X} = \min_X(-\log P(X, Y \mid \sigma_Y^2, \sigma_X^2)) = \min_X \sum_{i=1}^{N}\sum_{j=1}^{M} -\log P(y_{i,j} \mid x_{i,j}, \sigma_{y_{j,j}}^2) \\ -\log P(x_{i,j} \mid Pa_{x_{i,j}}, \sigma_{x_{j,j}}^2)$$

$$= \min_X \sum_{i=1}^{N}\sum_{j=1}^{M} -\log\left(\frac{1}{\sqrt{2\pi}\sigma_{y_{j,j}}^2} + \frac{1}{\sqrt{2\pi}\sigma_{x_{j,j}}^2}\right) + \frac{1}{2}\left(\frac{(y_{i,j} - x_{i,j})^2}{\sigma_{y_{j,j}}^2} + \frac{(x_{i,j} - Pa_{x_{i,j}})^2}{\sigma_{x_{j,j}}^2}\right) \tag{2.19}$$

It is important to note that the cost function given in Eq. 2.19 is a combination of measurement and process model, thus resulting in an unconstrained optimization problem formulation. When prior information of individual source nodes is available, maximum likelihood estimation (MLE) can be re-cast as maximum–a–posteriori (MAP) estimation problem in Bayesian network setting which is discussed in the following section.

2.5.2 Maximum-a-Posteriori Estimation

When prior information of individual source nodes is available, maximum likelihood estimation problem can be extended to maximum–a–posteriori estimation problem by incorporating prior information of individual nodes of the process Bayesian network.

With the inclusion of prior information of individual nodes, MLE cost function in Eq. 2.19 gets modified into a MAP cost function represented as follows.

$$\hat{X} = \min_{X}(-\log P(X, Y \mid \sigma_Y^2, \sigma_X^2)) = \min_{X} \sum_{i=1}^{N}\sum_{j=1}^{M} -\log P(y_{i,j} \mid x_{i,j}, \sigma_{y_{j,j}}^2) \\ -\log P(x_{i,j} \mid Pa_{x_{i,j}}, \sigma_{x_{j,j}}^2) - \log P(Pa_{x_{source}}, \sigma_{x_{source}}^2)$$

$$= \min_{X} \sum_{i=1}^{N}\sum_{j=1}^{M} -\log\left(\frac{1}{\sqrt{2\pi}\sigma_{y_{j,j}}^2} + \frac{1}{\sqrt{2\pi}\sigma_{x_{j,j}}^2}\right) + \frac{1}{2}\left(\frac{(y_{i,j} - x_{i,j})^2}{\sigma_{y_{j,j}}^2} + \right. \\ \left. \frac{(x_{i,j} - Pa_{x_{i,j}})^2}{\sigma_{x_{j,j}}^2} + \frac{(Pa_{x_{source}} - \mu_{source})^2}{\sigma_{x_{source}}^2}\right) \tag{2.20}$$

Given the cost function in Eq. 2.20, estimates of the states are obtained by solving the optimization problem and these estimates are interpreted as reconciled values. Quality of the estimates varies depending upon the prior distribution chosen. In the present work, it is assumed that the prior information of the nodes follows Gaussian distribution. Mean of the source (prior) is estimated in MAP optimization routine and the variance is estimated based on Cramer – Rao inequality [30, 31], which provides the lower bounds for the variance of unbiased estimates as given in Eq. 2.21

$$\Sigma_{X_{source}} = \sigma_{x_{source}}^2 = [I_L + I_P]^{-1} \tag{2.21}$$

where, I_L and I_P are the Fischer information matrix of likelihood of the state and measurement and the prior. On expanding the Eq. 2.21 further, approximation of prior variance can be obtained as follows.

$$\Sigma_{X_{source}} = \left[\left(- \frac{\partial^2}{\partial X_s^2}\log\left(P(Y_s \mid X_s)P(X_s \mid Pa_{X_s})\right)\right) + \right. \\ \left. \left(\left(\frac{\partial}{\partial X_s}\log P(Pa_{X_s})\right)\left(\frac{\partial}{\partial X_s}\log P(Pa_{X_s})\right)\right)\right]^{-1} \tag{2.22}$$

On expanding Eq. 2.22 under the consideration that conditional distribution follows Gaussian distribution, simple close form expression can be obtained for the variance of the prior as follows.

$$\Sigma_{X_{source}} = [\Sigma_{Y_s}^{-1} + \Sigma_{X_s}^{-1} + \left((X_s - X_{past})^T(\Sigma_{X_{past}}^{-2})(X_s - X_{past})\right)]^{-1} \tag{2.23}$$

where Y_s and X_s are the measurement and state of the source node with Σ_{Y_s} and Σ_{X_s} being the variance of measurement and state of the corresponding source node. X_{past} and $\Sigma_{X_{past}}$ are the mean and the variance of the state variables calculated from the data repository.

2.5.3 Simultaneous Data Reconciliation and Uncertainty Parameter Estimation

In actual setting, parameters representing uncertainties in states and measurements (σ_x^2, σ_y^2) are not available. In the absence of any knowledge about these uncertainties, reconciliation algorithms developed in the previous sections using maximum likelihood estimation (MLE) or maximum-a-posteriori (MAP) estimation cannot be directly applied unless the uncertainty parameters (σ_x^2, σ_y^2) are estimated simultaneously along with the reconciled states. In the case of Bayesian network models, due to their hierarchical nature, it would be difficult to obtain analytical solutions for uncertainty parameter estimation under maximum likelihood estimation (MLE) or under maximum–a–posteriori estimation (MAP) framework [32, 33, 34]. Even if we manage to obtain an analytical expressions for Bayesian network model, the solution will be problem specific due to the network structure. Therefore, in this work, Particle Expectation Maximisation (Particle-EM) algorithm is developed to obtain a general solution to the problem of simultaneous state and uncertainty estimation.

Expectation Maximization (EM) is an iterative algorithm which yields approximate maximum likelihood estimates. EM algorithm is implemented iteratively in two stages - Expectation step (E–step) and Maximization step (M-step). In the E–step, expectation of the joint log-likelihood is evaluated with guessed parameter values (updated in the next iteration) and in the M–step, parameters are estimated by maximizing the expectation of log-likelihood (Q function). In Particle-EM, E–step is evaluated through Monte Carlo simulations to estimate the state and M–step is evaluated using conventional optimization approach [34].

Detailed derivation of the Particle-EM algorithm for data reconciliation and simultaneous estimation of uncertainty parameters is presented in this section. Joint likelihood with the observed measurements (Y) and the parameters Θ can be represented as follows.

$$L(Y;\Theta) = \log P(Y \mid \Theta) = \log \int P(X, Y \mid \Theta) dX \tag{2.24}$$

Here, (X) is the hidden state, Θ is the parameter representing the measurement and state uncertainty (variance: $\theta_y = \text{diag}(\Sigma_y)$, $\theta_x = \text{diag}(\Sigma_x)$) and $\Theta \in (\theta_y \cup \theta_x)$. On multiplying and dividing Eq. 2.24 by $P(X \mid Y, \Theta^k)$ we get,

$$\log P(Y \mid \Theta) = \log \int \frac{P(X, Y \mid \Theta)}{P(X \mid Y, \Theta^k)} P(X \mid Y, \Theta^k) dX \tag{2.25}$$

Further, Eq. 2.25 can be expressed in terms of conditional expectation as the following.

$$\log P(Y \mid \Theta) = \log \mathbb{E}_{X|Y,\Theta^k}\left[\frac{P(X,Y \mid \Theta)}{P(X \mid Y,\Theta^k)} \mid Y,\Theta^k\right] \tag{2.26}$$

On further simplification and by applying Jensen's Inequality [35] to Eqn. (20), following expressions are obtained.

$$\log P(Y \mid \Theta) \geq \mathbb{E}_{X|Y,\Theta^k}[\log P(X,Y \mid \Theta) \mid Y,\Theta^k] - \mathbb{E}_{X|Y,\Theta^k}[\log P(X \mid Y,\Theta^k) \mid Y,\Theta^k] \tag{2.27}$$

$$\log P(Y \mid \Theta) \geq Q(\Theta \mid \Theta^k) - H(\Theta^k \mid \Theta^k) \tag{2.28}$$

where, $Q(\Theta \mid \Theta^k)$ is $\mathbb{E}_{X|Y,\Theta^k}[\log P(X,Y \mid \Theta) \mid Y,\Theta^k]$, $H(\Theta^k \mid \Theta^k)$ is $\mathbb{E}_{X|Y,\Theta^k}[\log P(X \mid Y,\Theta^k) \mid Y,\Theta^k]$ and Θ^k represents the parameter estimated during the k^{th} iteration of EM algorithm. $Q(\Theta \mid \Theta^k)$ is maximized w.r.t parameters, which tends to maximize the log-likelihood given in Eq. 2.27 since H is not a function of Θ. EM algorithm can be implemented by following steps.

Expectation Step (E-Step)

In the E – Step, estimates of the true state are obtained by evaluating the Q function over fixed parameters obtained at k^{th} iteration. On decomposing the joint likelihood in the Q function, based on the knowledge of process Bayesian network (Markov property), into conditional probability distribution, we arrive at the following equation.

$$\log P(X,Y \mid \Theta) = \sum_{i=1}^{N}\sum_{j=1}^{M} \log[P(y_{i,j} \mid x_{i,j},\theta_{y_{j,j}})P(x_{i,j} \mid Pa_{x_{i,j}},\theta_{x_{j,j}})] \tag{2.29}$$

By substituting Eq. 2.29 in Q function of Eq. 2.27, the Q function can be expressed as follows.

$$Q(\Theta \mid \Theta^k) = \mathbb{E}_{X|Y,\Theta^k}\left[\sum_{i=1}^{N}\sum_{j=1}^{M} \log[P(y_{i,j} \mid x_{i,j},\theta_{y_{j,j}})P(x_{i,j} \mid Pa_{x_{i,j}},\theta_{x_{j,j}})] \mid y_{i,j},\theta^k_{y_{j,j}},\theta^k_{x_{j,j}}\right] \tag{2.30}$$

$$Q(\Theta \mid \Theta^k) = \int\int \sum_{i=1}^{N}\sum_{j=1}^{M} \log[P(y_{i,j} \mid x_{i,j},\theta_{y_{j,j}})P(x_{i,j} \mid Pa_{x_{i,j}},\theta_{x_{j,j}})] \; P(Pa_{x_{i,j}} \mid y_{i,j},\theta^k_{y_{j,j}})P(x_{i,j} \mid Pa_{x_{i,j}},\theta^k_{x_{j,j}})dx_{i,j}dPa_{x_{i,j}} \tag{2.31}$$

In the Q function (Eq. 2.31), it can be observed that conditional distribution of the state conditioned over the measurements, is inferred as the posterior distribution w.r.t the parameter from the k^{th} iteration. Now, the posterior distribution in Eq. 2.31 is sampled from an empirical distribution in order to compute the Q function in the expectation step. The empirical sampling distribution (proposal distribution) ($g(\cdot)$) is defined as Gaussian distribution based on the parameter from k^{th} iteration, which is represented as follows [34].

$$P(Pa_{x_{i,j}} \mid y_{i,j}, \theta^k_{y_{j,j}}) P(x_{i,j} \mid Pa_{x_{i,j}}, \theta^k_{x_{j,j}}) = P(x_{i,j}, Pa_{x_{i,j}} \mid y_{i,j}, \Theta^k) \tag{2.32}$$
$$\approx \frac{1}{N_{sample}} \sum_{l=1}^{N_{sample}} g\Big((x_{i,j})_l, (Pa_{x_{i,j}})_l \mid y_{i,j}, \Theta^k\Big)$$

Here, N_{sample} represents the number of samples generated during Monte Carlo simulation and $(x_{i,j})_l$ is the value of the samples obtained using Gibbs sampler [36] w.r.t the state and parameter from the empirical distribution for the i^{th} sample of the j^{th} process variable. Now substituting Eq. 2.32 in Eq. 2.31, Q function takes the following form

$$Q(\Theta \mid \Theta^k) =$$

$$\int\int \sum_{i=1}^{N} \frac{1}{N_{sample}} \sum_{l=1}^{N_{sample}} \left(\sum_{j=1}^{M} \log[P(y_{i,j} \mid x_{i,j}, \theta_{y_{j,j}}) P(x_{i,j} \mid Pa_{x_{i,j}}, \theta_{x_{j,j}})] \right) \tag{2.33}$$
$$g((x_{i,j})_l, (Pa_{x_{i,j}})_l \mid y_{i,j}, \Theta^k) dx_{i,j} dPa_{x_{i,j}}$$

In Eq. 2.33, empirical distribution can be approximated as a Dirac delta function [34] and using the convolution property of the function, Eq. 2.33 can be simplified further as follows

$$Q(\Theta \mid \Theta^k) = \sum_{i=1}^{N} \frac{1}{N_{sample}} \sum_{l=1}^{N_{sample}} \left(\sum_{j=1}^{M} \log[P(y_{i,j} \mid x_{i,j}, \theta_{y_{j,j}}) P(x_{i,j} \mid Pa_{x_{i,j}}, \theta_{x_{j,j}})] \right)_l \tag{2.34}$$

where, $x_{i,j}$ is sampled from the proposal distribution $g(\cdot)$. Eq. 2.34 can be interpreted as, for every i^{th} sample out of N available process measurements, Monte Carlo simulations were carried out with N_{sample} of $x_{i,j}$ generated from the empirical distribution $g(\cdot)$. Theoretically, by sum of large numbers, Q function is expected to converge to the expected value [34]. Further, to reduce the variance in the computed expected value and to reduce the computational cost in re-sampling at every iteration, samples are drawn from the initial distribution and weights are provided for the expected

value. These weights are computed using the following equation [34].

$$w_l = \frac{g(x_l, Pa_{x_l} \mid y, \Theta^k)}{g(x_l, Pa_{x_l} \mid y, \Theta^0)} \tag{2.35}$$

where, $g(x_l, Pa_{x_l} \mid y, \Theta^k)$ is the distribution w.r.t parameter Θ^k used for obtaining new weights at the k^{th} iteration and $g(x_l, Pa_{x_l} \mid y, \Theta^0)$ is the proposal distribution provided at the initial iteration from which states are sampled. Hence, the Q function given in Eq. 2.34, with incorporation of weights given in Eq. 2.35, modifies as follows.

$$Q(\Theta \mid \Theta^k) = \sum_{i=1}^{N} \frac{1}{N_{sample}} \sum_{l=1}^{N_{sample}} w_l \left(\sum_{j=1}^{M} \log[P(y_{i,j} \mid x_{i,j}, \theta_{y_{j,j}}) P(x_{i,j} \mid Pa_{x_{i,j}}, \theta_{x_{j,j}})] \right)_l \tag{2.36}$$

Therefore, on evaluating the Q function (Eq. 2.36) over fixed parameter, estimate of the state ($\hat{X}$) can be obtained by averaging the samples from the empirical distribution. At the first iteration, i.e. $k = 0$, all the samples are provided with unit weight or weights of equal importance. As the iterations proceed, weights on the states sampled from $g(x_l, Pa_{x_l} \mid y, \Theta^0)$ begin to vary, eventually correcting the states and making the Q function converge to the expected value. Accuracy in the estimate can be achieved over certain iterations of the parameter. The algorithm for parameter update at each iteration is discussed in the maximization step (M –Step).

Maximization Step (M-Step)

With the given Q function in Eq. 2.31, objective in the M- Step is to maximize the Q function w.r.t parameters (Θ) as follows.

$$\Theta^{k+1} = arg \max_{\Theta} Q(\Theta \mid \Theta^k) \tag{2.37}$$

On computing the derivative of Q function (Eq. 2.31) w.r.t individual parameters (θ_y^{-1} & θ_x^{-1}) and equating them to zero, closed form expression is obtained for the vector of parameters to be updated in the E – Step. Steps for obtaining the closed form expression to update the parameters are explained below:

The Q function in Eq. 2.31 can be represented in the vector form (Eq. 2.38), in which $y_j \in \mathbb{R}^{N \times 1}$ denotes the measurement vector, $\hat{x}_j \in \mathbb{R}^{N \times 1}$ and $Pa_{\hat{x}_j} \in \mathbb{R}^{N \times 1}$ denote the estimated vectors of the j^{th} state variable obtained at the k^{th} iteration of the

Particle-EM algorithm in the E-Step through Particle simulation.

$$Q(\Theta \mid \Theta^k) = \sum_{j=1}^{M} \big(\log(P(y_j \mid \hat{x}_j, \theta_{y_{j,j}})) + \log(P(\hat{x}_j \mid Pa_{\hat{x}_j}, \theta_{x_{j,j}}))\big) \tag{2.38}$$

$$P(Pa_{\hat{x}_j} \mid y_j, \theta^k_{y_{j,j}}) P(\hat{x}_j \mid Pa_{\hat{x}_j}, \theta^k_{x_{j,j}})$$

$$Q(\Theta \mid \Theta^k) = \sum_{j=1}^{M} \big(\log(P(y_j \mid \hat{x}_j, \theta_{y_{j,j}})) P(Pa_{\hat{x}_j} \mid y_j, \theta^k_{y_{j,j}}) P(\hat{x}_j \mid Pa_{\hat{x}_j}, \theta^k_{x_{j,j}}) \tag{2.39}$$

$$+\log(P(\hat{x}_j \mid Pa_{\hat{x}_j}, \theta_{x_{j,j}})) P(Pa_{\hat{x}_j} \mid y_j, \theta^k_{y_{j,j}}) P(\hat{x}_j \mid Pa_{\hat{x}_j}, \theta^k_{x_{j,j}})\big)$$

On expanding the logarithmic terms in Eq. 2.39 using conditional Gaussian distribution, Q function can be obtained in the following form.

$$Q(\Theta \mid \Theta^k) = \sum_{j=1}^{M} \Bigg[\frac{1}{2}(\log(\theta^{-1}_{y_{j,j}})) P(Pa_{\hat{x}_j} \mid y_j, \theta^k_{y_{j,j}}) P(\hat{x}_j \mid Pa_{\hat{x}_j}, \theta^k_{x_{j,j}}) - \tag{2.40}$$

$$\frac{1}{2}((y_j - \hat{x}_j)^T (\theta^{-1}_{y_{j,j}})(y_j - \hat{x}_j)) P(Pa_{\hat{x}_j} \mid y_j, \theta^k_{y_{j,j}}) P(\hat{x}_j \mid Pa_{\hat{x}_j}, \theta^k_{x_{j,j}}) \Bigg]$$

$$+ \sum_{j=1}^{M} \Bigg[\frac{1}{2}(\log(\theta^{-1}_{x_{j,j}})) P(Pa_{\hat{x}_j} \mid y_j, \theta^k_{y_{j,j}}) P(\hat{x}_j \mid Pa_{\hat{x}_j}, \theta^k_{x_{j,j}}) -$$

$$\frac{1}{2}((\hat{x}_j - Pa_{\hat{x}_j})^T (\theta^{-1}_{x_{j,j}})(\hat{x}_j - Pa_{\hat{x}_j})) P(Pa_{\hat{x}_j} \mid y_j, \theta^k_{y_{j,j}}) P(\hat{x}_j \mid Pa_{\hat{x}_j}, \theta^k_{x_{j,j}}) \Bigg]$$

By taking derivative of Eq. 2.40 w.r.t (θ_y^{-1}&θ_x^{-1}) and equating it to zero, expressions in Eq. 2.43 and Eq. 2.44 are obtained, after necessary algebraic manipulations, for updating the parameters in the E-Step.

$$\frac{\partial Q(\Theta \mid \Theta^k)}{\partial \theta_y^{-1}} = \sum_{j=1}^{M} \Bigg[-\frac{1}{2}(\theta^{-1}_{y_{j,j}}) P(Pa_{\hat{x}_j} \mid y_j, \theta^k_{y_{j,j}}) P(\hat{x}_j \mid Pa_{\hat{x}_j}, \theta^k_{x_{j,j}}) + \tag{2.41}$$

$$\frac{1}{2}((y_j - \hat{x}_j)^T (\theta^{-2}_{y_{j,j}})(y_j - \hat{x}_j)) P(Pa_{\hat{x}_j} \mid y_j, \theta^k_{y_{j,j}}) P(\hat{x}_j \mid Pa_{\hat{x}_j}, \theta^k_{x_{j,j}}) \Bigg] = 0$$

$$\frac{\partial Q(\Theta \mid \Theta^k)}{\partial \theta_x^{-1}} = \sum_{j=1}^{M} \Bigg[-\frac{1}{2}(\theta^{-1}_{x_{j,j}}) P(Pa_{\hat{x}_j} \mid y_j, \theta^k_{y_{j,j}}) P(\hat{x}_j \mid Pa_{\hat{x}_j}, \theta^k_{x_{j,j}}) + \tag{2.42}$$

$$\frac{1}{2}((\hat{x}_j - Pa_{\hat{x}_j})^T (\theta^{-2}_{x_{j,j}})(\hat{x}_j - Pa_{\hat{x}_j})) P(Pa_{\hat{x}_j} \mid y_j, \theta^k_{y_{j,j}}) P(\hat{x}_j \mid Pa_{\hat{x}_j}, \theta^k_{x_{j,j}}) \Bigg] = 0$$

$$\theta_y^{k+1} = \frac{\sum_{i=1}^{M} P(Pa_{\hat{x}_j} \mid y_j, \theta_{y_{j,j}}^k)(\hat{x}_j - y_j)(\hat{x}_j - y_j)^T}{\sum_{j=1}^{M} P(Pa_{\hat{x}_j} \mid y_j, \theta_{y_{j,j}}^k)} \tag{2.43}$$

$$\theta_x^{k+1} = \frac{\sum_{i=1}^{M} P(\hat{x}_j \mid Pa_{\hat{x}_j}, \theta_{x_{j,j}}^k)(\hat{x}_j - Pa_{\hat{x}_j})(\hat{x}_j - Pa_{\hat{x}_j})^T}{\sum_{j=1}^{M} P(\hat{x}_j \mid Pa_{\hat{x}_j}, \theta_{x_{j,j}}^k)} \tag{2.44}$$

In the expressions obtained, only dependent parameters are retained and the independent parameters do not appear. Aforementioned derivation steps (E-Step and M-Step) can be summarized into a sequence of computation steps as presented in Algorithm 1.

Algorithm 1 Particle-EM Algorithm for Bayesian Network based Data Reconciliation

1: At iteration count, $k = 0$, define initial guess for the parameter of Θ^0, an empirical distribution and number of samples (N_{sample}) to be generated during Monte Carlo simulation.

2: Initialize the EM algorithm with samples from initial parameter guess value at iteration count, $k = 0$.

3: **E-Step:** Compute Q function given by Eq. 2.36 to obtain the estimate of state ($\hat{X}$).

4: **M-Step:** Maximize Q function to estimate unknown parameters Θ using Eq. 2.43 and Eq. 2.44.

5: Update the parameter $\Theta^k = \Theta^{k+1}$ until $\mid \Theta^k - \Theta^{k+1} \mid \leq \epsilon$
where, ϵ is the error threshold. Repeat Step. 3 and Step. 4 with updated parameters from Step. 5 until error is under the fixed threshold.

2.6 Case Studies

Four case studies covering three systems listed below are taken to test the performance of the Bayesian network based data reconciliation schemes (BN-MLE, BN-MAP and Particle-EM) proposed in this work and compared them with the results obtained using conventional MLE (Conv-MLE) and conventional MAP (Conv-MAP) methods.

- Simple flow network problem [9] widely considered as illustrative example in data reconciliation literature.
- Process without recycle streams: Mineral processing unit [24]
- Process with recycle streams: Mineral Beneficiation Process [25].
- Process with partial measurements: Mineral processing unit [24].

For the purpose of simulation, uncertainties in the state and measurements are deliberately introduced in the form of zero mean Gaussian noise with known covariance (Σ_x & Σ_y). The conventional MLE and MAP schemes make an attempt to estimate the reconciled states without taking these uncertainties in the state into consideration and thus assuming the steady state model to be an exact representation of the process. The BN-MLE and BN-MAP schemes estimate the reconciled values of the states using the Bayesian network model of the process with the assumption that the uncertainties in the state and measurements are known. These known uncertainties are taken as the state and measurement noise covariance (Σ_x & Σ_y) introduced in the simulation. Particle-EM algorithm is implemented with the assumption that the state and measurement noise statistics (Σ_x & Σ_y) are not known, which is a more realistic representation of any practical scenario. Particle-EM algorithm estimates the values of both the reconciled states and the unknown noise statistics simultaneously. The Particle-EM algorithm is validated by comparing the estimated noise statistics ($\hat{\Sigma}_x$ & $\hat{\Sigma}_y$) with the known noise statistics (Σ_x & Σ_y) used in the simulation. In all the case studies, 1000 particles are generated for Monte Carlo simulation used in the implementation of Particle-EM algorithm.

Assuming the knowledge of state and measurement uncertainties to be available for the implementation of BN-MLE and BN-MAP schemes is hypothetical, as such an assumption is not valid in any practical situation. However, the simulation results generated using BN-MLE and BN-MAP schemes can serve as a reference for comparing the performance of other schemes proposed in this work. It is for this reason, the simulation studies using BN-MLE and BN-MAP schemes are carried out and reported in this work. Further, it is to be noted that prior information about the individual source nodes is assumed to be available and incorporated in the implementation of BN-MAP scheme. This is just to demonstrate that the BN-MAP with incorporation of prior information will result in the best possible reconciled estimates compared to the other schemes.

In order to make the simulations independent of any particular realization, 10 (N_r) independent simulations are carried out for each case, using N measurement samples for each simulation run. Average Root Mean Square Error ($ARMSE$) is used as an index to assess the performance of data reconciliation schemes.

$$ARMSE = \left(\frac{1}{N_r} \sum_{k=1}^{N_r} \left(\sqrt{\frac{\sum_{i=1}^{N} (x_{i,j} - \hat{x}_{i,j})^2}{N}} \right)_k \right) \tag{2.45}$$

2.6.1 Simple Flow Network - Illustrative Case Study

A simple flow network [9], described in section 4, is taken as an illustrative example to demonstrate the performance of the proposed data reconciliation schemes. Process network model with 4 process units and 6 process variables is shown in Figure 2.6 and the corresponding Bayesian Network model in Figure 2.7. Steady state measurement data of 1000 samples is generated using the process model. Covariance corresponding to uncertainty in measurement Σ_y and state Σ_x is taken as.

$$\Sigma_y = diag \begin{bmatrix} 0.6 & 0.65 & 0.50 & 0.45 & 0.55 & 0.50 \end{bmatrix}$$

$$\Sigma_x = diag \begin{bmatrix} 0.05 & 0.02 & 0.025 & 0.03 & 0.025 & 0.03 \end{bmatrix}$$

Results corresponding to the estimates of only 4 significant variables X_1, X_2, X_5 and X_6 are presented in Table 3.1 for the sake of brevity. Compared to the conventional MLE and MAP (Conv-MLE and Conv-MAP) approaches for data reconciliation, the corresponding Bayesian network based schemes (BN-MLE and BN-MAP) proposed in this work for known uncertainties in state and measurements obtain state estimate values that are much closer to the true states. Between BN-MLE and BN-MAP, performance of BN-MAP is relatively better due to the incorporation of prior information. The results obtained from the implementation of Conv-MLE, Conv-MAP, BN-MLE and BN-MAP schemes in the simple flow network case show that accounting for state uncertainties (BN-MLE and BN-MAP) will always result in a better estimate of state compared to the case (Conv-MLE and Conv-MAP) in which the state uncertainties are not accounted for. These results clearly demonstrate the advantage of formulating the data reconciliation problem in the Bayesian network framework for systems with state uncertainties.

Table 2.1: Simple Flow Network – ARMSE for known (*) & unknown uncertainty (**)

State Variables	ARMSE				
	Conv-MLE	Conv-MAP	BN-MLE*	BN-MAP*	Particle-EM**
X_1	1.099	0.9723	0.5060	0.4745	0.5447
X_2	0.710	0.6918	0.5004	0.4896	0.5156
X_5	0.749	0.7298	0.4820	0.4547	0.4953
X_6	1.092	0.9270	0.4495	0.4340	0.4891

In the more realistic scenario of unknown uncertainties in state and measurements, the ability of Particle-EM algorithm to accurately capture the unknown noise statistics is evident from the results presented in Table 2.2 In this case, it is observed that the estimates of state and measurement covariance ($\hat{\Sigma}_x$ & $\hat{\Sigma}_y$) are much closer to the true values (Σ_x & Σ_y). As a result of the accuracy in estimation of noise statistics achieved by Particle-EM algorithm, it is observed from the results presented in Table 2.1 that the estimated values of the reconciled states obtained by Particle-EM are closer to ones estimated by BN-MLE scheme. These results prove the capability of the proposed Particle-EM algorithm in estimating the values of reconciled states in the absence of any knowledge about the state and measurement noise as accurately as the state estimate values obtained by the BN-MLE algorithm using complete knowledge of these noise statistics. From the histogram of estimate residues shown in Figure 2.11, it is observed that the residues of state estimates obtained using Bayesian network based data reconciliation schemes (BN-MLE,BN-MAP and Particle-EM) are closer to zero mean compared to the state estimate residues obtained using conventional (Conv-MLE and Conv-MAP) methods.

Table 2.2: Simple Flow Network - True and estimated noise covariance of States $(\Sigma_x, \hat{\Sigma}_x)$ & Measurements $(\Sigma_y, \hat{\Sigma}_y)$

State Variables	True		Estimate	
	Σ_x	Σ_y	$\hat{\Sigma}_x$	$\hat{\Sigma}_y$
X_1	0.05	0.6	0.0421	0.535
X_2	0.02	0.65	0.0171	0.592
X_3	0.025	0.5	0.0271	0.513
X_4	0.03	0.45	0.0244	0.412
X_5	0.025	0.55	0.0231	0.542
X_6	0.03	0.5	0.0289	0.503

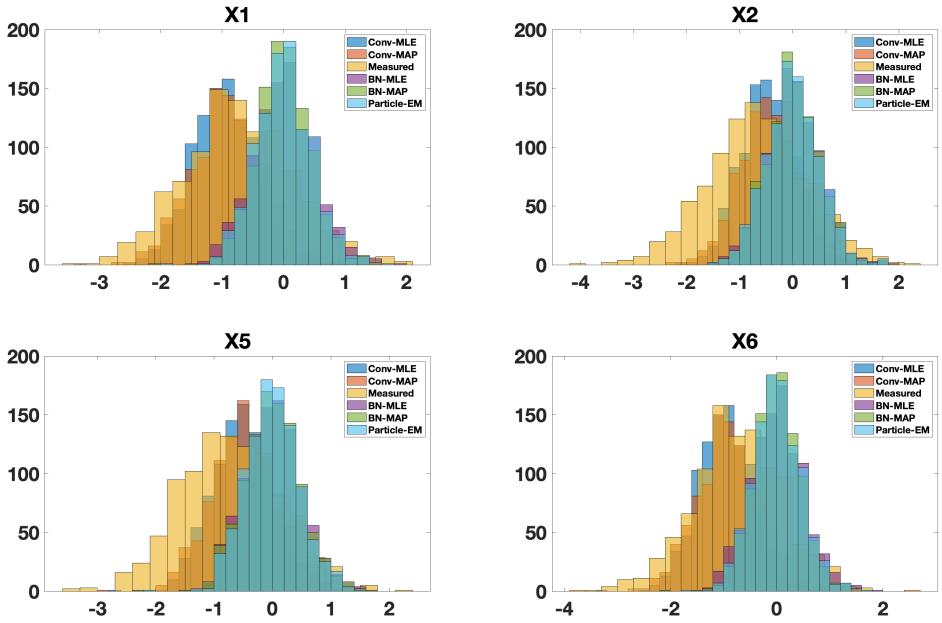

Figure 2.11: Error Histogram of Data reconciliation Algorithms for Simple Flow Network

2.6.2 Mineral Processing Unit - Process without Recycle Stream

Implementation of the proposed data reconciliation schemes on the Brunswick Mineral Processing unit [24] is discussed in this section. Figure 2.12 shows a simplified

representation of a larger mineral processing unit, with 8 process units and 15 process variables. Measurements of all the 15 process variables are assumed to be available. Steady state linear mass balance equations representing the process model and the corresponding probabilistic interpretations are given in Eq. 2.46. Process Bayesian Network developed from the steady state process model is shown in Figure 2.13.

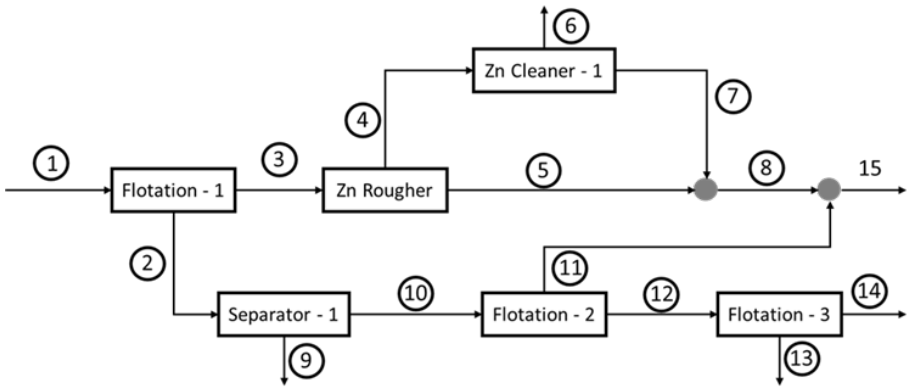

Figure 2.12: Mineral Processing Unit Flow sheet

Process Unit	Mass Balance	Probabilistic Model
Flotation - 1	$X_1 = X_2 + X_3$	$P(X_3 \mid X_2, X_1)$
Zn Rougher	$X_3 = X_4 + X_5$	$P(X_5 \mid X_3, X_4)$
Cu Separator	$X_2 = X_9 + X_{10}$	$P(X_9 \mid X_2, X_{10})$
Zn Cleaner	$X_4 = X_6 + X_7$	$P(X_6 \mid X_4, X_7)$
Mixer – 1	$X_5 + X_7 = X_8$	$P(X_8 \mid X_5, X_7)$
Pyrite Flotation	$X_{10} = X_{11} + X_{12}$	$P(X_{12} \mid X_{10}, X_{11})$
Pb –Zn Flotation	$X_{14} = X_{12} + X_{13}$	$P(X_{14} \mid X_{12}, X_{13})$
Mixer - 2	$X_{15} = X_8 + X_{11}$	$P(X_{15} \mid X_8, X_{11})$

(2.46)

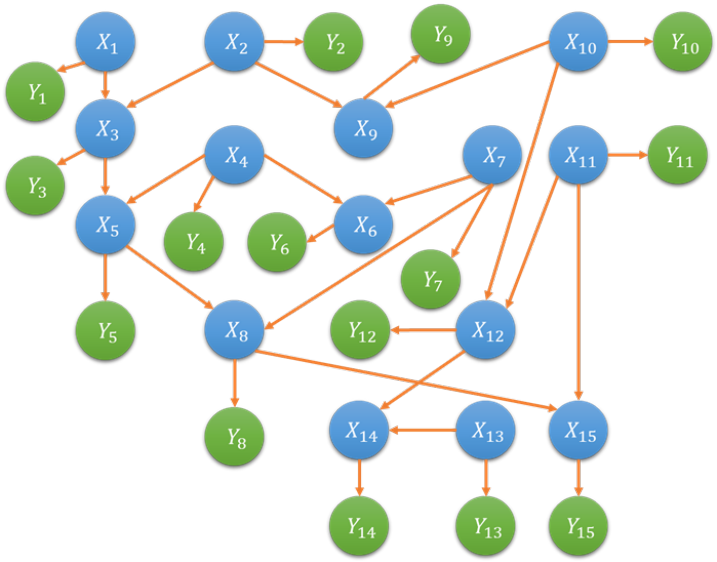

Figure 2.13: Bayesian Network of Mineral Processing Unit

Given the process Bayesian Network and the measurements of process variables, data reconciliation is performed using various methods proposed in this work. Steady state measurements of 1500 samples are generated using the process model. Covariance of measurement uncertainties reported for this process in the literature (Sadeghi et al. (2018)) is used here:

$$\Sigma_y = diag \begin{bmatrix} 0.325 & 0.425 & 0.305 & 0.315 & 0.340 & 0.225 & 0.42 & .. \\ 0.335 & 0.52 & 0.42 & 0.25 & 0.324 & 0.52 & 0.42 & 0.415 \end{bmatrix}$$

Covariance of state uncertainties is taken as

$$\Sigma_x = diag \begin{bmatrix} 0.015 & 0.015 & 0.015 & 0.015 & 0.02 & 0.025 & 0.075 & .. \\ 0.062 & 0.0115 & 0.015 & 0.065 & 0.0175 & 0.0215 & 0.0135 & 0.0142 \end{bmatrix}$$

Results of only 4 significant state variables X_1, X_4, X_{13} and X_{15} are presented here. Simulation results presented in Table 3.3 show that the BN-MLE and BN-MAP schemes make an estimate of state variable values closer to the true values compared to the values estimated using conventional MLE and MAP methods. Further, as a result of incorporation of prior information, BN-MAP scheme is observed to perform better than BN-MLE. Due to the availability of information on state and measurement uncertainties, BN-MLE and BN-MAP schemes perform better than the conventional MLE and MAP methods which do not take these state uncertainties into account.

Table 2.3: Mineral Processing Unit – ARMSE for known (*) & unknown(**) uncertainty

State variables	ARMSE				
	Conv-MLE	Conv-MAP	BN-MLE*	BN-MAP*	Particle-EM**
X1	1.9271	0.9460	0.5824	0.5698	0.5992
X4	2.7688	2.2870	0.5355	0.5264	0.5403
X13	0.6844	0.6926	0.6365	0.6275	0.6596
X15	8.8378	9.3345	0.5972	0.5781	0.7043

With no knowledge about the state and measurement uncertainties being available, results presented in Table 2.4 show that the Particle-EM algorithm can make accurate estimate of these uncertainties by estimating the state and measurement covariance ($\hat{\Sigma}_x$ & $\hat{\Sigma}_y$) values closer to the true values (Σ_x & Σ_y). As a result of this, the reconciled values of state estimates obtained using Particle-EM algorithm are closer to the ones estimated using BN-MLE as reported in Table 2.3. Thus, performance of Particle-EM achieved with no knowledge of state and measurement uncertainties is closer to the performance of BN-MLE achieved with complete knowledge of state and measurement noise. Histogram of estimate residues shown in Figure 2.14 reveals that the state estimate residues obtained using BN-MLE, BN-MAP and Particle-EM algorithms compared to the ones calculated using conventional methods are closer to zero mean.

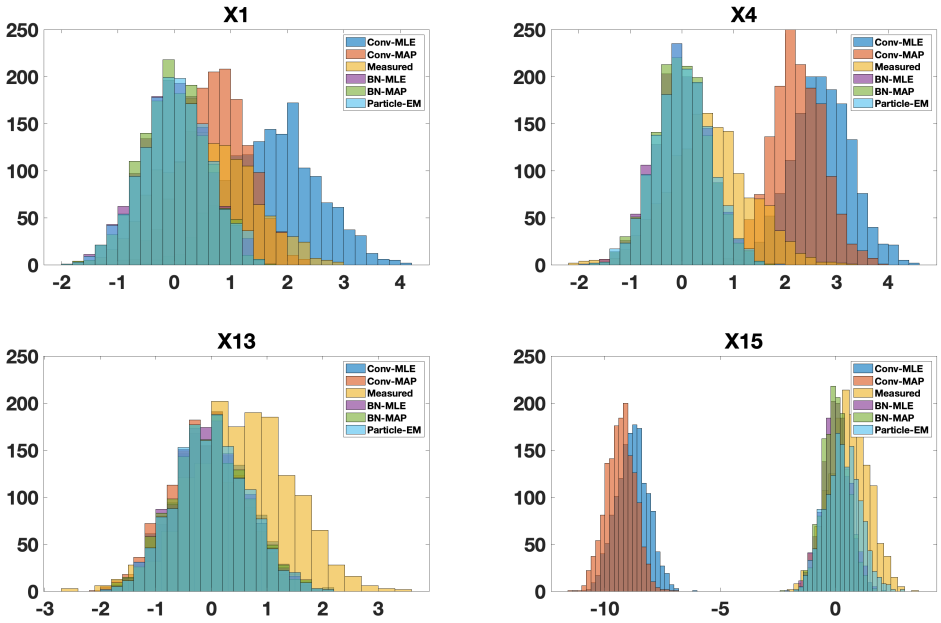

Figure 2.14: Error Histogram of Data reconciliation algorithms for Mineral Processing Unit

Table 2.4: Mineral Processing Unit - True and estimated noise covariance of States $(\Sigma_x, \hat{\Sigma}_x)$ & Measurements $(\Sigma_y, \hat{\Sigma}_y)$

State Variables	True		Estimate		State Variables	True		Estimate	
	$\Sigma_x \times 10^{-2}$	Σ_y	$\hat{\Sigma}_x \times 10^{-2}$	$\hat{\Sigma}_y$		$\Sigma_x \times 10^{-2}$	Σ_y	$\hat{\Sigma}_x \times 10^{-2}$	$\hat{\Sigma}_y$
X_1	1.5	0.325	1.38	0.3461	X_8	6.2	0.335	5.21	0.321
X_2	1.5	0.425	1.47	0.428	X_9	1.15	0.52	1.18	0.517
X_3	1.5	0.305	1.50	0.325	X_{10}	1.5	0.42	1.37	0.468
X_4	1.5	0.315	1.2	0.312	X_{11}	6.5	0.25	5.9	0.285
X_5	2	0.34	2.18	0.329	X_{12}	1.75	0.324	1.72	0.317
X_6	2.5	0.225	2.39	0.215	X_{13}	2.15	0.52	2.30	0.546
X_7	7.5	0.42	7.2	0.436	X_{14}	1.35	0.42	1.37	0.437
					X_{15}	1.42	0.415	1.20	0.371

2.6.3 Mineral Beneficiation Process - Process with Recycle Stream

Mineral Beneficiation Process [25] with recycle streams is taken as a case study to illustrate the application of Bayesian Network based data reconciliation schemes proposed in this work for process networks with recycle. Row echelon reduction method proposed in Section. 3.1 for process networks with recycle streams is used to construct Bayesian Network model with acyclic structure. Mineral beneficiation process shown in Figure 2.15, with 7 process units and 12 process variables, is a simplified representation of a larger process unit. It is assumed that measurements of all the 12 variables are available.

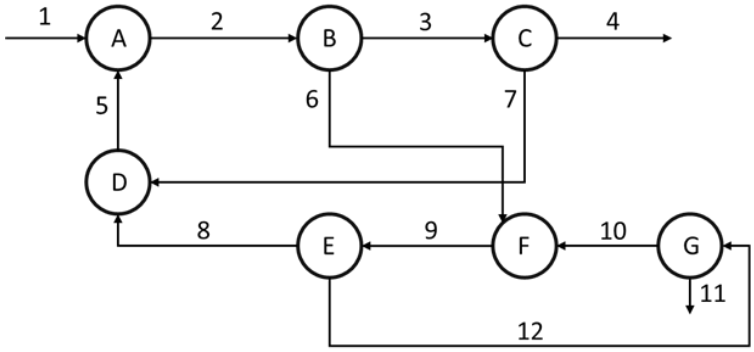

Figure 2.15: Mineral Beneficiation Process Flow sheet

Applying row echelon reduction (Eq. 2.15) to the mass balance model of the process given in Eq. 2.47 and writing the dependent variables $X_1, X_2, X_3, X_5, X_6, X_8, X_{10}$ as a linear combination of independent variables $X_4, X_7, X_9, X_{11}, X_{12}$, reduced model equations are obtained for the process. Reduced process model and the corresponding probabilistic interpretations are listed in Eq. 2.47.

Process Unit	Mass Balance	Reduced Model	Probabilistic Model
A	$X_1 + X_5 = X_2$	$X_1 = X_4 + X_{11}$	$P(X_1 \mid X_4, X_{11})$
B	$X_2 = X_3 + X_6$	$X_2 = X_4 + X_7 + X_9 + X_{11} - X_{12}$	$P(X_2 \mid X_4, X_7, X_9, X_{11}, X_{12})$
C	$X_3 = X_4 + X_7$	$X_3 = X_4 + X_7$	$P(X_3 \mid X_4, X_7)$
D	$X_7 + X_8 = X_5$	$X_5 = X_7 + X_9 - X_{12}$	$P(X_5 \mid X_7, X_9, X_{12})$
E	$X_9 = X_{12} + X_8$	$X_6 = X_9 + X_{11} - X_{12}$	$P(X_6 \mid X_9, X_{11}, X_{12})$
F	$X_{10} + X_6 = X_9$	$X_8 = X_9 - X_{12}$	$P(X_8 \mid X_9, X_{12})$
G	$X_{12} = X_{10} + X_{11}$	$X_{10} = X_{12} - X_{11}$	$P(X_{10} \mid X_{11}, X_{12})$

(2.47)

Bayesian Network with acyclic structure is constructed from the reduced steady state model of the process (Figure 2.16).

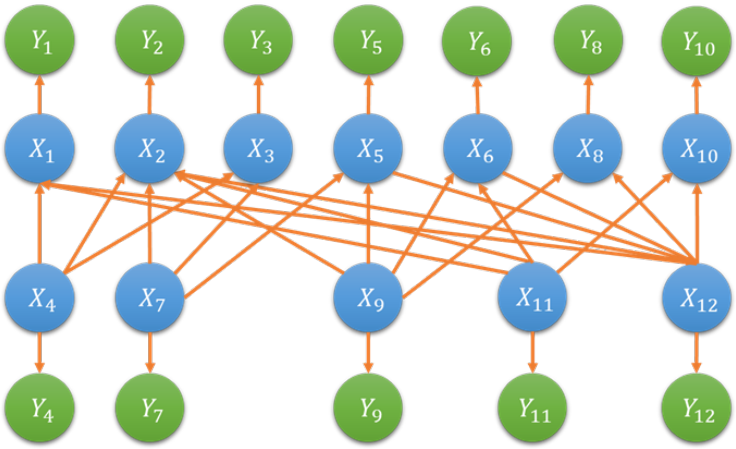

Figure 2.16: Bayesian Network of the Mineral Beneficiation process

Steady state data of 1000 measurement samples are generated. Covariance of measurement and state uncertainties are taken as:

$$\Sigma_y = diag \begin{bmatrix} 0.35 & 0.42 & 0.28 & 0.325 & 0.175 & 0.155 & ... \\ 0.215 & 0.3 & 0.245 & 0.45 & 0.24 & 0.312 & \end{bmatrix}$$

$$\Sigma_x = diag \begin{bmatrix} 0.025 & 0.021 & 0.032 & 0.027 & 0.022 & 0.024 & ... \\ 0.032 & 0.025 & 0.0172 & 0.0165 & 0.0235 & 0.0205 & \end{bmatrix}$$

These state uncertainties are incorporated into the reduced process network obtained after row echelon transformation of the original process network. Taking the Bayesian network model (Figure 2.16) obtained after row echelon transformation of the original process network and assuming the state and measurement noise statistics to be not known, the Particle-EM algorithm is used to make an estimate of the reconciled values of the states along with the uncertainties in state and measurement. These results are compared with the reconciled state estimate values obtained using conventional MLE and MAP methods. Results corresponding to 4 significant state variables X_1, X_4, X_{11}, X_{12} out of 12 state variables are presented here.

Table 2.5: Mineral Beneficiation Process – ARMSE

State Variables	ARMSE		
	Conv-MLE	Conv-MAP	Particle-EM
X1	0.8123	0.7963	0.6053
X4	0.5241	0.5149	0.5136
X11	0.6134	0.6127	0.5209
X12	0.8118	0.8036	0.6421

These results presented in Table 2.5 show that the Particle-EM yields state estimate values that are closer to the true values compared to the ones estimated by conventional MLE and MAP methods. This is due to the fact that the Particle-EM is able to make a good estimate of unknown noise statistics as reported in Table 2.6, where the estimated covariance of state and measurement noise ($\hat{\Sigma}_x$ & $\hat{\Sigma}_y$) are found to be closer to the true covariance values (Σ_x & Σ_y). From the histogram of estimate residues shown in Figure 2.17, it is observed that the Particle-EM yields state estimate residues that are closer to the zero mean compared to the residues obtained using conventional methods.

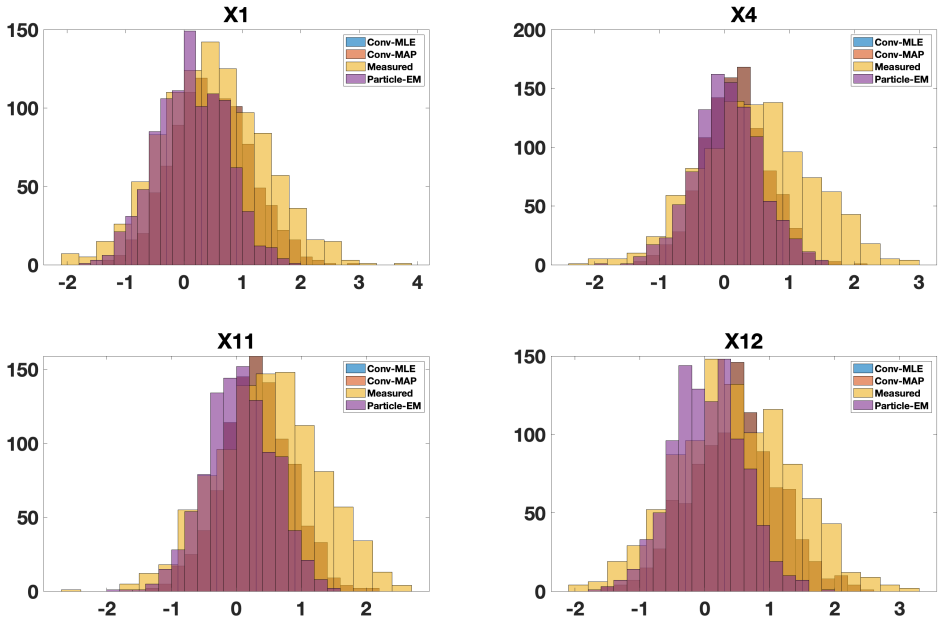

Figure 2.17: Error Histogram of Data reconciliation algorithms for Mineral Beneficiation process

Table 2.6: Mineral Beneficiation Process - True and estimated noise covariance of States ($\Sigma_x, \hat{\Sigma}_x$) & Measurements ($\Sigma_y, \hat{\Sigma}_y$)

State Variables	True		Estimate		State Variables	True		Estimate	
	Σ_x	Σ_y	$\hat{\Sigma}_x$	$\hat{\Sigma}_y$		Σ_x	Σ_y	$\hat{\Sigma}_x$	$\hat{\Sigma}_y$
X_1	0.025	0.35	0.0215	0.329	X_7	0.032	0.215	0.03	0.1635
X_2	0.021	0.42	0.023	0.396	X_8	0.025	0.3	0.019	0.34
X_3	0.032	0.28	0.0316	0.298	X_9	0.017	0.245	0.023	0.1764
X_4	0.027	0.325	0.029	0.319	X_{10}	0.0165	0.45	0.0117	0.476
X_5	0.022	0.175	0.026	0.189	X_{11}	0.023	0.24	0.027	0.185
X_6	0.024	0.155	0.023	0.1502	X_{12}	0.02	0.312	0.020	0.317

This case study has clearly demonstrated that the proposed row echelon reduction method is very effective for constructing a Bayesian network model with acyclic structure given a process network with recycle streams. Further, for process networks with

recycle streams, it is illustrated that the Particle-EM algorithm is capable of making an accurate estimate of unknown noise statistics along with the reconciled values of the states.

2.6.4 Mineral Processing Unit - Process with Partial Measurements

Bayesian network based data reconciliation for partially measured systems is demonstrated using the method proposed in Section 3.2, by taking the mineral processing unit (Section 5.2) as the case study. It is assumed that 7 process variables $X_2, X_4, X_6, X_8, X_9, X_{12}, X_{13}$ are measured and the remaining 8 variables X_1, X_3, X_5, $X_7, X_{10}, X_{11}, X_{14}, X_{15}$ are unmeasured. Applying the method proposed in Section 6, the reduced model (Eq. 2.48) is obtained for the partially measured system. This reduced model is used to construct Bayesian network (Figure 2.18) and to perform data reconciliation.

Process Unit	Reduced Mass Balance Model	Probabilistic Model
Flotation - 1	$X_1 = X_2 + X_6 + X_8$	$P(X_1 \mid X_2, X_6, X_8)$
Zn Rougher	$X_3 = X_6 + X_8$	$P(X_3 \mid X_6, X_8)$
Cu Separator	$X_2 = X_9 + X_{10}$	$P(X_9 \mid X_2, X_{10})$
Zn Cleaner	$X_7 = X_4 - X_6$	$P(X_7 \mid X_4, X_6)$
Mixer – 1	$X_{10} = X_2 - X_9$	$P(X_{10} \mid X_2, X_9)$
Pyrite Flotation	$X_{11} = X_2 - X_9 - X_{12}$	$P(X_{11} \mid X_2, X_9, X_{12})$
Pb –Zn Flotation	$X_{14} = X_{12} - X_{13}$	$P(X_{14} \mid X_{12}, X_{13})$
Mixer - 2	$X_{15} = X_2 + X_8 - X_9 - X_{12}$	$P(X_{15} \mid X_2, X_8, X_9, X_{12})$

(2.48)

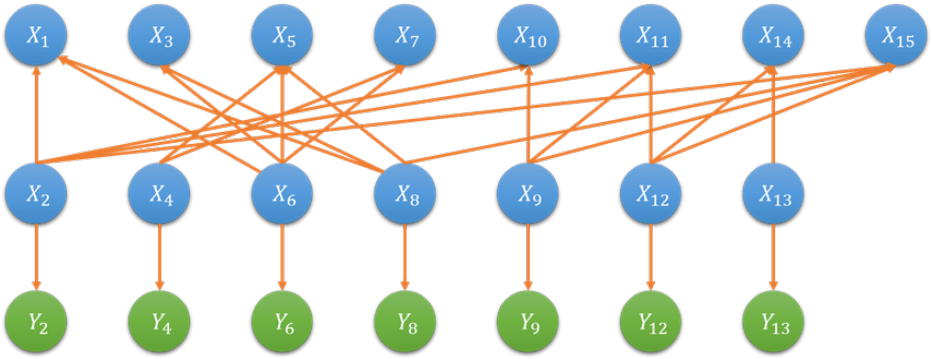

Figure 2.18: Bayesian Network of Partially measured system

Steady state data of 1500 measurement samples are generated for X_2, X_4, X_6, X_8, X_9, X_{12} &X_{13}. Covariance of uncertainties in measurements and states is taken respectively as:

$$\Sigma_y = diag\begin{bmatrix}0.425 & 0.315 & 0.225 & 0.335 & 0.52 & 0.324 & 0.52\end{bmatrix}$$

$$\Sigma_x = diag\begin{bmatrix}0.015 & 0.015 & 0.025 & 0.0625 & 0.0115 & 0.0175 & 0.0215\end{bmatrix}$$

Here, like in the case of process with recycle streams, state uncertainties are incorporated only after transforming the process network using row echelon approach. Simulation results showing the reconciled estimates of the measured and unmeasured state variables are presented in Table 2.7. Results of the state estimates obtained using conventional QR factorization method and the other Bayesian network based estimation methods (BN-MLE, BN-MAP and Particle-EM) are reported. The state estimates obtained using the conventional QR factorization method deviate by distinct margin from the true states compared to the state estimates obtained using the proposed Bayesian network schemes. The possible reason for this deviation is that the measured variable matrix A_M turns out to be not a full rank matrix. During the projection of A_M on to the column space of Q in QR factorization, if A_M is not of full rank, it may affect the estimates of the measured and reconstructed state variables. The ARMSE statistics reported in Table 2.7 validates this deviation in the estimates obtained using QR approach.

In the absence of any knowledge about the state and measurement (for the measured state variables) uncertainties, the results reported in Table 2.8 show that the Particle-EM is able to make an estimate of state and measurement noise covariance ($\hat{\Sigma}_x$ & $\hat{\Sigma}_y$) that are closer to the true values (Σ_x & Σ_y). As a result of this, reconciled state estimates obtained using Particle-EM are reported (Table 2.7) to be as good as

the state estimates obtained using BN-MLE that uses the known knowledge of noise statistics for state estimation.

Table 2.7: Partially Measured System – ARMSE for measured and unmeasured state variables

State Variables		ARMSE			
		QR Estimate	BN-MLE	BN-MAP	Particle-EM
Measured	X_4	0.9665	0.7439	0.7418	0.7688
	X_9	1.0723	0.8479	0.8423	0.8587
	X_{12}	0.9802	0.7735	0.7723	0.7921
	X_{13}	1.0535	0.8397	0.8368	0.8462
Unmeasured	X_7	142.59	0.9923	0.9923	1.0530
	X_{10}	26.952	1.1836	1.1836	1.1880
	X_{11}	14.553	1.5537	1.4230	1.4426
	X_{14}	14.297	1.1687	1.1687	1.2524

Table 2.8: Mineral Processing Unit (Partially Measured case) - True and estimated noise covariance of States ($\Sigma_x, \hat{\Sigma}_x$) & Measurements ($\Sigma_y, \hat{\Sigma}_y$)

State Variables (Measured)	True		Estimate	
	Σ_x	Σ_y	$\hat{\Sigma}_x$	$\hat{\Sigma}_y$
X_2	0.015	0.425	0.0151	0.428
X_4	0.015	0.315	0.0147	0.319
X_6	0.025	0.225	0.0253	0.218
X_8	0.0625	0.335	0.0620	0.322
X_9	0.0115	0.52	0.0119	0.514
X_{12}	0.0175	0.324	0.0179	0.320
X_{13}	0.0215	0.52	0.0226	0.515

The results presented here illustrate the capability of the proposed row echelon reduction method in accurately estimating the reconciled values of the states for systems with partial measurement in a Bayesian network framework.

2.7 Summary

Conventional data reconciliation techniques do not take uncertainties in state into consideration and as a result they may lead to inconsistent estimates of reconciled states. In this work, a novel framework for data reconciliation using Bayesian network has been proposed accounting for uncertainties in states. Depending upon the availability of information on state and measurement uncertainty, Bayesian network based reconciliation is formulated as MLE, MAP and Particle-EM statistical inference problems. In the course of development of the reconciliation framework using Bayesian network, a row echelon reduction method is proposed in this work in order to achieve an acyclic construction of the network for processes with recycle. This row echelon reduction approach is also extended to systems with partially measured data. Performance of the proposed Bayesian network-based data reconciliation schemes has been evaluated on three examples namely simple flow network, mineral processing unit and mineral beneficiation process.

Simulation studies were carried out to evaluate the performance of i) BN-MLE and BN-MAP schemes with the assumption that the state and measurement uncertainties are known and ii) Particle-EM scheme assuming that the state and measurement uncertainties are not known. Assuming the knowledge of state and measurement uncertainties to be available for the implementation of BN-MLE and BN-MAP schemes is a hypothetical case, which is used in this work to primarily generate simulation results that can serve as a benchmark for assessing the performance of other data reconciliation schemes proposed in this study. It is observed from the results that, in all the case studies, BN-MLE and BN-MAP schemes, due to the availability of knowledge on state and measurement uncertainties, make a far better estimate of reconciled states compared to the conventional MLE and MAP schemes that do not take these state uncertainties into account. These results validate the need for taking state uncertainties into consideration for achieving a better estimate of states. Between BN-MLE and BN-MAP, BN-MAP performs better due to incorporation of prior information. In a realistic scenario, where no knowledge about the state and measurement uncertainties are available, it is observed in all the cases that the Particle-EM algorithm is able to make an accurate estimate of unknown noise statistics and as a result, the state estimates calculated using Particle-EM are reported to be as good as the state estimates obtained using BN-MLE algorithm. Thus, in the absence of any knowledge about state and measurement uncertainties, the Particle-EM is able to achieve a performance that is closer to the performance achieved by BN-MLE

scheme using the complete available knowledge about state and measurement noise statistics. The results presented in this work have also demonstrated the ability of the proposed row echelon reduction method in dealing with process networks with recycle and processes with partial measurement of state variables.

This research work has clearly highlighted the advantage of formulating the data reconciliation problem in the Bayesian network framework for system with state uncertainties. Overall reason for the improvement in the estimates of the true states using the proposed schemes may be attributed to independent parameterization property [6] exhibited by Bayesian network, in which each of the nodes is parametrized separately based on conditional independence property. As a result of this property, each one of the variables is represented as nodes of the Bayesian network and is inferred effectively using statistical inference techniques through relevant nodes in the network.

Chapter 3

Prediction of Flooding & Weeping in Process Operation using Causality Analysis

3.1 Introduction

Flooding and Weeping are quite predominant in tall columns used for separation in process industries. Usually, flooding is observed in both packed bed and tray tower columns. However, weeping can happen only in tray tower columns. These two phenomena can be understood from design and operational perspective. From design perspective, $\left(\frac{V}{L}\right)$ ratio (vapor to liquid flow ratio) is considered to be an important parameter in the column design. Usually, columns are designed with high $\left(\frac{V}{L}\right)$ ratio, otherwise known as near flooding condition in order to achieve high separation efficiency. At the same time, low $\left(\frac{V}{L}\right)$ ratio leading to a weeping condition should be avoided, to reduce the energy consumption, equipment damage and also poor separation efficiency. Thus, the $\left(\frac{V}{L}\right)$ ratio is a crucial design parameter utilised in regular column operation to achieve high separation efficiency. Also, in the routine operation, $\left(\frac{V}{L}\right)$ ratio indicates the onset of abnormal conditions leading to flooding and weeping as indicated in Figure 3.1.

Apart from the $\left(\frac{V}{L}\right)$ ratio, during flooding condition, high pressure drop is set to occur on the tray that is located below the point of flooding and the trays that are above

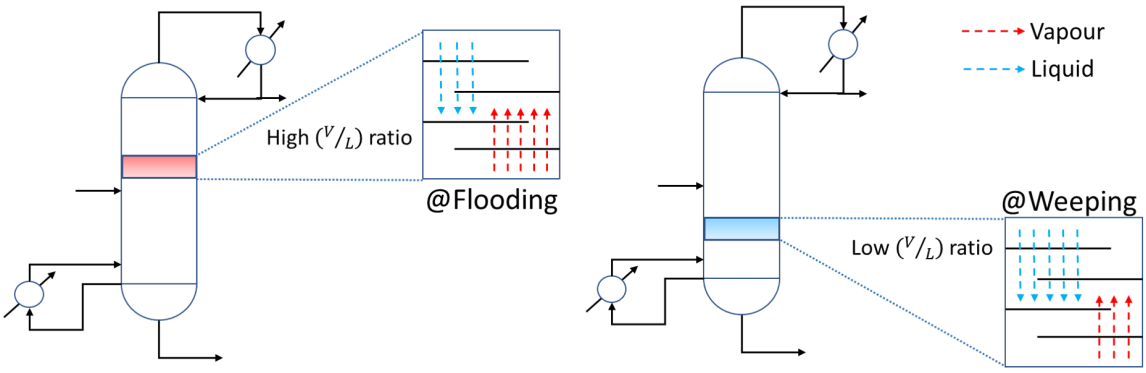

Figure 3.1: Schematic of Flooding & Weeping conditions based on $\frac{V}{L}$ ratio

this point are said to flood as well. Similarly during weeping, the temperature drops drastically at the bottom section of the column. These pressure and temperature variations in the column are considered to be the effects of the flooding and weeping phenomena and these are detected during the routine operation much after the onset of these events. Upon detection, necessary actions are taken by the operators to control the flooding and weeping events. Since these events are detected and controlled after their onset, product quality and energy consumption gets affected drastically and at times process is also driven to temporary shutdown. In some of the current industrial practices [37, 38], column pressure drop is monitored and timely control actions are taken to control the flooding. In the absence of pressure drop measurement and monitoring tools, reactive measures are taken by the operators after the onset of flooding events to mitigate its effect in overall process operation. In this work, in order to ensure a smooth operation, the problem of flooding and weeping is formulated using causality analysis, where underlying reasons for flooding and weeping are determined and effective measures are proposed for early prediction and possible prevention of these abnormal events.

Causality analysis helps in understanding the relationship among the process variables from the data. Causality analysis is vital in domains such as economics, biology and climate science etc [39]. In chemical engineering, especially in process systems engineering, applications of causality analysis in root cause analysis [40] and control loop oscillation detection [41] have been reported in the literature. In process systems, causality naturally exists due to complex physical inter-connections among process units and presence of control systems. Time series models and first principle models have been widely used for causality analysis. However, time series models are usually preferred over first principle models for its ease in use, especially when the processes are complex and have too many variables to model in the first principle framework.

Among the different time series models, vector auto-regressive (VAR) model, vector auto-regressive model with exogenous inputs (VARX) and vector auto-regressive moving average (VARMA) model [42, 43] are usually considered for analysing the causal relationship. The most common and very well-known method for causality analysis using time series data is Granger causality analysis [44]. A time series x_1 is expected to Granger cause time series x_2 if the past information of x_1 improves the prediction of x_2 compared to the prediction based only on the past information of x_2. The improvement in prediction is quantified by means of Granger score [42] and causal relationship among the variables is determined in pairwise manner using statistical hypothesis testing. However, the complexity involved in pairwise hypothesis testing increases with dimension of the data. It is important to understand that in the actual processes not all the variables are causally associated with one another, which makes the true causal relationship to be sparse. However, direct use of causal modelling techniques, at times, yields results that show all process variables to be causally related to one another, which leads to spurious outcomes. Therefore, to overcome this issue, sparsity constraint is enforced on the model parameter during the identification step [45, 46, 47], which makes the parameter vector sparse in representation, thereby reducing the spurious connections.

The idea of sparsity plays a vital role in the field of signal processing, image processing, Statistics and Mathematics etc [48, 49]. Given a high dimensional data, sparsity constraint can interpret the given data with high accuracy and minimum number of variables without the problem of over-fitting. Usually, sparsity is promoted on the parameters with the help of L_0 norm [50], L_1 norm [51] and combination of L_1 & L_2 norm [52]. To achieve most sparse solution, L_0 norm is preferred followed by L_1 norm and a combination of L_1 & L_2. However, L_0 is non-convex and NP-hard to solve. Therefore, the original problem is either relaxed to L_1 constrained convex optimization problem [53, 54] or solved using greedy methods [55]. In terms of application, sparsity constraint is introduced in problems like non-negative matrix factorization, regression, principle component analysis and network reconstruction etc [48].

In general, analysing causation is important in process industries to have an event free and a safe day to day operation. In this work, a two-step methodology involving one step to analyse the causation and another step to predict the abnormal events such as flooding and weeping is proposed. In the first step for analysing causation, finite impulse response (FIR) model is used to identify possible causal variables and then the cause-effect direction among the identified causal variables is verified using the

information about the flow direction embedded in the process flow-diagram. Reasons for using FIR model over output feedback models such as ARX and ARMAX models are (i) its capability for capturing complex dynamics with simple model structure, (ii) its open loop structure, which helps to reduce the effect of output feedback during the identification step and (iii) in the present problem of interest, since output process variable is known, FIR model structure helps in modelling the input/output relationship explicitly, thereby allowing us to determine the significant input process variables that affect the output. Inspite of the aforementioned advantages, non-parsimonious nature of the FIR model can be cited as its drawback. However, this issue is resolved with the help of L_0 norm and L_1 norm sparsity promoting constraint on the parameters that makes the model parsimonious [56, 50]. After identifying the causal variables and cause-effect directions, this causal information is used to construct a set of hypotheses, that validate the results of causality analysis. In the second step, hypotheses derived from the causality analysis are translated into monitoring rules, which are then used for the early prediction of abnormal events in routine process operation.

The main contribution of this work is the development of a methodology to predict flooding and weeping using causality analysis. An approach that integrates data-driven model with the process knowledge is proposed for the reconstruction of causal network. Finite impulse response model is identified with L_0 & L_1 constraint to extract the information of possible causal variables. In the course of addressing the problem, FIR model with L_0 constraint is identified using greedy sparse simplex algorithm and the necessary analytical expressions are derived. An hypotheses driven approach is presented for the prediction of flooding and weeping in process operation.

3.2 FIR Model Identification with Sparsity constraint

Finite impulse response (FIR) model of a process is a linear mapping of the output variable $y[t]$ with time lagged input variables $x[t-p]$ [57]. FIR model can be represented as

$$y[t] = \sum_{p=1}^{P} x[t-p]\theta[t-p] + \epsilon[t] \tag{3.1}$$

Eq. 3.1 can be written in the matrix form as.

$$Y = X\theta + \epsilon \tag{3.2}$$

$$Y = \begin{bmatrix} y_1 & y_2 & ..... & y_{N-1} & y_N \end{bmatrix}^T$$

$$\theta = \begin{bmatrix} \theta_{1,t-1} & \theta_{1,t-2} & ... & \theta_{1,t-p} & ..... & \theta_{M,t-1} & ... & \theta_{M,t-p+1} & \theta_{M,t-p} \end{bmatrix}^T$$

$$X = \begin{bmatrix} x^1_{1,t-1} & x^1_{1,t-2} & ... & x^1_{1,t-p} & ... & x^1_{M,t-1} & ... & x^1_{M,t-p} \\ x^2_{1,t-1} & x^2_{1,t-2} & ... & x^2_{1,t-p} & ... & x^2_{M,t-1} & ... & x^2_{M,t-p} \\ . & . & ... & . & ... & . & ... & . \\ x^{N-1}_{1,t-1} & x^{N-1}_{1,t-2} & ... & x^{N-1}_{1,t-p} & ... & x^{N-1}_{M,t-1} & ... & x^{N-1}_{M,t-p} \\ x^N_{1,t-1} & x^N_{1,t-2} & ... & x^N_{1,t-p} & ... & x^N_{M,t-1} & ... & x^N_{M,t-p} \end{bmatrix}$$

where, $Y \in \mathbb{R}^{N\times 1}$ is the output process variable, $X \in \mathbb{R}^{N\times M(t-p)}$ is input process variables, θ is the parameter vector of dimension $\mathbb{R}^{M(t-p)\times 1}$, $\epsilon_i \overset{i.i.d}{\sim} \mathcal{N}(0,\Sigma)$ is white noise, N is sample dimension, M is variable dimension and p is order of time-lag. Estimation of the parameter vector θ, given X and Y of the FIR model is usually posed as the least square optimization problem.

$$\hat{\theta} : arg\min_{\theta} \quad f(\theta) \Rightarrow arg\min_{\theta} \quad \|Y - X\theta\|_2^2 \tag{3.3}$$

$$\hat{\theta} = arg\min_{\theta} \quad Y^TY - 2(X\theta)^TY + (X\theta)^TX\theta \tag{3.4}$$

On taking derivative of Eq. 3.4 and equating it to zero, analytical expression for the estimate of θ is obtained as

$$\hat{\theta} = \left(X^TX\right)^{-1}X^TY \tag{3.5}$$

This estimated parameters encode the input-output relationship among the variables. However, using Eq. 3.5 for parameter estimation may result in estimation error, inaccurate mapping of variables and over fitting caused due to the non-parsimonious nature of FIR model and also due to accounting for the effect of some less significant input process variables in the model equations. It is possible to reduce the estimation error and improve the accuracy of mapping by penalizing or ignoring the parameters corresponding to less significant input variables. This can be achieved by modifying the least square parameter estimation problem as a constrained optimization problem with a sparsity promoting norm constraint imposed on the parameter vector. In this context, zero norm constraint on the parameter vector can be considered as a natural choice to achieve at most sparsity. Thus, minimization problem in Eq. 3.3 is modified as the following.

$$\hat{\theta}_{l_0} = \min_{\theta} \|Y - X\theta\|_2^2 \; s.t. \; \|\theta\|_0 \leq s \tag{3.6}$$

However, L_0 norm constraint formulation of sparse regression is a NP-hard problem. As an alternative way to overcome this problem, a convex relaxation using L_1 norm

constraint is considered and the optimization problem in Eq. 3.6 is reformulated as follows.

$$\hat{\theta}_{l_1} := arg\min_{\theta} \quad \|Y - X\theta\|_2^2 + \alpha\|\theta\|_1 \tag{3.7}$$

where, α is the regularization parameter. The selection of optimal value of α is discussed in Appendix. A.1. Aforementioned optimization problem is commonly known as LASSO [51] and they are solved using techniques such as coordinate descent, alternating direction method of multipliers (ADMM) [53] and interior point methods [54] etc. In this work, optimization problem in Eq. 3.7 is solved using ADMM. Theoretical insights and the calculation steps of ADMM can be found in [53]. In some cases, L_1 norm constraint enforced on the parameter might result in some spurious estimate of $\hat{\theta}_{l_1}$. Though L_0 norm constraint problem is regarded as NP-hard to solve and non-convex in nature, these issues are addressed in the literature using first-order methods [50] and greedy methods. In general, aforementioned optimization problem can be solved using different greedy algorithms such as matching pursuit [55] and greedy sparse simplex (GSS) [8]. In this work, L_0 norm constrained non-convex optimization problem is solved using greedy sparse simplex to achieve near global optimal solution. Reasons behind using the aforementioned greedy sparse simplex over matching pursuit algorithms [8] are (i) the most sparse vector initialization of the guess vector instead of complete zero vector, (ii) correction mechanism to remove incorrectly chosen parameters and (iii) continuing iterations for parameter correction even after the vector of desired dimension is recovered. Details about the greedy sparse simplex are presented in Appendix A.2. Further, derivation steps involved in the identification of FIR model using the aforementioned framework are discussed in Appendix A.3.

Thus, in this work, FIR model identification with sparsity constraint is proposed as an effective way of identifying the causal variables from the process data and this method uses the estimated values of the sparse FIR model parameters for pruning out less contributing input variables and picking up only the most significant process variables. This proposed method is tested on the process described in the following section and results of this study are discussed in section 3.4.

3.3 Process & Problem Description

3.3.1 Process Description

Flooding and weeping events are observed to occur extensively in an industrial deethanizer column associated with a fluid catalytic cracking process presented in Figure. 3.2. Primary feed for the process enters the pre-heating unit followed by fluid catalytic cracking unit. During the cracking process, pre-heated feed cracks down into different products and exits the unit from the top in gaseous state. The product in gaseous state enters the fractionator column for separation and the separated products enter as feed for different downstream process units. In this, top product from the fractionator reaches a multi-stage condenser and condensed product from the unit enters the storage tank. Product from the storage tank splits into two streams and one of the streams enters the absorber as feed and the other stream enters the deethanizer unit after compression. Deethanizer unit is also connected with reboiler and reflux unit to improve the product quality. Especially, reboiler is used for controlling the temperature inside the column.

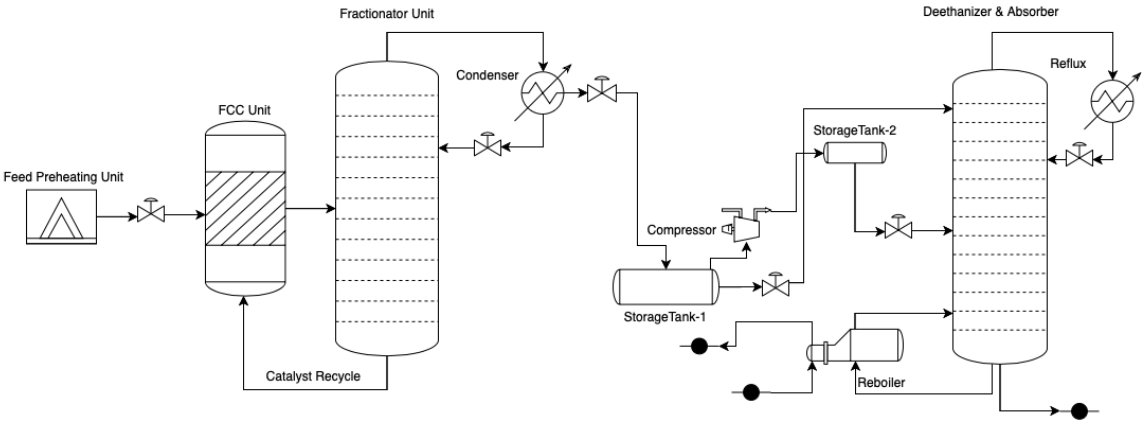

Figure 3.2: Process & Instrumentation Diagram of FCC Unit

3.3.2 Problem Description

A brief description of the problem of flooding and weeping prediction in the industrial Deethanizer column is presented here. Flooding is a phenomenon in which excessive flow of vapour at high pressure occurs inside a column thereby causing entrainment of liquid flowing in the counter current direction. Similarly, weeping is a phenomenon,

where liquid flows down through the sieve holes in the trays of the column without undergoing separation. Usually, pressure drop in the middle region or outlet flowrate above the point of flooding is considered to be flooding indicators. In this work, outlet flowrate measured at top of the column is considered as the flooding indicator. Temperature at the bottom region of the column is taken as the weeping indicator. Flooding and weeping events cause major disruptions in routine operations. In order to overcome such operational difficulties, the problem of flooding and weeping is formulated in this work in the context of causality analysis, where the root cause for flooding and weeping is identified. Based on the identified causal variables, monitoring rules are constructed for the early prediction of flooding and weeping events.

3.4 Flooding & Weeping Prediction using Causality Analysis

A method for detecting flooding and weeping events in process operations is introduced here. A summary of steps used in the proposed method is illustrated in Figure 3.3. The approach consists of data pre-processing step, causal network reconstruction, construction of monitoring rules followed by final implementation. In the first step, after data pre-processing, causal relation is reconstructed using the process data and it is verified using the available process knowledge such as process flow-sheet and the physics of the process. Then in the second step, causal knowledge obtained in the first step is used for construction of monitoring rules to predict the early onset of flooding and weeping. In the forthcoming subsections, these steps are discussed in detail.

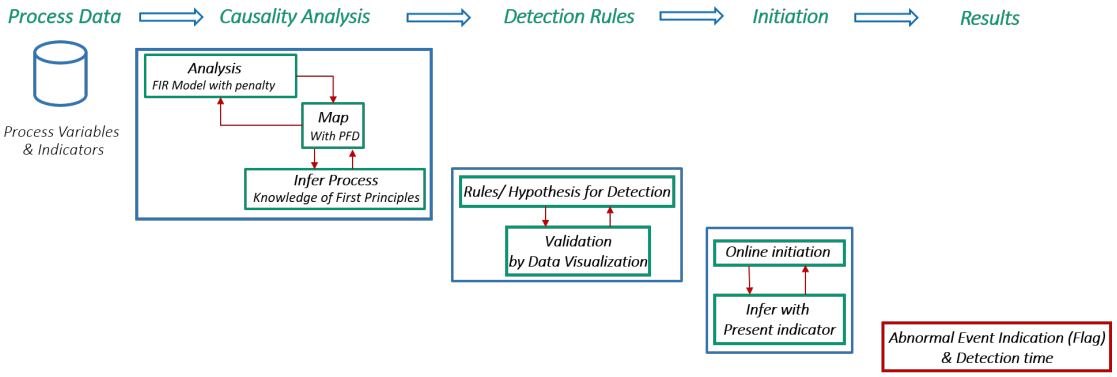

Figure 3.3: Methodology for Predicting Flooding & Weeping

3.4.1 Data Pre-processing

For causality analysis, process data from regular operation is considered. Process variables include flow rates, pressure and temperature, sampled every minute for a duration of twelve months. These twelve months of data are further classified on bi-monthly basis and causality analysis is carried out on bi-monthly sets of data to ensure consistency of the results provided by the proposed methods. For the sake of brevity, result from one of the sets is illustrated for explaining the causality analysis.

3.4.2 Causality Analysis using Sparse FIR Model & Process Knowledge

Process flow-diagram helps in understanding the pathway of propagation, when any-one of the process variables is changed during the plant operation. However, due to complex interconnections among the process units and large number of process variables, identifying the propagation pathway and the causal variables is difficult. In this section, a causal network reconstruction method that makes use of sparsity constrained FIR model, with consideration of physics of the process and connectivity information embedded in the process flow-diagram is presented for the industrial case. In the first step, sparse FIR model is identified and the corresponding sparse parameter vector is obtained. On obtaining the sparse parameter vector, the process variables associated with this parameter vector are considered for further analysis. Results of sparse FIR model identification with L_1 and L_0 norm constraints on the parameters with respect to flooding indicators are presented in Figure. 3.4. For this case, the list of contributing parameters obtained in the identification step and the corresponding process variables are illustrated in Figure. 3.5. Similarly, Figure. 3.6 shows the results of sparse FIR model identification with respect to weeping indicator. The contributing parameters recovered and the corresponding process variables for this case are shown in Figure. 3.7. These results indicate that, in general, L_0 norm constrained estimator yields the most sparse parameter vector compared to L_1 norm constrained estimator, although in some cases, both L_1 and L_0 norm constrained estimators may result in parameter vectors of equal sparsity. Hence, for further analysis, most sparse solution obtained with L_0 norm constraint is considered.

The process variables corresponding to the contributing parameters recovered using L_0 norm constrained estimator are taken to be significant in the causation of flooding

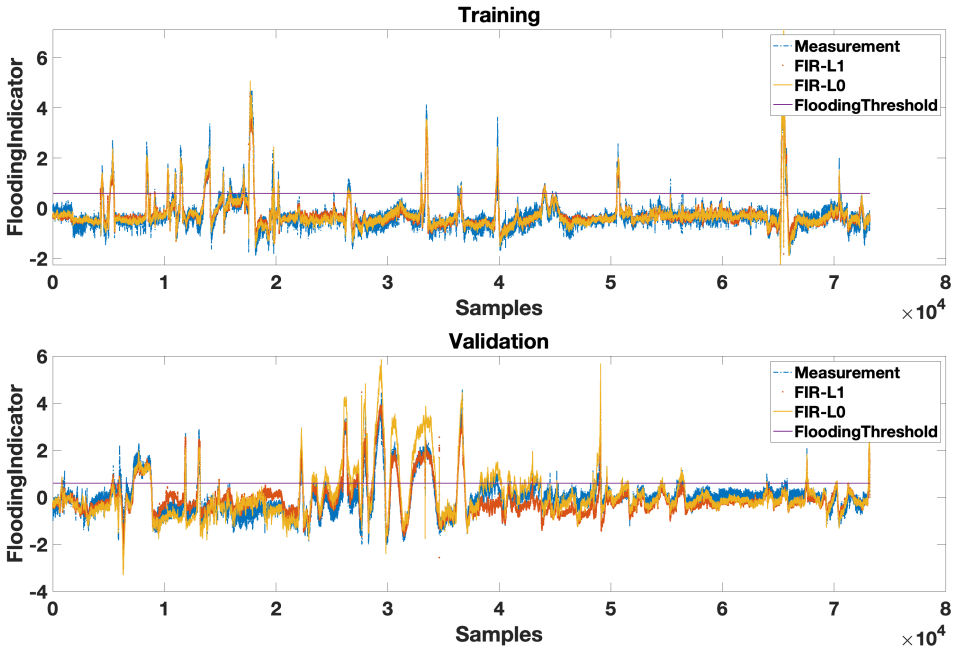

Figure 3.4: FIR Model Identification (Flooding). $(R^2_{train})_{L_0} = 0.894$; $(R^2_{val})_{L_0} = 0.854$ & $(R^2_{train})_{L_1} = 0.822$; $(R^2_{val})_{L_1} = 0.725$

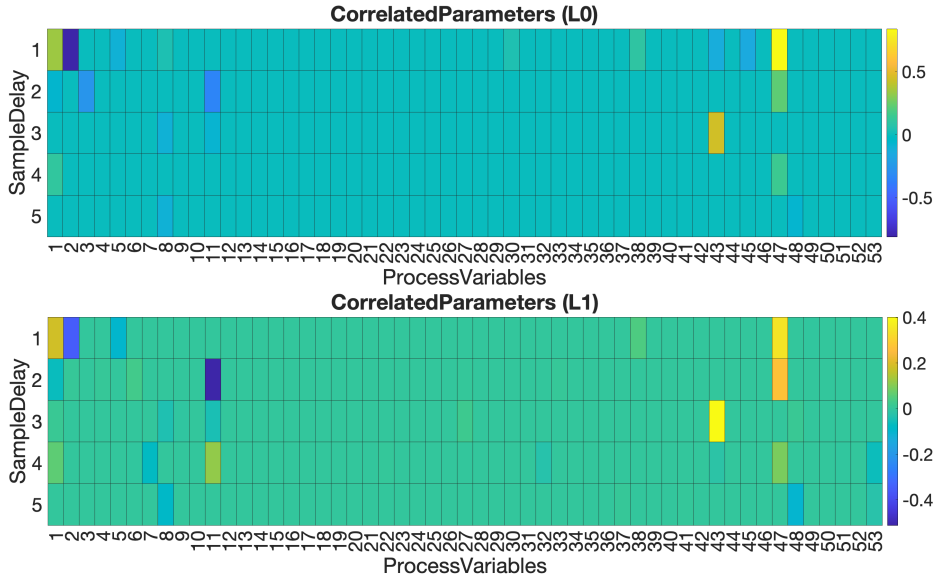

Figure 3.5: Sparse parameter vector recovered with L_0 & L_1 constraint for Flooding. Significantly correlated parameters are presented in a distinct color. Number of non-zero parameters recovered with L_0 constraint is 20 and with L_1 constraint is 40

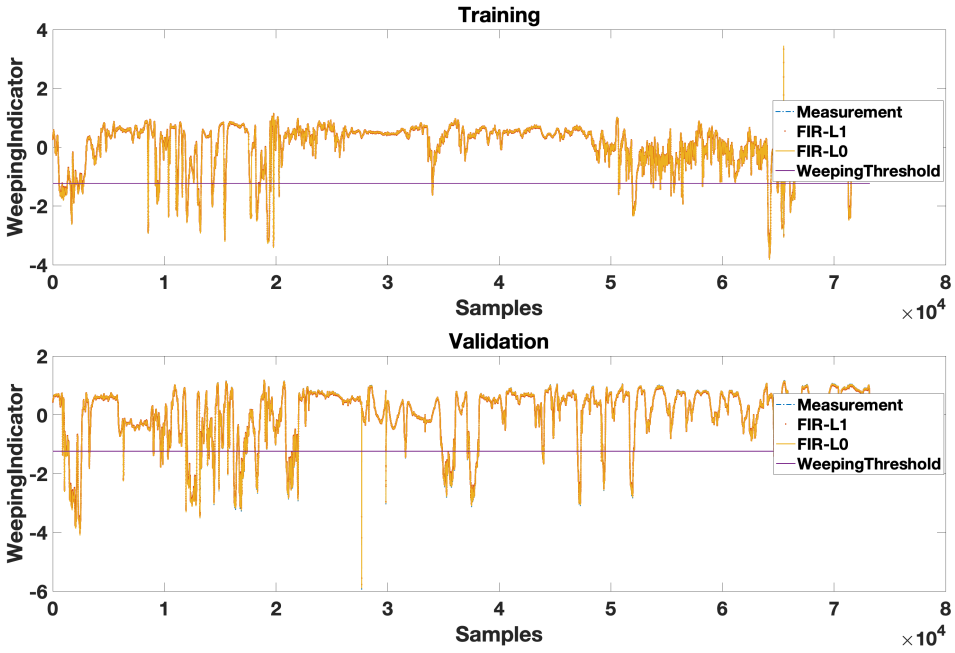

Figure 3.6: FIR Model Identification (Weeping). $(R^2_{train})_{L_0} = 0.99$; $(R^2_{val})_{L_0} = 0.987$ & $(R^2_{train})_{L_1} = 0.992$; $(R^2_{val})_{L_1} = 0.976$

and weeping events. These significantly contributing process variables are tagged in the process flow-diagram shown in Figure 3.8. Description of these process variables tagged in the process flow-diagram, are detailed in Table. 3.1.

Next, a causal network is constructed showing the cause-effect direction among the identified process variables. The first level causal network can be constructed based on the input-output relationship of FIR model. This is illustrated in Figure 3.10. Once the first level causal network construction is completed, corresponding process variables are mapped on to the process flow-diagram to ascertain if the causal direction matches with the mass flow direction of the actual process. Further, to avoid any ambiguity of cause-effect direction in the causal network, the response of process variables are visualized and based on this, the causal direction is switched. For instance, in the first level causal network (Figure 3.10), based on the input-output relation of FIR model, $DBF \rightarrow FIV$ (DBF causes FIV) was defined initially. Then, by visualizing the process variables DBF and FIV as presented in Figure 3.9, one can understand that FIV responds first followed by DBF. Hence, the causal relationship is switched and the direction is updated as $FIV \rightarrow DBF$ in the first level causal network. Similarly, $WI_1 \rightarrow FIV$ and $WI_2 \rightarrow FIV$ are switched as $FIV \rightarrow WI_1$ and $FIV \rightarrow WI_2$ respectively.

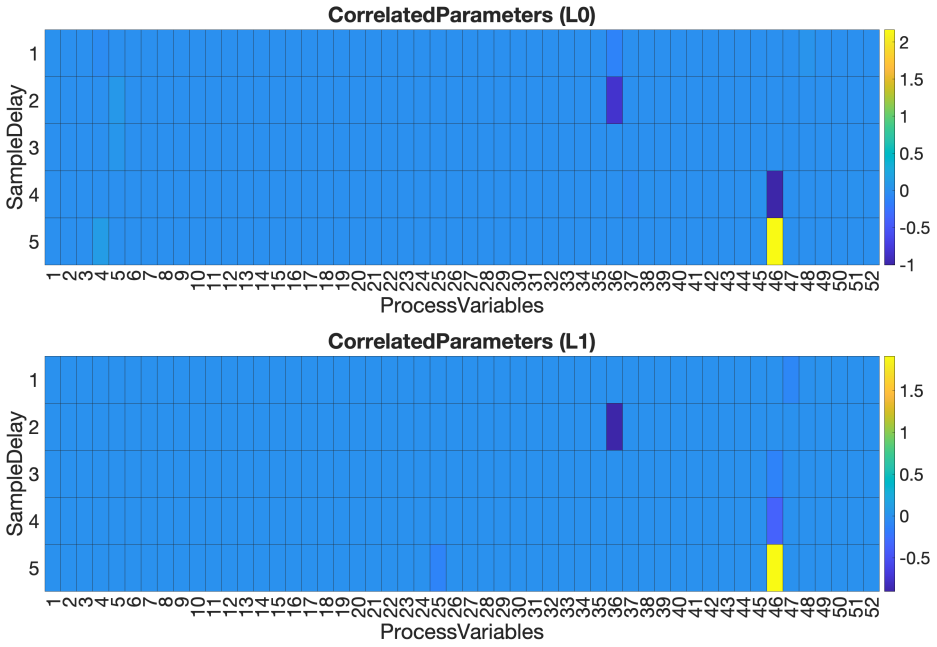

Figure 3.7: Sparse parameter vector recovered with L_0 & L_1 constraint for Weeping. Significantly correlated parameters are presented in a distinct color. Number of non-zero parameters recovered is 7 for both L_0 & L_1 norm constraints

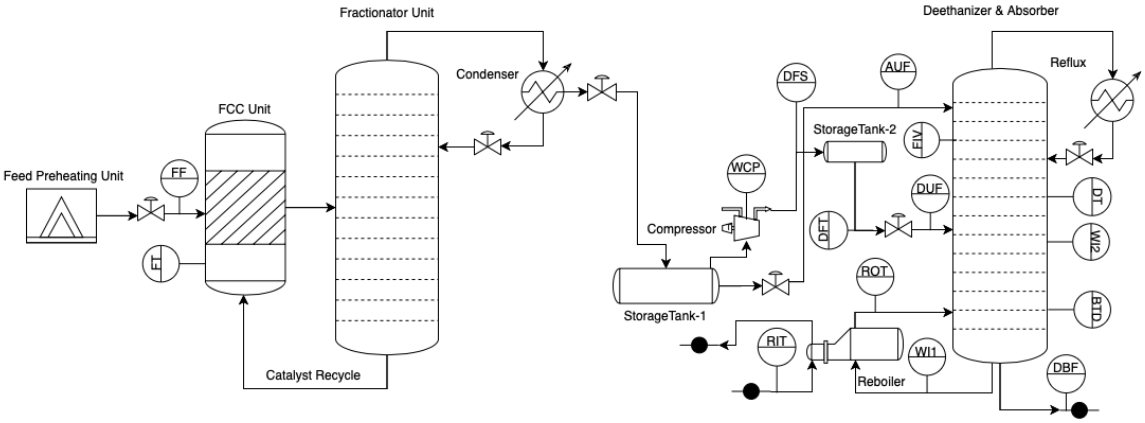

Figure 3.8: Process & Instrumentation Diagram of FCC Unit with the information of contributing process variables

Then, first level causal map is further updated by representing the relationship among other process variables. To construct the second level causal map, the process variable that has significantly contributed in predicting the flooding indicator is considered based on the parameter with highest magnitude. For instance, in this case DUF

Table 3.1: Process variables description (Flooding & Weeping)

Tag (PV No.)	**Process Variable Description**	**Tag** (PV No.)	**Process Variable Description**
DUF (2)	Deethanizer Unit Feed	WI_1 (3)	Weeping Ind-(1) (Bottom Tray Temp.)
RIT (30)	Reboiler Inlet Temperature	ROT (38)	Reboiler Outlet Temperature
WCP (5)	Wet Gas Compressor Pressure	DBF (11)	Deethanizer Bottom Flow stream
AUF (8)	Absorber Feed	WI_2 (4)	Weeping Ind-(2) (Bottom Mid Tray Temp)
DT (47)	Deethanizer Temperature	FT (53)	FCC Temperature
DFT (1)	Deethanizer Feed Temperature	FF (48)	FCC Feed
BTD (43)	Bottom Tray Temp in Deethanizer	FIV (46)	Flooding Indicator (Outlet Flow-rate)
DFS (27)	Deethanizer Feed Separator		

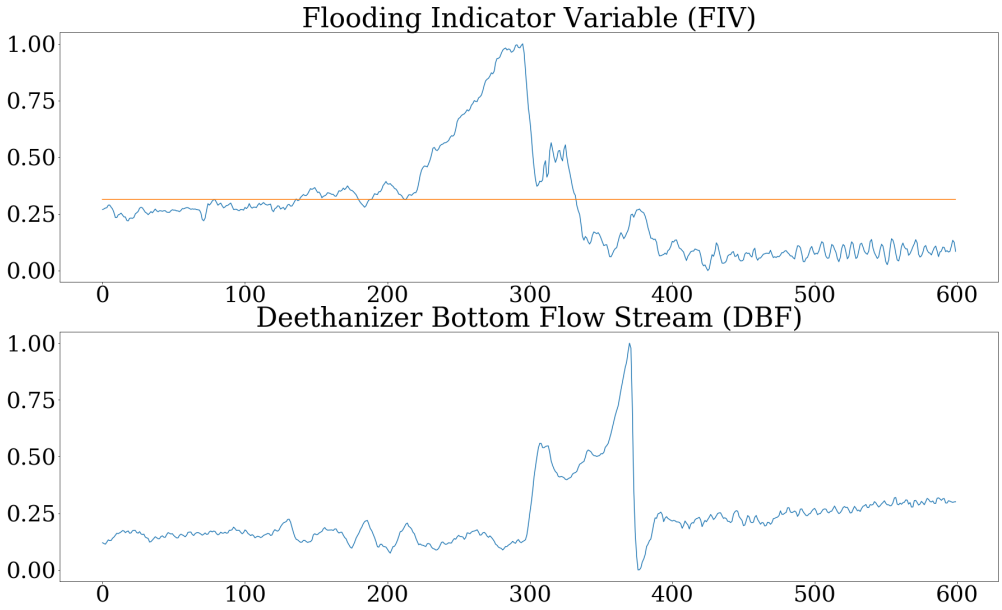

Figure 3.9: Validation of causal direction through process variable visualization

is selected. This newly selected process variable is considered to be the new output variable for the sparse FIR model. Using the new set of process variables, first level of causal map is updated based on the input-output relationship of FIR model and also by using the information obtained from visualization of process variables. In the final step, causal network construction is completed by identifying the FIR model among the subset of process variables that are present in the first level causal map. Resulting final causal network for flooding and weeping is illustrated in Figure. 3.11. Based on the causal network constructed, it is possible to identify that there are five primary nodes, which can be considered as probable causes for the flooding and weeping in the deethanizer. Using this information, sets of hypothesis explaining the physical phenomena of flooding and weeping can be constructed. In this problem, a total of four hypotheses are proposed and they are presented below.

Hypothesis-1 (H_1): Effect of change in Feed for the FCC unit

First hypothesis analyzes the effect of feed change in FCC unit along with the propagation of this effect in the downstream units. Whenever the feed for FCC unit happens to change drastically, feed for the corresponding downstream process units also changes considerably thereby causing a kind of disturbance in the process operations. A reduction in FCC feed would cause a reduction in flow of liquid as feed into the deethanizer. As a result of this, pre-occupied liquid in the deethanizer would get vaporized and an excessive flow of vapour relative to the flow of liquid is expected to

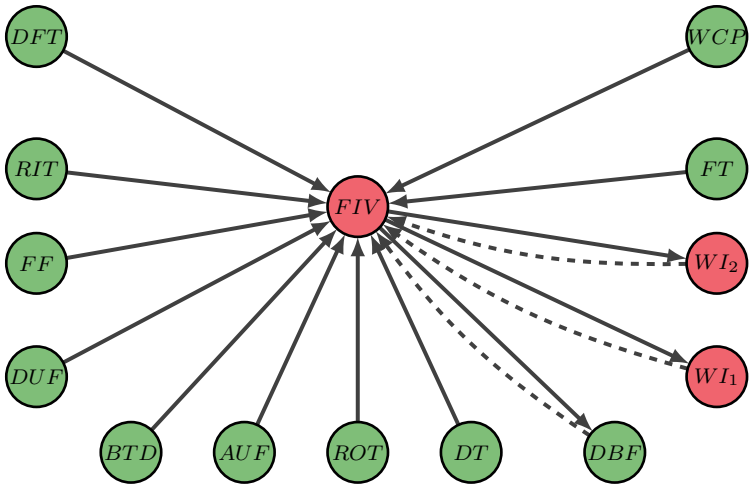

Figure 3.10: First level of Causal Network for Flooding & Weeping. Dashed line indicates the causal relationship before switching

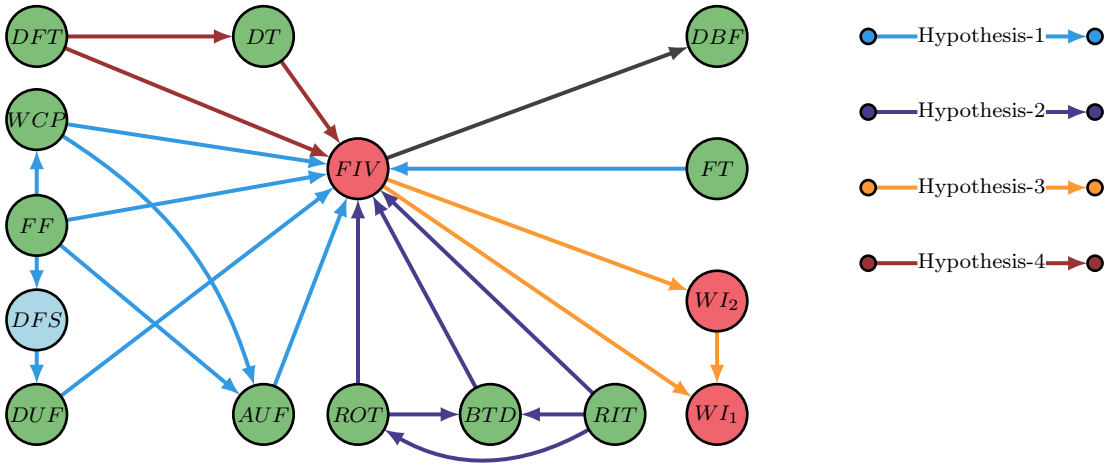

Figure 3.11: Resultant Causal Network for Flooding & Weeping

happen in the process unit. Over a period of time, continuous and excessive flow of vapour at high pressure in the column would lead to flooding. This hypothesis can be validated using the causal network presented in Figure. 3.11. In the given network, it can be noticed that the FCC feed (FF) has direct influence on the flooding indicator variable (FIV) and also on the feed of the absorber (AUF) and the deethanizer (DUF).

Hypothesis-2 (H_2): Effect of Reboiler operation

Second hypothesis accounts for operating conditions of the reboiler associated with

the deethanizer. Whenever the reboiler load is kept unchanged for decreasing flow of FCC feed or increased for a constant flow of FCC feed, excessive vapour generation occurs inside the deethanizer column. This excessive flow of vapour is expected to cause flooding to occur. To validate this claim, complete causal network given in Figure. 3.11 is considered. In the causal network, it is observed that the shell side inlet temperature of the reboiler (RIT) is affecting the tube side outlet temperature (ROT) and the bottom tray temperature of the deethanizer (BTD). Similarly, change in ROT causes a change in BTD. Altogether, three aforementioned process variables are affecting the flooding indicator variable (FIV).

Hypothesis-3 (H_3): Effect of Flooding control on Weeping

Third hypothesis considers the weeping problem. Based on the physics, weeping can be understood as excessive flow of liquid without undergoing separation. This condition is expected to happen specially after flooding is being controlled. To control the flooding, temperature of the reboiler is reduced which eventually reduces the vapour pressure inside column. Due to reduction in pressure, entrained liquid gets released at high flow-rate and as an effect, bottom tray temperature of the column reduces drastically. As a validation of the current hypothesis, causal network indicates that Flooding (FIV) is the cause and the weeping indicated by WI_1&WI_2 is the effects.

Hypothesis-4 (H_4): Effect of Deethanizer Feed temperature

Fourth hypothesis takes deethanizer feed temperature into account. Whenever there is a slow and gradual increase in the deethanizer feed temperature, energy balance of the deethanizer gets affected. Over a period, accumulated temperature increases the vapour pressure thereby favouring flooding condition in deethanizer. Based on the causal network, it can be validated that, an increase in deethanizer feed temperature (DFT) causes an increase of deethanizer (DT) temperature and correspondingly increases vapour pressure, thereby causing flooding (FIV) to occur in the process unit.

3.4.3 Construction of Monitoring rules using Causal Hypotheses

Once the causal map is reconstructed for flooding and weeping problem, information from the causal map is used for constructing the hypothesis set and monitoring rules

to detect the abnormal events in a logical manner. In general, hypothesis explains the physics behind the occurrence of abnormal event in process operations. These hypotheses are then tested for logical validation using offline measurements and also by visualization like the one illustrated in Figure 3.9. When implemented online, flags are raised if the hypothesis is considered to be true. After the initiation of all the hypotheses, existing indicator for the abnormal event is considered as the reference and time difference is computed between the event flag and the indicator to determine the detection time. For prediction of flooding and weeping in the deethanizer column, monitoring rules are implemented. To begin with, process variables in each of the hypotheses are segregated and they are visualized in a sequence that is given in the causal network. Once the visualization is completed, thresholds are given for the process variables and monitoring rules are constructed for the prediction of flooding and weeping events. At first, process variables associated with the hypotheses are classified based on the information from the causal network given in Figure. 3.11.

H_1 **Variables:** $\{FF, DFS, WCP, DUF, FT \ \& \ AUF\}$

H_2 **Variables:** $\{RIT, ROT \ \& \ BTD\}$

H_3 **Variables:** $\{FIV \ \& \ ROT\}$

H_4 **Variables:** $\{DFT \ \& \ DT\}$

Upon classification of hypotheses set and process variables, logical monitoring rules are constructed for prediction of flooding and weeping. Sequence of prediction starts with the parent/ primary variable of the hypotheses set followed by second variable of the same set and this is continued until the last variable of the set is reached. This detection procedure is repeated until all the hypothesis sets are validated. Construction of monitoring rules based on the hypothesis is detailed for H_1 as follows.

- First variable of the set FF is considered. By hypothesis 1, it is understood that drastic reduction in FF leads to flooding. At the same time, it is found that increase in cracking temperature (FT) also leads to flooding. Therefore, first logical criterion to be satisfied is defined as $FF < \alpha_1 \ \& \ FT > \alpha_2$.
- Once the first criteria is satisfied, then second variable of the hypothesis set, WCP is considered and based on this hypothesis it is known that an increase in WCP influences flooding. Therefore, second logical criterion can defined as $WCP > \alpha_3$.
- Upon satisfying the first and the second criteria, third logical criterion is con-

structed using DUF and AUF. From the hypothesis, it can be understood that as WCP increases, AUF decreases and DUF increases. Therefore, third logical criterion can be stated as $AUF < \alpha_4$ & $DUF > \alpha_5$.

Similarly, rules are constructed for other three hypotheses. In second hypothesis, three key process variables can be noticed as possible reason for flooding. Based on the physics, it can be understood that when RIT increases, ROT and BTD increase. Therefore the rules are defined as, $RIT > \beta_1$ and $ROT > \beta_2$ & $BTD > \beta_3$. Third hypothesis is related to weeping, where control of flooding causes weeping. When FIV is changed, existing value of ROT alters the process condition that is favourable to weeping. Based on the physical understanding, rules to predict the onset of weeping can be defined as $FIV < \gamma_1$ & $ROT < \gamma_2$. Similarly from the fourth hypothesis, it can be inferred that increase in feed temperature of deethanizer, DFT, leads to increase in temperature inside the deethanizer DT, which eventually causes flooding. Therefore, prediction rules can be constructed as $DFT > \kappa_1$ & $DT > \kappa_2$.

Once all the four monitoring rules are satisfied, flags for the onset of flooding and weeping are indicated. Here, bounds for process variables in monitoring rules $\alpha, \beta, \gamma, \kappa$ are fixed by visualizing the trends of each one of the process variables that are present in hypotheses. For instance, in the third hypothesis, values of $\gamma_1 = 0.26$ and $\gamma_2 = 0.25$ are obtained by visualizing the trends of ROT and FIV shown in Figure 3.12.

It is to be noted that switching happens from $H_1 \rightarrow H_2$ only if H_1 is not satisfied. Once the flags are obtained, time difference between the flag and the current event indicator is calculated to determine the prediction duration. Results of flooding and weeping prediction are given in Figure. 3.13 and Figure. 3.14. In the results presented for flooding, it can be noticed that different flags have been indicated earlier than expected. Each of these flags corresponds to hypothesis which detected the event. Similar interpretation can be given for weeping prediction as well. The proposed approach for causal network reconstruction and abnormal event prediction applied for the problem of flooding and weeping and yielded physically interpretable results and is also able to predict them using its source variable.

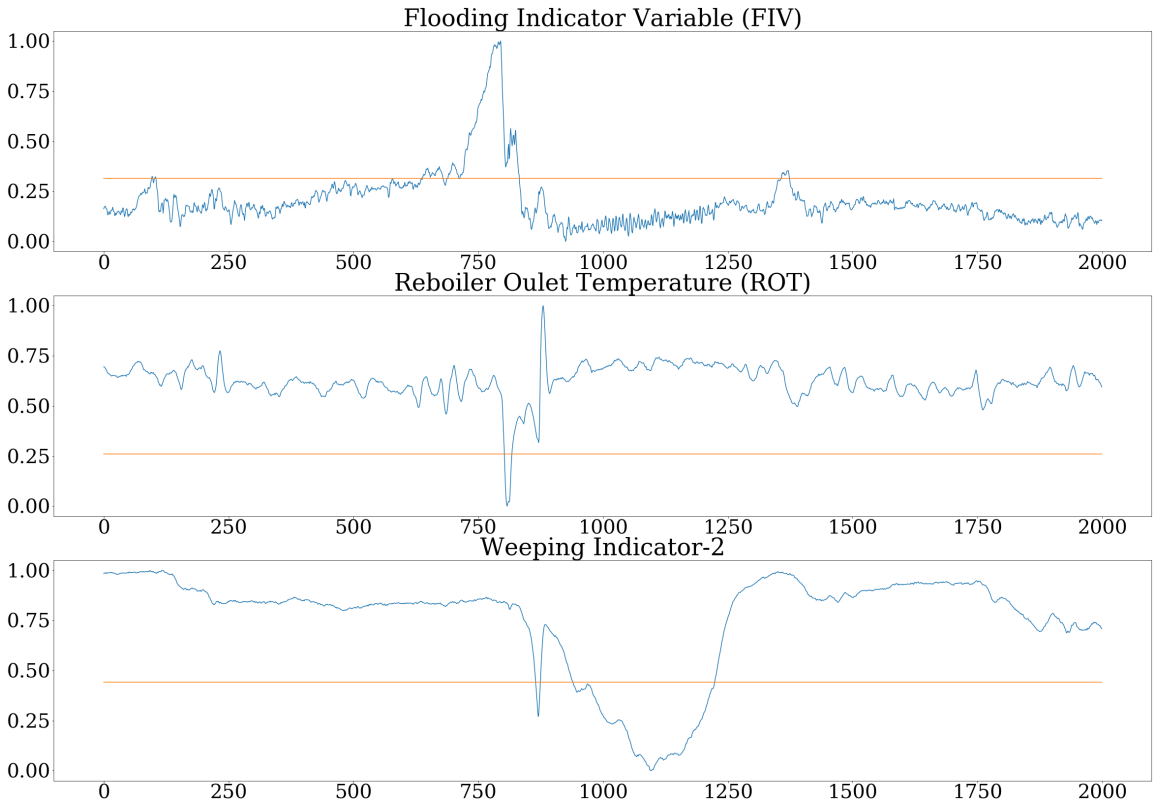

Figure 3.12: Validation & definition of bounds (orange line) for the variables in monitoring rules (hypothesis-3)

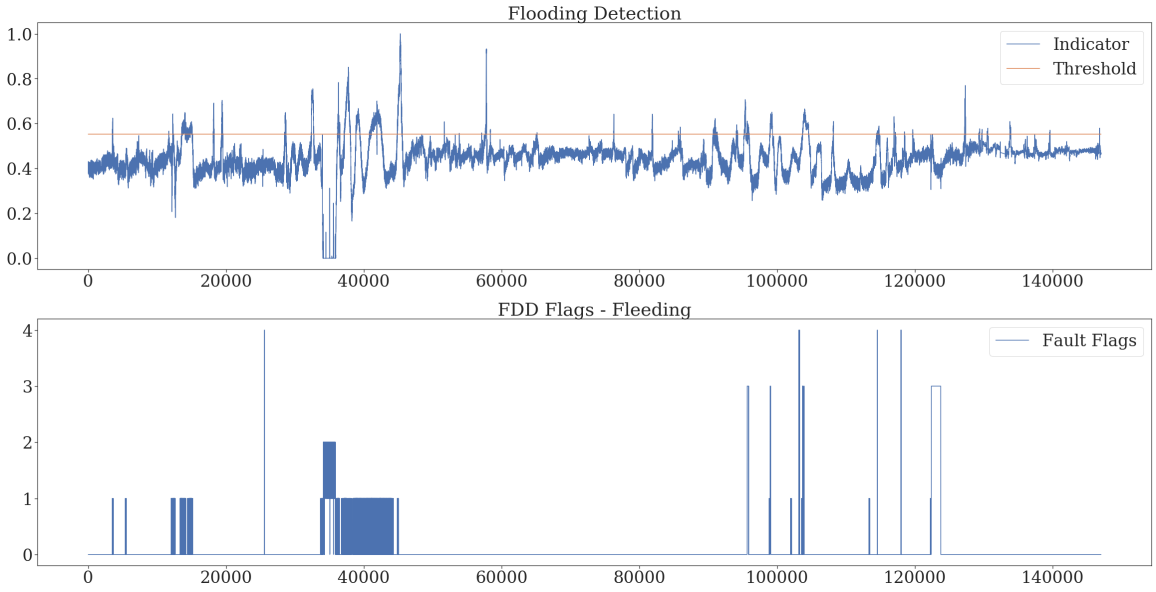

Figure 3.13: Prediction of Flooding by Hypothesis approach

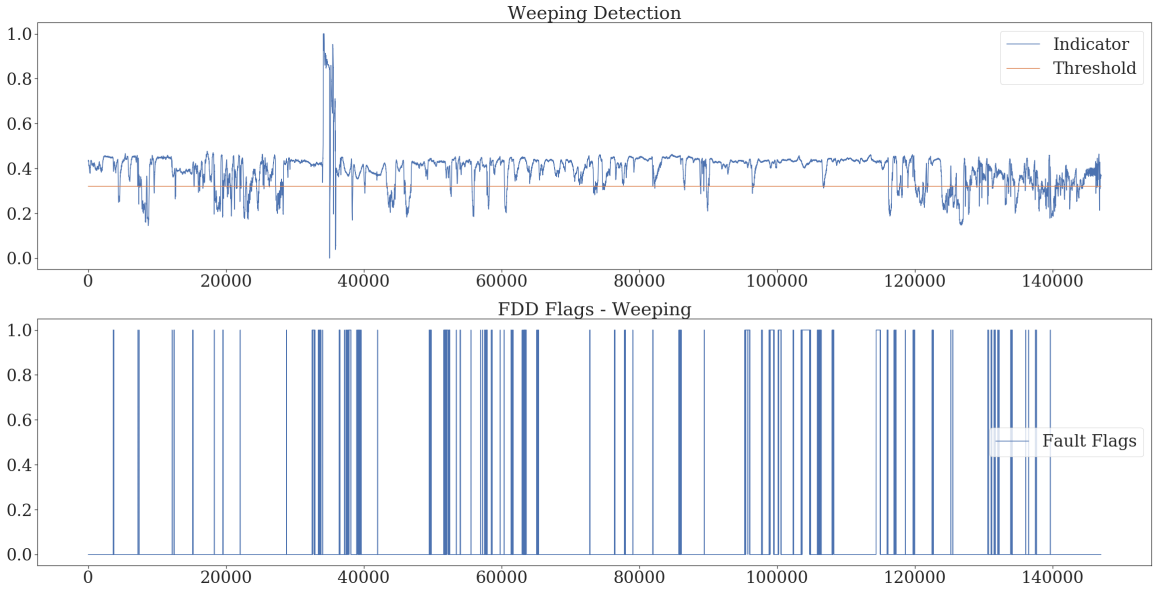

Figure 3.14: Prediction of Weeping by Hypothesis approach

3.5 Results & Outcome of Industrial Implementation

Consistent results were obtained for other five bi-monthly data set with minor modifications in the reconstructed causal network. Some of the causes are not consistent throughout and they occur only once in a while. Effect of deethanizer feed temperature (DFT) and temperature of FCC reactor (FT) are the causes that do not influence flooding all the time. This information is updated in the causal network for flooding and weeping illustrated in Figure 3.11 using a distinct representation. The causal network for the span of twelve months is presented in Figure 3.15. Comprehensive results of flooding and weeping prediction are given in Table. 3.2.

Table 3.2: Comprehensive results of flooding & weeping detection

	Flooding	Weeping
Actual Events	64	113
Detected Events	55 (85%)	101 (89%)
Undetected Events	9	15
False positive	14	22
Average prediction time	∼1.5 Hrs	@ Onset of Flooding

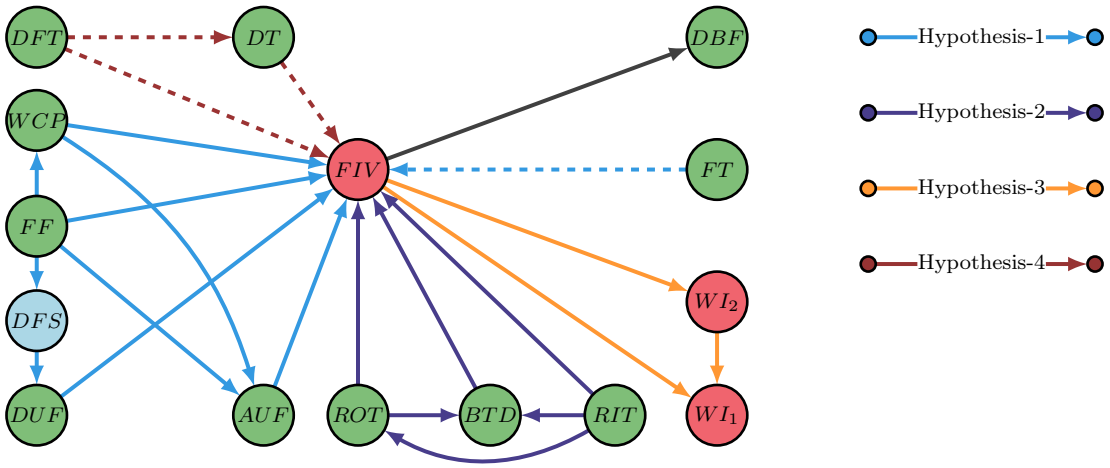

Figure 3.15: Resultant Causal Network for Flooding & Weeping considering results for the span of 12 months

The findings of the methodology proposed for causality analysis have been implemented in real-time to predict and control flooding and weeping in deethanizer column for the process given in Section 3.3. On one instance for example, based on the information obtained from the causal network and the proposed prediction algorithm, bottom tray temperature of the deethanizer was reduced using robust-model predictive controller present around the reboiler section of the deethanzier to successfully prevent flooding. Due to the pro-active measure taken based on the prediction algorithm, flooding events were prevented. It is also observed that, once the flooding is controlled on time, due to the underlying physics of the problem, weeping is also controlled.

3.6 Summary

In this work, a novel methodology is presented for the prediction of flooding and weeping events in an industrial process using causality analysis. The method involves two-steps, where in the first step causal network is reconstructed using a data-driven approach coupled with process knowledge. In the second step, hypothesis based prediction of abnormal event in process operation is carried out by utilising the causal information. In causal network reconstruction step, finite impulse response model with sparsity promoting norm constraints, L_1 & L_0 norm, on the parameter is used for the selection of possible causal variables and knowledge of process flow-sheet is used

to validate the direction of causation. In the event prediction step, process oriented monitoring rules are constructed to predict the events ahead of time. The efficacy of the proposed approach is demonstrated in the industrial application of flooding and weeping prediction in a deethanizer column. From the analysis it is found that drastic feed change, abnormality in reboiler operation and deethanizer feed temperature are considered to be possible cause for flooding and it is also found that improper control of flooding leads to weeping. The proposed causality driven approach for abnormal event prediction is able to predict flooding event on an average of 1.5 Hrs before onset and the weeping events were detected immediately after the onset of flooding. These findings are then implemented in an actual industrial setting and positive outcomes were achieved by avoiding the occurrence of flooding and weeping.

Chapter 4

Sparse Inverse Covariance Estimation for Causal Inference in Process Data Analytics

4.1 Introduction

In Chapter 3, we proposed causality analysis approach using sparse FIR model combined with the process knowledge and applied it in flooding and weeping event prediction in a deethanizer column of an industrial process. In this approach, it is to be noted that the process knowledge is essential in addition to the process data for causality analysis. In the case of non availability of the process knowledge, there is a need for developing a causal inference technique that makes use of only the process data. In this chapter, a data-driven approach for causal inference using sparse inverse covariance is proposed and investigated.

Causal inference emphasizes on decoding the relationship among the variables from the data. Based on the knowledge gained from causal analysis, applications across different domains such as economics, reaction networks, gene networks etc., are available in the literature [58, 59]. In the domain of process systems engineering, causal relationships are generally embedded in process data and process flow sheets. Using the information of causal relationship in process systems, several challenges such as root cause analysis of process faults [40], detection of plant-wide oscillations [41]

and plant connectivity reconstruction [60] etc., can be addressed. To understand the causal relationships, graphical models are generally considered as a viable tool and different techniques have been proposed in the literature [58, 39] to address this problem. Among these methods, time series models such as vector auto-regressive (VAR) models have been used to determine the causality [61]. Similarly, vector auto-regressive exogenous (VARX) models along with factor analysis (FA) models are used for causal analysis along with contemporaneous correlation feature inference in Variational Bayesian framework [62]. A Bayesian network structure is also learned from the data using score based learning algorithm [63] to determine the causal relationship. Apart from the aforementioned techniques, causal relations can also be determined using the method of intervention of variables [64]. During the construction of causal graph, it can be noted that not all variables are associated with one another. Therefore, the concept of sparsity is also introduced in causal modelling in order to reduce the detection of spurious connections in a network [65, 45, 66].

The idea of sparsity has been extensively used in areas such as machine learning, image and signal processing, Mathematics and Statistics etc. [67, 68]. Given the data with large number of variables, introduction of sparsity constraints helps in explaining the data with minimum number of variables. In general, a sparsity constraint can be induced through regularization of parameters with L_0 (Zero) norm [8] or L_1 norm (LASSO) [51] or a combination of L_1 and L_2 norms (Elastic Net, CLOT) [52, 69]. Among the regularization techniques, L_0 provides the most sparse solution followed by L_1 and a combination of both L_1 and L_2 norms. Using the sparsity constraint, problems such as regression, principle component analysis (PCA) and graph construction have been formulated and solved [68]. To reconstruct an undirected graph, estimation of an inverse covariance matrix has been considered as it has the structural information of Gaussian graphical model. During the reconstruction step, any of the aforementioned norm constraints can be induced to estimate the sparse inverse covariance matrix. It is to be noted that L_0 norm is usually preferred as it promotes better sparsity over its counterparts [70]. However, the problem becomes hard to solve due to the NP-hard nature of L_0 norm constraint. Therefore, the original problem is addressed by relaxing it to its convex equivalent i.e., L_1 norm constraint. To solve the convex relaxation problem, different approaches such as first-order methods [71], Block coordinate ascent (BCA) [72] and Alternating direction method of multipliers (ADMM) [73] are available. To solve the non-convex optimization problem i.e., L_0-norm minimization, there are methods in the literature [70, 74], which are guaranteed to converge to at least a local minimum. Since convergence of co-ordinate

wise minimum (defined in Appendix A.2.1) is stronger than a local minimum [8], an algorithm that converges to the former is used in the current work.

Since, inferring the causal direction is important in the field of process systems engineering but many of the aforementioned methods infer an undirected graph from the data, it is essential to have methods which can infer the directed graph from data. Therefore, the problem of inferring causal relations is addressed in this work by combining the estimation of sparse inverse covariance matrix with the dynamic likelihood score. In the current approach, a two-step algorithm is proposed. In the first step, a zero-norm constraint is introduced while estimating the sparse inverse covariance matrix in order to reconstruct a sparse relational network of the process from the data. In the second step, existing likelihood score is extended for dynamic models and dynamic likelihood score is computed to infer causal direction among the associated variables in the reconstructed sparse network from the first step. As mentioned earlier, inverse covariance has the information of Gaussian graphical model. Therefore, when sparsity constraint is introduced, some of the elements in the inverse covariance matrix becomes zero, which makes that variable conditionally independent of other variables. Due to the existence of conditional independence among the variables [75], information in the Gaussian graphical models can be interpreted from causality perspective.

The main contributions of this work are summarized as follows. To solve the aforementioned non-convex optimization problem in the first step of the proposed method, a greedy approach is used to achieve near global optimal solution. In particular, due to its accuracy over others, greedy sparse simplex method [8] is considered and is adapted to the current framework of estimation. The algorithm is also modified to account for the additional positive semi-definite constraint on the inverse covariance matrix. To infer the causal direction, a dynamic likelihood score is utilized. The proposed approach for causal analysis is illustrated with a numerical and an industrial case study. In particular, the root cause and causal map for flooding and weeping in a deethanizer associated with Fluid catalytic cracking (FCC) is identified in the industrial case study.

4.2 Graph

A graph (G) is defined as set of objects that are related to each other in some aspect. Mathematically, a graph (G) is represented using a set of nodes (N) and edges (E) as

$$G = (N, E)$$

where, N denotes the set of all variables and E denotes set of ordered pairs where each pair represents the link connecting the variables. A graph can be classified into directed and undirected as illustrated in Figure 4.1. In directed graph, nodes are connected by edges with an arrow pointed at a particular direction, where as in an undirected graph, edges do not have the information about the direction.

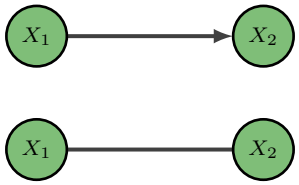

Figure 4.1: Representation of directed and undirected graph

A graph can also be represented in the form of a square matrix, known as adjacency matrix (A_{adj}). In an undirected graph, adjacency matrix will be symmetric with a value of 1 at $(i, j)^{th}$ and $(j, i)^{th}$ components of the matrix if the variables i and j are connected in the graph and zero otherwise. For the directed graph, only $(i, j)^{th}$ component takes a value of 1 if the information is transferred from variable i to j and zero otherwise. A graph structure can also be constructed from the adjacency matrix by connecting the non-zero entries of the matrix. However in practice, graph structure is not known a-priori. In this context, methods for estimating the graph structure from data has gained significance in the recent years [76]. In the following subsection, the method of inverse covariance estimation, an approach to estimate the graph structure from the data, will be discussed.

4.3 Sparse Inverse Covariance Estimation

The problem of inferring the connectivity from data can be formulated as an estimation of inverse covariance matrix, which encodes the information of conditional independence [72, 77] among the variables. Therefore, the underlying relationships

among the variables can be inferred from the data by estimating the inverse of covariance matrix in the framework of maximum likelihood (ML) estimation.

Proposition. *Given a graph G with M variables, $X \coloneqq \{x_i, i = 1, 2, \cdots, M\}$ following a multivariate Gaussian distribution i.e., $X \sim \mathcal{N}(0, \Sigma)$, where Σ is regular and let $\Gamma = \{1, 2, \cdots, M\}$. Then for $i, j \in \Gamma$ with $i \neq j$,*

$$x_i \perp\!\!\!\perp x_j | x_{\Gamma \setminus \{i,j\}} \iff (\Sigma^{-1})_{i,j} = 0$$

i.e., the inverse of the covariance matrix encodes the information of conditional independence among the variables.

Proof. Refer to Proposition 5.2 in [77]. □

In the current work, the data matrix is represented by $X \in \mathbb{R}^{M \times N}$ where, N is the number of samples and M is the number of variables. It is further assumed that the data follows multivariate Gaussian distribution with zero mean ($\mu \in \mathbb{R}^{M \times 1}$) and covariance $\Sigma \in \mathbb{R}^{M \times M}$.

Based on the aforementioned assumption, the probability distribution of the data can be expressed as

$$P(X) = \frac{1}{\sqrt{2\pi}} \Big((det(\Sigma))^{-1/2} \Big) \exp \Big(-\frac{1}{2} X^T \Sigma^{-1} X \Big) \tag{4.1}$$

In Eq. (4.1), inverse of the covariance (Σ^{-1}) is replaced by Θ and logarithmic form of $P(X)$ is considered to have tractable computation. Thus, the expression in the following form is obtained as,

$$\log(P(X)) = \frac{1}{2} \log(det(\Theta)) - \frac{1}{2} \Big(X^T \Theta X \Big) \tag{4.2}$$

Further, Eq. (4.2) can be modified as,

$$\log(P(X)) = \frac{1}{2} \log(det(\Theta)) - \frac{1}{2} \mathrm{Tr} \left(\left(\frac{1}{N} \sum_{i=1}^{N} (x_i)(x_i)^T \right) \Theta \right) = \frac{1}{2} \log(det(\Theta)) - \frac{1}{2} \mathrm{Tr}(S\Theta) \tag{4.3}$$

where, S is the sample covariance computed from the data and Θ is the inverse covariance to be estimated. In order to estimate the inverse of covariance, the problem is presented in the maximum likelihood estimation framework as

$$\hat{\Theta} = arg \min_{\Theta \succeq 0} \Big(-\log(det(\Theta)) + \mathrm{Tr}(S\Theta) \Big) \tag{4.4}$$

In general, ML estimate of the inverse covariance matrix will lead to dense graphical model. Therefore, inferring the connectivity among the variables becomes a challenging task and it may also lead to spurious connections. In order to overcome this issue, a sparsity constraint in terms of L_0 norm on the inverse of covariance matrix is considered.

It is a well known fact that L_0 norm minimization is combinatorial and is NP-hard to solve. Therefore, the original L_0 problem for inverse covariance estimation is generally transformed to its convex counterpart by relaxing the constraint to L_1 norm [71, 53, 72]. Another way of handling the original L_0 problem is to use greedy methods, which makes locally optimal choice at every stage with a goal to reach the global optimum [78, 8]. As the greedy methods promote better sparsity over convex relaxations, the former is used in the current work. In the following subsections, details that are essential to understand both the convex formulations and greedy methods will be explained by considering a general function $f : \mathbb{R}^n \rightarrow \mathbb{R}$.

4.3.1 One Norm Constrained Optimization Algorithm: Convex Formulation

A convex equivalent solution to the problem of inverse covariance estimation given in Eq. (4.4) is obtained by incorporating L_1 constraint on the decision variable to the objective function as

$$\hat{\Theta} = arg \min_{\Theta \succeq 0} \log(det(\Theta)) - \mathrm{Tr}(S\Theta) + \alpha \left\|\Theta\right\|_1 \tag{4.5}$$

To solve the aforementioned problem, ADMM is most prominently used. In this section, an overview of ADMM method for a general convex function $f(\theta) := h(\theta) + g(\theta)$ is presented in brief and its extension for sparse inverse covariance estimation is also detailed in the later parts. Consider a minimization problem of a general convex function $f(\cdot)$ as

$$\begin{aligned} \hat{\theta} &= arg \min_{\theta} f(\theta) \\ &= arg \min_{\theta} h(\theta) + g(\theta) \end{aligned}$$

The aforementioned problem can be solved using different approaches such as first-order methods [71], block coordinate ascent (BCA) [72] and alternating direction method of multipliers (ADMM) [73]. In BCA, convergence becomes non-monotonic

for non-smooth function because of which, the estimate converges to a sub-optimal solution. In order to avoid this issue, a new variable (z) for θ is introduced in function $g(\cdot)$ and the unconstrained optimization problem is converted into a constrained form as

$$\hat{\theta} = arg\min_{\theta} \; h(\theta) + g(z)$$
$$s.t \; (\theta - z = 0)$$

This formulation, often referred to as ADMM, has the advantage of decomposability from dual descent and convergence properties from the method of multipliers [53]. The aforementioned problem is then converted into unconstrained form by introducing the method of multipliers and the final steps of estimating the parameters in ADMM method are as follows

$$\theta^{k+1} = arg\min_{\theta} J_p(\theta, z^k, y^k)$$
$$z^{k+1} = arg\min_{z} J_p(\theta^{k+1}, z, y^k)$$
$$y^{k+1} = y^k + \rho(\theta^{k+1} - z^{k+1})$$

where, $\rho > 0$ and $J_p(\theta, z, y) = h(\theta) + g(z) + y^T(\theta - z) + \frac{\rho}{2}\|\theta - z\|^2$.

In order to extend this approach to the case of estimation of sparse inverse covariance matrix i.e., Eq. (4.5), the cost function defined in Eq. (4.5) is first separated into smooth ($h(\Theta)$=$\log(det(\Theta)) - \mathrm{Tr}(S\Theta)$) and non-smooth functions ($g(Z)$=$\|\Theta\|_1$). Applying the final steps of estimating the parameters in ADMM method for inverse covariance estimation, an analytical expression for inverse covariance matrix as given in Algorithm 2 is obtained [53].

Algorithm 2 Sparse Inverse Covariance Estimation: ADMM (Convex Formulation)

1: $\Theta^{k+1} = Q\tilde{\Theta}^k Q^T$ ▷ Smooth function update
2: $Z^{k+1} = \left(1 - \frac{\alpha}{\rho}|(\Theta^{k+1} + U^k)|^{-1}\right)$ ▷ Non-smooth function update
3: $U^{k+1} = U^k + \Theta^{k+1} - Z^{k+1}$ ▷ Dual update

In Algorithm 2, Θ^k is the estimated inverse covariance, Z^k is the variable which regularizes the estimate with L_1 norm, U is the dual variable of Θ, and Q is the matrix with orthonormal vectors obtained from singular value decomposition of Θ. The resultant graph structure estimated with L_1 constraint might make the structure

dense if the regularization factor (α) is not tuned well, which may again lead to spurious relations.

Since greedy methods promote better sparsity over convex formulations, the former is used in the current work of estimation of inverse covariance matrix. Therefore, the problem of estimation of inverse covariance is formulated as

$$\begin{aligned} \hat{\Theta} = arg\min_{\Theta \succeq 0}(-\log(det(\Theta)) + \mathrm{Tr}(S\Theta)) \\ s.t. \|\Theta\|_0 \leq s \end{aligned} \tag{4.6}$$

Further details on solving the problem in Eq. (4.6) are discussed in detail in Section 4.5. Once the graph structure is estimated, the next objective is to infer the direction in which the variables are related, which is discussed in detail in the following subsection.

4.4 Inferring Causation in Sparse Inverse Covariance

Given the inverse covariance matrix, causal direction is determined by computing the likelihood score, which is a metric that is used to compute the causal direction among the variables in an undirected graph. To explain further details on inference of causal direction using the likelihood score, two random variables x_i and x_j are considered. Given the functions $\hat{f}, \hat{g} : \mathbb{R} \to \mathbb{R}$ which are prediction of x_j from x_i and prediction of x_i from x_j, respectively. Let the prediction residuals be defined as $\eta_{x_j,\hat{f}} \coloneqq x_j - \hat{f}(x_i)$ and $\eta_{x_i,\hat{g}} \coloneqq x_i - \hat{g}(x_j)$.

To infer causal relation among continuous random variables, differential entropy (denoted by $H(\cdot)$) is used [79]. For a continuous random variable $x \in X$, differential entropy can be defined as $H(x) = \mathbb{E}\left[-\ln P(x)\right]$. Similarly, joint entropy can be represented as the sum of conditional differential entropy and marginal of the joint differential entropy using the chain rule of differential entropy [80] as

$$\begin{aligned} H(x_i, x_j) &= H(x_j) + H(x_i \mid x_j) \\ &= H(x_j) + H(\eta_{x_i,\hat{g}} \mid x_j) \\ &= H(x_j) + H(\eta_{x_i,\hat{g}}) - I(x_j, \eta_{x_i,\hat{g}}) \end{aligned}$$

where, $I(\cdot,\cdot)$ represents differential mutual information. For instance, given two ran-

dom variables x_1, x_2, $I(x_1, x_2) \coloneqq \mathbb{E}\left[\ln\left(\frac{p(x_1|x_2)}{p(x_2)}\right)\right]$ where $p(\cdot)$ represents the probability density function.

Similarly,

$$\begin{aligned} H(x_i, x_j) &= H(x_i) + H(x_j \mid x_i) \\ &= H(x_i) + H(\eta_{x_j,\hat{f}} \mid x_i) \\ &= H(x_i) + H(\eta_{x_j,\hat{f}}) - I(x_i, \eta_{x_j,\hat{f}}) \end{aligned}$$

The aforementioned equations of differential entropy leads to

$$H(x_i) + H(\eta_{x_j,\hat{f}}) - I(x_i, \eta_{x_j,\hat{f}}) = H(x_j) + H(\eta_{x_i,\hat{g}}) - I(x_j, \eta_{x_i,\hat{g}}) \tag{4.7}$$

In the case that the random variables x_i, x_j either satisfies an additive noise model with $x_i \to x_j$ or $x_j \to x_i$, but not both, then the mutual information of the corresponding term is zero [81, 79] i.e., when the causal structure is given to be $x_i \to x_j$, then $I(x_i, \eta_{x_j,\hat{f}}) = 0$ and $I(x_j, \eta_{x_i,\hat{g}}) > 0$ and vice versa. Therefore, the differential entropy given in Eq. (4.7), for the causal structure $x_i \to x_j$ can be written as

$$\begin{aligned} H(x_j - \hat{f}(x_i)) + H(x_i) &= H(x_i - \hat{g}(x_j)) + H(x_j) - I(x_i - \hat{g}(x_j), x_j) \\ \Rightarrow H(x_j - \hat{f}(x_i)) + H(x_i) &\leq H(x_i - \hat{g}(x_j)) + H(x_j) \end{aligned} \tag{4.8}$$

The proof for non-negativity of mutual information and its relationship to causal structure identification is presented in Appendix A.4. Further, when the random variables are assumed to be Gaussian, differential entropy can be related to variance [79] and the following expression is obtained.

$$\log Var(x_j - \hat{f}(x_i)) + \log Var(x_i) \leq \log Var(x_i - \hat{g}(x_j)) + \log Var(x_j) \tag{4.9}$$

where $\hat{f}(\cdot)$ is a function that represents the relation between the variables x_i and x_j. From Eq. (4.9), it can be noted that the $L_{x_i \to x_j} < L_{x_j \to x_i}$ for the case when x_i causes x_j and $L_{x_j \to x_i} < L_{x_i \to x_j}$ when x_j causes x_i.

In the current paper, the aforementioned likelihood score is applied to the case when the function $\hat{f}(\cdot)$ is considered to be in the form of linear FIR dynamic models. Since negative log-likelihood is most commonly used to infer the estimate of the parameters from the data for dynamic models, the dynamic likelihood score i.e., $L^d_{x_i \to x_j}$ can be defined in the context of differential entropy as

$$L^d_{x_i \to x_j} : -\log\big(\hat{\Sigma}_{(x_j)_t|(x_i)_{t:t-K+1}}\big) - \log\big(\hat{\Sigma}_{x_i}\big) \tag{4.10}$$

where $\hat{\Sigma}_{(x_j)_t|(x_i)_{t:t-K+1}} = Var((x_j)_t - \hat{h}((x_i)_{t:t-K+1}))$ and $\hat{h}(\cdot)$ represents the linear FIR model. The dynamic likelihood score is expected to be $L^d_{x_i \to x_j} > L^d_{x_j \to x_i}$ for the case when x_i causes x_j and $L^d_{x_j \to x_i} > L^d_{x_i \to x_j}$ when x_j causes x_i. Hence, this information can be used to infer the direction in the estimated undirected graph, thereby transforming undirected graph into a directed graph. It has to be noted that this score for computing the causal direction is only applicable if the variables are assumed to be Gaussian. For more details about the likelihood score refer to Mooij et.al. 2016 [79] and Peters et.al. 2017 [64].

4.5 Sparse Inverse Covariance Estimation using Greedy Sparse Simplex

In this section, Greedy sparse simplex approach is utilized to solve the inverse covariance estimation problem with zero-norm constraint i.e., Eq. (4.6) along with positive semi-definite constraint for estimating the sparse graph structure. In particular, the expressions for minimization steps in GSS algorithm i.e., Eqs. (A.1) and (A.4) when the function $f(\cdot)$ is expressed using Eq. (4.6) are detailed in this section. Further, gradient based methods are used to perform the minimization steps of Eq. (A.1) and (A.4) due to the convex nature of the objective function $f(\cdot)$. The main difference between the general structure of GSS approach and the method of minimization used in the current work is that the optimization variable in this approach is a symmetric matrix. Therefore, a structured indicator matrix E, instead of an indicator vector e, is used to iterate through the elements of the matrix in an orderly sequence. The final steps in the GSS algorithm are also modified to account for the constraint of positive semi-definiteness of the solution matrix.

Considering Eq. (A.1), when the function f is expressed using Eq. (4.6), the minimization problem reduces to,

$$\begin{aligned}
\delta_{i,j} &= arg\min_{\delta \in \mathbb{R}} f(\Theta^k + \delta E_{i,j}) \\
&= arg\min_{\delta \in \mathbb{R}} -\log(det(\Theta^k + \delta E_{i,j})) + \mathrm{Tr}(S(\Theta^k + \delta E_{i,j})) \\
&= arg\min_{\delta \in \mathbb{R}} -\log(det(\Theta^k + \delta E_{i,j})) + \mathrm{Tr}(S\Theta^k) - \delta Tr(SE_{i,j}) \qquad (4.11)
\end{aligned}$$

where, $i = 1, 2, \ldots, M$, $j = i, i+1, \ldots, M$ and $E_{i,j}$ is a symmetric matrix with 1 at $(i,j)^{\text{th}}$ position and zeros elsewhere. Since gradient based methods are used to

solve the minimization problem, it is essential to compute the derivative of Eq. (4.11) with respect to δ. As the derivative computation is independent of indices i and j, for simplicity in notation, $E_{i,j}$ is replaced with E in the following derivation and the indices are specified wherever required. Therefore,

$$\begin{aligned}\frac{df(\Theta^k+\delta E)}{d\delta} &= 0 \\ &\Rightarrow -\frac{1}{det(\Theta^k+\delta E)}\mathrm{Tr}[(det(\Theta^k+\delta E)(\Theta^K+\delta E)^{-1}E)] + \mathrm{Tr}(SE) = 0 \\ &\Rightarrow -\mathrm{Tr}[(\Theta^k+\delta E)^{-1}E] + \mathrm{Tr}(SE) = 0\end{aligned} \tag{4.12}$$

Based on the inversion lemma for sum of matrices [82], $(\Theta^k+\delta E)^{-1}$ in Eq. (4.12) can be given as the following.

$$(\Theta^k+\delta E)^{-1} = (\Theta^k)^{-1} - \frac{\delta}{1+\delta\mathrm{Tr}(E(\Theta^k)^{-1})}(\Theta^k)^{-1}(E)(\Theta^k)^{-1} \tag{4.13}$$

In Eq. (4.13), $\frac{\delta}{1+\delta\mathrm{Tr}(E(\Theta^k)^{-1})}$ is denoted as β. On substituting the inverse expression in Eq. (4.12) and after rearranging the terms, an expression of the following form can be obtained.

$$\beta\mathrm{Tr}\left(\left(\left(\Theta^k\right)^{-1}E\right)^2\right) = \mathrm{Tr}\left(\left(\Theta^k\right)^{-1}E\right) - \mathrm{Tr}(SE) \tag{4.14}$$

Using the *symmetric polynomial property* [83], for any square matrix A, $\mathrm{Tr}(A^2) = [\mathrm{Tr}(A)]^2 - 2\sum_{i<j}\lambda_i\lambda_j$ where, λ denotes the eigenvalue. Further, when the rank(A) is 1 & $A_{i,i} \neq 0$ then $\mathrm{Tr}(A^2) = [\mathrm{Tr}(A)]^2$

In the current problem, $((\Theta^k)^{-1}E)$ has the rank of 1 when E operates on the diagonal element ($i = j$) and it has the rank of 2 when E operates on off diagonal elements($i \neq j$) due to symmetric nature of $(\Theta^k)^{-1}$. Therefore,

$$\mathrm{Tr}[((\Theta^k)^{-1}E)^2] = \begin{cases}[\mathrm{Tr}((\Theta^k)^{-1}E)]^2 \text{ for } i = j \\ [\mathrm{Tr}((\Theta^k)^{-1}E)]^2 - 2\sum_{i<j}\lambda_i\lambda_j \text{ for } i \neq j\end{cases} \tag{4.15}$$

Further, denote $\mathrm{Tr}[(\Theta^k)^{-1}E]$ as γ and $\mathrm{Tr}(SE)$ as κ. Then, for the case when $i \neq j$, Eq. (4.14) can be modified as

$$\frac{\delta}{1+\delta\gamma}\left(\gamma^2 - 2\sum_{i<j}\lambda_i\lambda_j\right) = \gamma - \kappa \tag{4.16}$$

which can be further simplified as

$$\delta = \frac{\gamma - \kappa}{\gamma\kappa - 2\sum_{i<j} \lambda_i \lambda_j} \tag{4.17}$$

Note that when $i = j$, $\delta = \frac{1}{\kappa} - \frac{1}{\gamma}$.

Since the function is convex, the minimum of Eq. (A.1) is unique and is given by Eq. (4.17). Now the function in Eq. (A.2) can be estimated as

$$f_{i,j}(\Theta^k + \delta E_{i,j}) = -\log\Big(det\Big(\Theta^k + \Big(\frac{\gamma - \kappa}{\gamma\kappa - 2\sum_{i<j} \lambda_i \lambda_j}\Big) E_{i,j}\Big)\Big) + \mathrm{Tr}(S\Theta^k) + \Big(\frac{\gamma - \kappa}{\gamma\kappa - 2\sum_{i<j} \lambda_i \lambda_j}\Big)\kappa \tag{4.18}$$

Then, $(\hat{i}, \hat{j}) = arg\min\{f_{i,j}, i = 1, 2, \cdots, M, j = i, i+1, \cdots, M\}$ and the inverse covariance matrix can be updated as

$$\Theta^{k+1} = \begin{cases} \Theta^k + \Big(\frac{\gamma - \kappa}{\gamma\kappa - 2\sum_{i<j} \lambda_i \lambda_j}\Big)\hat{E}, \text{ when } \hat{i} \neq \hat{j} \\ \Theta^k + \Big(\frac{1}{\kappa} - \frac{1}{\gamma}\Big)\hat{E}, \text{ when } \hat{i} = \hat{j} \end{cases} \tag{4.19}$$

where $\hat{E}$ is a symmetric matrix with 1 at $(\hat{i}, \hat{j})^{\text{th}}$ position and zeros elsewhere.

To ensure the positive semi-definiteness of inverse covariance matrix, the update will be modified [84, 85] as

$$\begin{aligned} [U_{k+1}, D_{k+1}, V_{k+1}] &= \mathrm{svd}(\Theta^{k+1}) \\ \hat{\Theta}^{k+1} &= U_{k+1}\max(D_{k+1}, 0)V_{k+1} \end{aligned} \tag{4.20}$$

Consider Eq. (A.4), when the function $f(\cdot)$ is expressed using Eq. (4.6), the minimization problem reduces to,

$$\delta^{i,j}_{i_1,j_1} = arg\min_{\delta \in \mathbb{R}} f(\Theta^k - \Theta^k_{i,j} E_{i,j} + \delta E_{i_1,j_1})$$

$$= arg\min_{\delta \in \mathbb{R}} -\log(det(\Theta^k - \Theta^k_{i,j} E_{i,j} + \delta E_{i_1,j_1})) + \mathrm{Tr}(S\Theta^k) - \mathrm{Tr}(\Theta^k_{i,j} S E_{i,j}) + \delta \mathrm{Tr}(S E_{i_1,j_1}) \tag{4.21}$$

where $i_1 = 1, 2, \ldots, M$, $j_1 = i_1, i_1 + 1, \ldots, M$, $(i, j) \in I(\Theta^k)$ with $I(\Theta^k)$ being a set of all non-zero indices of the matrix Θ^k and $E_{i,j}$ is a symmetric matrix with 1 at $(i, j)^{\text{th}}$ position and zeros elsewhere. For simplicity in notation, $E_{i,j}$ is represented as E_1

and E_{i_1,j_1} is represented as E_2 in the following derivation. Equating the derivative of Eq. (4.21) with respect to δ to zero results in

$$\begin{aligned} -\mathrm{Tr}[(\Theta^k - \Theta^k_{i,j}E_1 + \delta E_2)^{-1}E_2] + \mathrm{Tr}(SE_2) = 0 \\ \Rightarrow \mathrm{Tr}[(\Theta^k + (\delta E_2 - \Theta^k_{i,j}E_1))^{-1}E_2] - \mathrm{Tr}(SE_2) = 0 \end{aligned} \tag{4.22}$$

Using the inversion lemma for sum of matrices [82], inverse portion in Eq. (4.22) can be replaced by

$$-\mathrm{Tr}\left[\left((\Theta^k)^{-1} - \frac{(\Theta^k)^{-1}(\delta E_2 - \Theta^k_{i,j}E_1)(\Theta^k)^{-1}}{1 + \mathrm{Tr}((\delta E_2 - \Theta^k_{i,j}E_1)(\Theta^k)^{-1})}\right)E_2\right] + \mathrm{Tr}(SE_2) = 0 \tag{4.23}$$

Denoting the term $\frac{1}{1+\mathrm{Tr}((\delta E_2 - \Theta^k_{i,j}E_1)(\Theta^k)^{-1})}$ in Eq. (4.23) as β^*, an expression of the following form is obtained after rearranging the terms as

$$\mathrm{Tr}[(\Theta^k)^{-1}E_2 + (-\beta^*)(\Theta^k)^{-1}(\delta E_2 - \Theta^k_{i,j}E_1)(\Theta^k)^{-1}E_2] - \mathrm{Tr}(SE_2) = 0 \tag{4.24}$$

Based on the properties of trace, aforementioned expression reduces to

$$\begin{aligned} -\mathrm{Tr}[(\Theta^k)^{-1}E_2] + \beta^*\delta\mathrm{Tr}[(\Theta^k)^{-1}E_2(\Theta^k)^{-1}E_2] - \beta^*\Theta^k_{i,j}\mathrm{Tr}[(\Theta^k)^{-1}E_1(\Theta^k)^{-1}E_2] \\ +\mathrm{Tr}(SE_2) = 0 \end{aligned} \tag{4.25}$$

To further simplify the notation, the trace terms in Eq. (4.25) are replaced using the following expressions.

$$\begin{gathered} \mathrm{Tr}[(\Theta^k)^{-1}E_1] = \gamma_1;\ \mathrm{Tr}[(\Theta^k)^{-1}E_2] = \gamma_2; \\ \mathrm{Tr}[(\Theta^k)^{-1}E_1(\Theta^k)^{-1}E_2] = \gamma_{12};\ \mathrm{Tr}[(\Theta^k)^{-1}E_2(\Theta^k)^{-1}E_2] = \gamma_{22}; \\ \mathrm{Tr}(SE_1) = \kappa_1;\ \mathrm{Tr}(SE_2) = \kappa_2 \end{gathered}$$

Thus, Eq. (4.25) can be simplified and represented as follows.

$$\gamma_2 - \kappa_2 + \frac{\Theta^k_{i,j}\gamma_{12}}{1 + \delta\gamma_2 - \Theta^k_{i,j}\gamma_1} = \frac{\delta\gamma_{22}}{1 + \delta\gamma_2 - \Theta^k_{i,j}\gamma_1} \tag{4.26}$$

Now, using the *symmetric polynomial property*, γ_{22} can be written as $\left((\gamma_2)^2 - 2\sum_{i<j}\lambda_i\lambda_j\right)$, where, λ_i and λ_j are the eigenvalues of $((\Theta^k)^{-1}E_2)$. On substituting the equivalent expression for γ_{22} in Eq. (4.26) and after simple algebraic manipulations, the following expression can be obtained.

$$\Theta^k_{i,j}(\gamma_{12} - \gamma_1\gamma_2 + \gamma_1\kappa_2) + \gamma_2 - \kappa_2 - \delta\kappa_2\gamma_2 = -2\delta\sum_{i<j}\lambda_i\lambda_j \tag{4.27}$$

Then by rearranging Eq. (4.27), the optimal expression for δ, when $i \neq j$, can be expressed as follows.

$$\delta = \frac{\gamma_2 - \kappa_2 + \Theta^k_{i,j}(\gamma_{12} - \gamma_1\gamma_2 + \gamma_1\kappa_2)}{(\kappa_2\gamma_2 - 2\sum_{i<j}\lambda_i\lambda_j)} \tag{4.28}$$

When, $i = j$, Eq. (4.28) modifies as the following.

$$\delta = \frac{1}{\kappa_2} - \frac{1}{\gamma_2} + \Theta^k_{i,j}\Big(\frac{\gamma_{12} - \gamma_1\gamma_2 + \gamma_1\kappa_2}{\kappa_2\gamma_2}\Big) \tag{4.29}$$

and the function in Eq. (A.5) is given as

$$f^{i,j}_{i_1,j_1}(\Theta^k - \Theta^k_{i,j}E_{i,j} + \delta E_{i_1,j_1}) =$$

$$-\log\Big(det\Big(\Theta^k - \Theta^k_{i,j}E_{i,j} + \Big(\frac{\gamma_2 - \kappa_2 + \Theta^k_{i,j}(\gamma_{12} - \gamma_1\gamma_2 + \gamma_1\kappa_2)}{(\kappa_2\gamma_2 - 2\sum_{i<j}\lambda_i\lambda_j)}\Big)E_{i_1,j_1}\Big)\Big) + \tag{4.30}$$

$$\mathrm{Tr}(S\Theta^k) - \mathrm{Tr}(\Theta^k_{i,j}SE_{i,j}) + \Big(\frac{\gamma_2 - \kappa_2 + \Theta^k_{i,j}(\gamma_{12} - \gamma_1\gamma_2 + \gamma_1\kappa_2)}{(\kappa_2\gamma_2 - 2\sum_{i<j}\lambda_i\lambda_j)}\Big)\mathrm{Tr}(SE_{i_1.j_1})$$

Now, $\{\hat{i}, \hat{j}, \hat{i_1}, \hat{j_1}\} = arg\min\{f^{i,j}_{i_1,j_1}; i_1 = 1, 2, \ldots, M, j_1 = i_1, i_1 + 1, \ldots, M, (i,j) \in I(\Theta^k)\}$ and the update expression for $\|\Theta^k\|_0 = s$ can be presented as follows.

$$\Theta^{k+1} = \begin{cases} \Theta^k - \Theta^k_{i,j}\hat{E}_1 + \Big(\frac{\gamma_2 - \kappa_2 + \Theta^k_{i,j}(\gamma_{12} - \gamma_1\gamma_2 + \gamma_1\kappa_2)}{(\kappa_2\gamma_2 - 2\sum_{i<j}\lambda_i\lambda_j)}\Big)\hat{E}_2, \text{ when } \hat{i} \neq \hat{j} \\ \Theta^k - \Theta^k_{i,j}\hat{E}_1 + \Big(\frac{1}{\kappa_2} - \frac{1}{\gamma_2} + \Theta^k_{i,j}\Big(\frac{\gamma_{12} - \gamma_1\gamma_2 + \gamma_1\kappa_2}{\kappa_2\gamma_2}\Big)\Big)\hat{E}_2, \text{ when } \hat{i} = \hat{j} \end{cases} \tag{4.31}$$

where $\hat{E}_1$ and $\hat{E}_2$ are symmetric matrices with 1 at $(\hat{i}, \hat{j})^{\text{th}}$ and $(\hat{i}_1, \hat{j}_1)^{\text{th}}$ position respectively and 0 elsewhere.

To ensure the positive semi-definiteness of inverse covariance matrix, the update equation will be modified [84, 85] as

$$\begin{aligned} [U_{k+1}, D_{k+1}, V_{k+1}] &= \mathrm{svd}(\Theta^{k+1}) \\ \hat{\Theta}^{k+1} &= U_{k+1}\max(D_{k+1}, 0)V_{k+1} \end{aligned} \tag{4.32}$$

The steps of GSS algorithm when the function f is expressed using Eq. (4.6) are detailed in Algorithm 3.

Implementing the steps detailed in Algorithm 3, an undirected sparse graph/ network structure can be estimated from the data. Finally, to infer the causal direction among the variables in the estimated network, likelihood score as detailed in Section 4.4 is utilised. The overall algorithm of the proposed method is given in Algorithm 4.

Algorithm 3 Sparse Inverse Covariance Estimation using Greedy Sparse Simplex Algorithm

- **Initialization:** Choose $\Theta_0 \in C_s$. Choosing an identity matrix or using as initial guess would be an efficient choice.
- **General step:** For, $k = 0, 1, 2, ...M$
  - If $\|\Theta\|_0 < s$
    - Estimate $(\hat{i}, \hat{j}) = arg\min\{f_{i,j}, i = 1, 2, \cdots, M, j = i, i+1, \cdots, M\}$ where $f_{i,j}$ is defined in Eq. (4.18).
    - If $f_{\hat{i},\hat{j}} < f(\Theta^k)$, update the covariance matrix using Eq. (4.20) and otherwise, stop the iteration.
  - If $\|\Theta\|_0 = s$,
    - Estimate $\{\hat{i}, \hat{j}, \hat{i_1}, \hat{j_1}\} = arg\min\{f^{i,j}_{i_1,j_1}; i_1 = 1, 2, \ldots, M, j_1 = i_1, i_1 + 1, \ldots, M, (i,j) \in I(\Theta^k)\}$ where, $f^{i,j}_{i_1,j_1}$ is defined using Eq. (4.30)
    - If $f^{\hat{i},\hat{j}}_{\hat{i}_1,\hat{j}_1} < f(\Theta^k)$, update parameter vector using Eq. (4.32); otherwise, stop the iteration.

Algorithm 4 Causal Analysis with Sparse Inverse Covariance

1. Estimate sparse inverse covariance matrix Θ using Algorithm 3.
2. Construct the undirected graph from Θ by connecting its non-zero components.
3. Compute pairwise likelihood score among the connected components in the graph using Eq. (4.10).
4. Accept the direction with maximum of computed likelihood score: $\max\left(L^d_{x_i \to x_j}, L^d_{x_j \to x_i}\right)$.
5. Repeat steps 3 & 4 for other pairs of variables.

4.6 Case Studies

To demonstrate the efficacy of the proposed algorithm, two case studies are considered in this work. The first case study is a numerical example where, a constructed system in which interactions among the variables are known a-priori is considered. The second case study is an industrial problem, in which the objective is to construct a causal network for inferring the phenomena of tower flooding and weeping in a deethanizer column associated with fluid catalytic cracking unit. Industrial process is same as the one presented in chapter 3, but for better understanding of the results, process and the problem have been discussed again in detail in the corresponding subsection.

4.6.1 Numerical Example

In this case, data with 6 variables are considered for the study. A network model representing the actual causal relationship among the variables is shown in Figure. 4.2. True inverse covariance or the precision matrix for the network in Figure. 4.2 is given

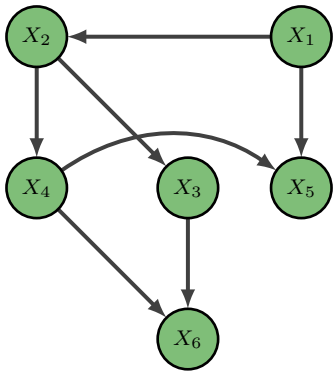

Figure 4.2: Actual network model for numerical case study

as follows.

$$\Theta_{true} = \begin{pmatrix} 14.475 & 4.80 & 0 & 0 & 3.90 & 0 \\ 4.80 & 8.4745 & 1.75 & 6.00 & 0 & 0 \\ 0 & 1.75 & 10.4745 & 0 & 0 & 3.40 \\ 0 & 6.00 & 0 & 11.4745 & 3.80 & 1.90 \\ 3.90 & 0 & 0 & 3.80 & 7.45 & 0 \\ 0 & 0 & 3.40 & 1.90 & 0 & 12.425 \end{pmatrix}$$

Considering the inverse covariance matrix given in Θ_{true} as a reference and with zero mean, 1000 samples of data for each node are generated. Using the computed covariance (S) from the generated data, sparse inverse covariance is estimated from the convex ($ADMM$) and non-convex (proposed) methods for the reconstruction of undirected network structure. Estimates of the inverse covariance matrix obtained using $ADMM$ after thresholding and the proposed GSS method are as follows.

$$\hat{\Theta}_{ADMM} = \begin{pmatrix} 13.51 & 4.35 & 0 & -0.21 & 3.53 & 0 \\ 4.35 & 7.39 & 1.46 & 5.49 & -0.19 & 0 \\ 0 & 1.46 & 10.04 & 0 & 0 & 3.02 \\ -0.21 & 5.49 & 0 & 10.71 & 3.49 & 1.71 \\ 3.53 & -0.19 & 0 & 3.49 & 7.12 & 0 \\ 0 & 0 & 3.02 & 1.71 & 0 & 11.90 \end{pmatrix}$$

$$\hat{\Theta}_{GSS} = \begin{pmatrix} 14.204 & 4.823 & 0 & 0 & 3.763 & 0 \\ 4.823 & 8.165 & 1.69 & 5.709 & 0 & 0 \\ 0 & 1.69 & 10.462 & 0 & 0 & 3.511 \\ 0 & 5.709 & 0 & 11.086 & 3.624 & 1.793 \\ 3.763 & 0 & 0 & 3.624 & 7.284 & 0 \\ 0 & 0 & 3.511 & 1.793 & 0 & 12.178 \end{pmatrix}$$

By connecting the non-zero components of the estimated matrix, it can be noted that the proposed method is able to accurately reconstruct the true underlying structure. On the other hand, spurious connections are present in the estimate obtained using ADMM method. Further to quantify the accuracy of the estimate, Frobenius norm ($\|\cdot\|_F$, defined as the square root of sum of squares of all the elements in the matrix) is computed between $\hat{\Theta}$ and Θ_{true}. For the numerical case study, a value of 0.937 is obtained for GSS and a value of 2.03 for ADMM is obtained. From these results, it can be concluded that the proposed approach provides relatively more accurate estimate compared to its convex counterpart. Also, number of non-zero entries in the estimate obtained using the proposed method is less than that of the estimate obtained using ADMM, from which it can be concluded that the proposed method is promoting better sparsity.

To infer the causal direction, dynamic likelihood score is computed among the variables in the undirected network that is estimated using the proposed method. Scores

computed among the connected nodes in the estimated network are given in Table. 4.1.

Table 4.1: Likelihood scores for Numerical case study

Variable Pairs		$L^d_{x_i \to x_j}$	$L^d_{x_j \to x_i}$	$max\ (Score)$
X_i	X_j			
X_1	X_2	1.9278	1.4276	1.9278
X_1	X_5	2.00	1.3895	2.00
X_2	X_3	0.4610	0.3293	0.4610
X_2	X_4	0.3323	0.1329	0.3323
X_4	X_5	3.01	2.658	3.01
X_3	X_6	0.1964	0.1597	0.1964
X_4	X_6	0.3187	0.3038	0.3187

Using the estimated undirected network structure and the scores computed, directed network that explains the causal relation is constructed and is given in Figure. 4.3.

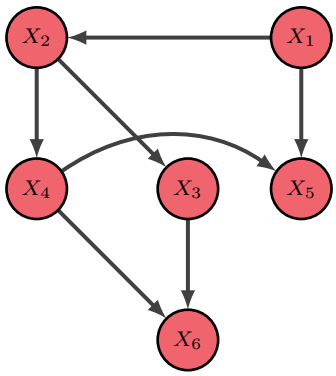

Figure 4.3: Reconstructed causal network using the proposed approach

4.6.2 Industrial Application: Tower Flooding & Weeping

In this section, the proposed method is applied to an industrial case study i.e., tower flooding & weeping problem. Flooding and weeping phenomena can occur in packed columns or tray towers (sieve trays / bubble columns) that are used for separation in process industries. Although flooding can occur in both packed column and tray

towers, weeping will happen only in tray towers. These two phenomena will lead to poor separation efficiency; thereby product quality is reduced and energy consumption is increased. Occasionally, these phenomena may drive the entire process to shutdown for days and weeks, and may sometimes also lead to severe equipment damage. In this particular case study, process upset and process throughput reductions are observed due to flooding and weeping. Therefore, it is essential to analyze the probable reasons for occurrence of such phenomena so that the plant can be operated in a normal mode. In this work, causality analysis is carried out by using the proposed method, in order to identify the source for such problems in tray tower distillation column. In the current study, the flooding and weeping phenomena occurring in the deethanizer column associated with the FCC unit are considered and the results of the proposed method are validated using the underlying physics of the process as well as subsequent application of the proposed solution in the actual process.

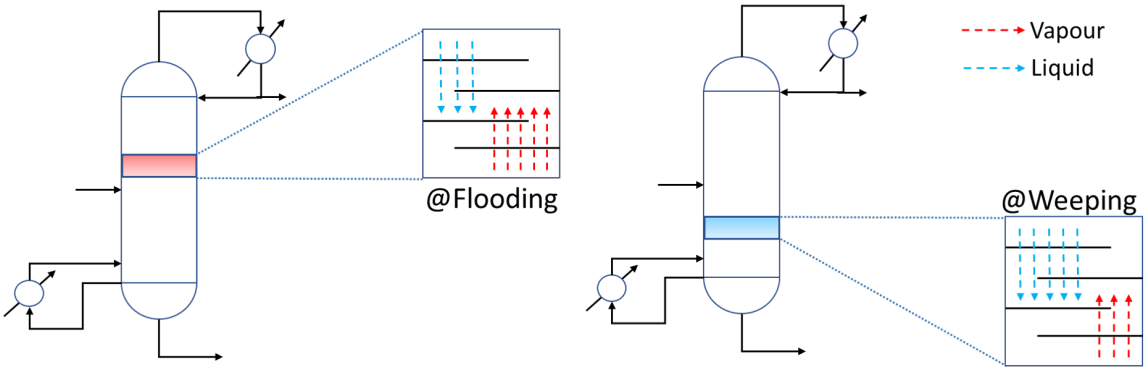

Figure 4.4: Illustration of Flooding & Weeping

Process description

In this study, Fluid Catalytic Cracking (FCC) and process units associated with it in the upstream and the downstream such as feed preheating unit, fractionator unit, condenser and deethanizer column are considered. A schematic of the entire process is given in Figure 4.5.

In this process, the products from the hydro-treating units enter the feed preheating unit as feed. Once the preheating is complete, feed enters the FCC unit where it undergoes cracking in the presence of catalyst. After cracking, the product enters the fractionator unit as feed in gaseous phase. During the separation, multiple side cuts are drawn at different temperatures and finally top product from the separation enters the condenser. The products from the condenser enters the storage tank-1 and then

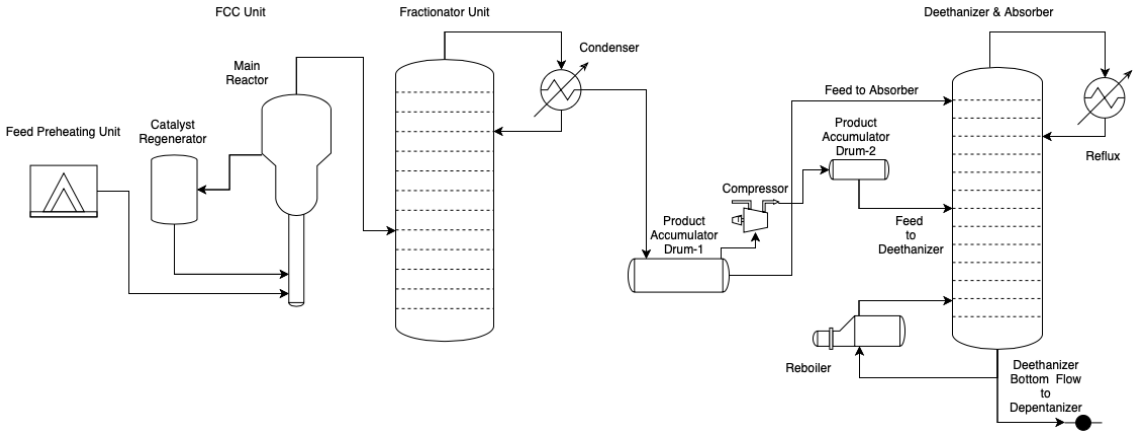

Figure 4.5: Schematic of the Industrial Process

splits into two streams, where the product in one of the streams enters the absorber and the product in the other stream is compressed and enters the deethanizer via storage tank-2 for further separation. Deethanizer unit has reboiler at the bottom and reflux on the top. In this process, reboiler is used as control handle to maintain the temperature of the trays at the bottom section of the deethanizer and at the same time, the tray temperatures are used to control the phenomena of flooding. Finally, the products from the bottom of the deethanizer are processed for further separation.

Flooding is a phenomenon in which liquid flowing in the counter-current direction from top of the distillation column gets entrained in the tray of a column due to the flow of vapour at high pressure from the bottom of the column. Similarly, weeping is the phenomenon that happens in a tray tower when the liquid starts flowing down through the sieve holes due to the lack of pressure exerted by the vapour flowing upwards. Both these phenomena are illustrated in Figure 4.4. Based on the process knowledge, a total of four hypotheses are expected to be the possible cause for the onset of either flooding or weeping in the deethanizer and these four possible hypothesis are listed below. It is to be noted that the existing method reported in the literature [86] utilises pressure drop information from the column to detect the on-set of flooding. In the present case study, the pressure drop information is not available and hence flooding and the primary causes for flooding are identified through other source variables determined by causal analysis.

Hypothesis-1

First hypothesis is considered to be the change of feed flowing into the Fluid catalytic cracking unit. Whenever there is a drastic feed change in FCC unit, it leads to

reduction in flow of feed to the subsequent process units. Eventually, this reduces the feed for the deethanizer. When feed for the deethanizer reduces, pre-occupied liquid in the bottom of the column vaporizes at higher rate and this causes flooding.

Hypothesis-2

Second hypothesis is with respect to the abnormal temperature in reboiler associated with the deethanizer. When increase of the temperature of the reboiler is not related to the feed entering the deethanizer, bottom tray temperature of the unit increases the flow of vapour inside the column. This excessive flow of vapour inside the column eventually causes flooding.

Hypothesis-3

Third hypothesis considers feed temperature of the deethanizer. When feed temperature increases at slower rate, energy balance of the column changes thereby causing flooding.

Hypothesis-4

Fourth hypothesis is associated with weeping. Based on the knowledge obtained from process operation, it is understood that improper control of flooding leads to weeping due to sudden change in operating condition of the deethanizer.

In the following subsection, nature of the process data will be detailed.

Process Data

In order to estimate the sparse inverse covariance matrix, process data from routine operation is considered. The process data includes 67 process variables such as flow rates, pressure and temperature associated with the process units (Figure 4.5). They are sampled every minute, over the period of five months i.e., approximately 200,000 samples.

Outcome

Upon computing the sample covariance from process data, sparse inverse covariance is estimated and causal direction is computed using dynamic likelihood score. Sparse inverse covariance estimated using greedy sparse simplex is given in Figure. 4.6 and

the one estimated using ADMM is given in Figure. 4.7.

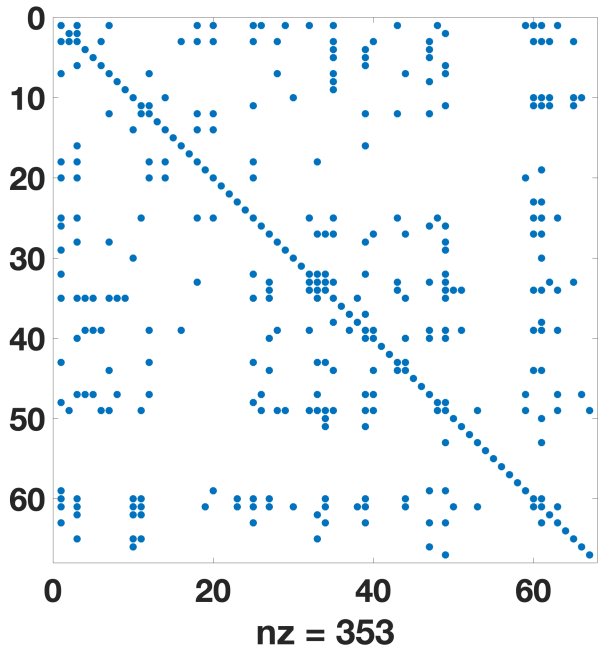

Figure 4.6: Estimate of the Proposed Method

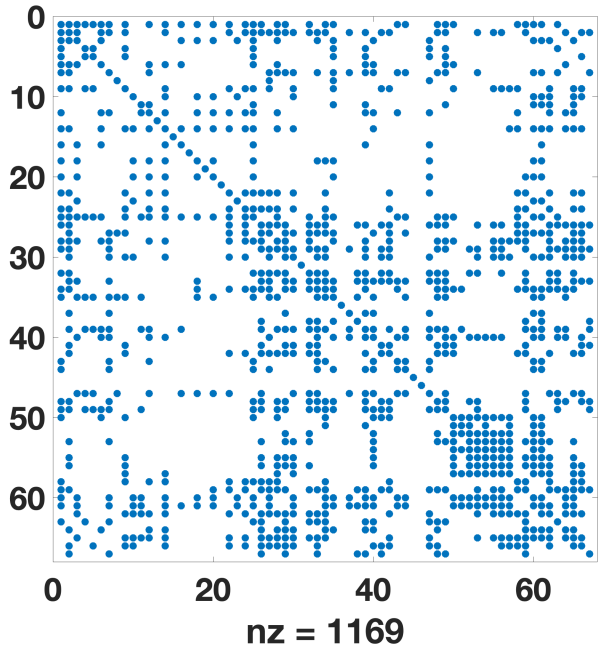

Figure 4.7: ADMM Estimate

In the given estimate, non-zero components represented in blue are connected to

reconstruct relationship among the variables. It can also be noted that the proposed method is promoting more sparsity than ADMM. Hence, the estimate obtained using the proposed method is used for the further analysis.

Since the primary objective of this work is to infer the causal map for the flooding and weeping phenomena, process variables that are associated to these indicators are used in the analysis. In Figure. 4.6, the first row has the information of flooding indicator and variables that are associated with it, and similarly, the third and eighteenth rows have the information of weeping and variables associated with them. Also, the variables that are redundant are not considered for causal analysis and the physical interpretation of the remaining associated variables are given in Table. 4.2.

Undirected graph constructed among the subset of variables associated with flooding and weeping is illustrated in Figure 4.8. In the graph, flooding and weeping indicators are shown in red and rest all in green. Upon constructing the undirected graph, direction of cause and the effect is inferred using likelihood score and the scores are given in Table. 4.3.

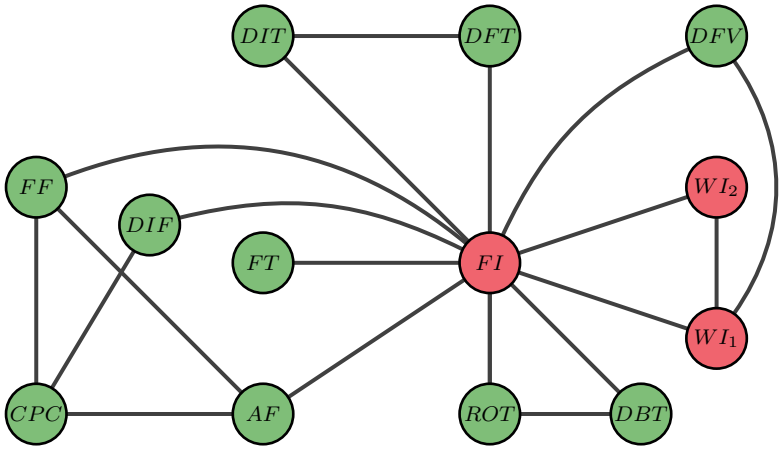

Figure 4.8: Estimated undirected graph for Flooding and Weeping

Using the information of dynamic likelihood score, presented in Table. 4.3, information of causal direction is incorporated to the undirected graph and the resulting causal network is presented in Figure. 4.9. To validate the causal network, connections in the network are interpreted using process knowledge. In the causal network, four primary variables for flooding and one primary variable for weeping have been indicated as possible primary cause along with their relation with other process variables. In the case of flooding, proposed approach indicates that changes in FF, DFT, ROT and FT have direct effect on FI. Along with this, the effect of propagation occurring

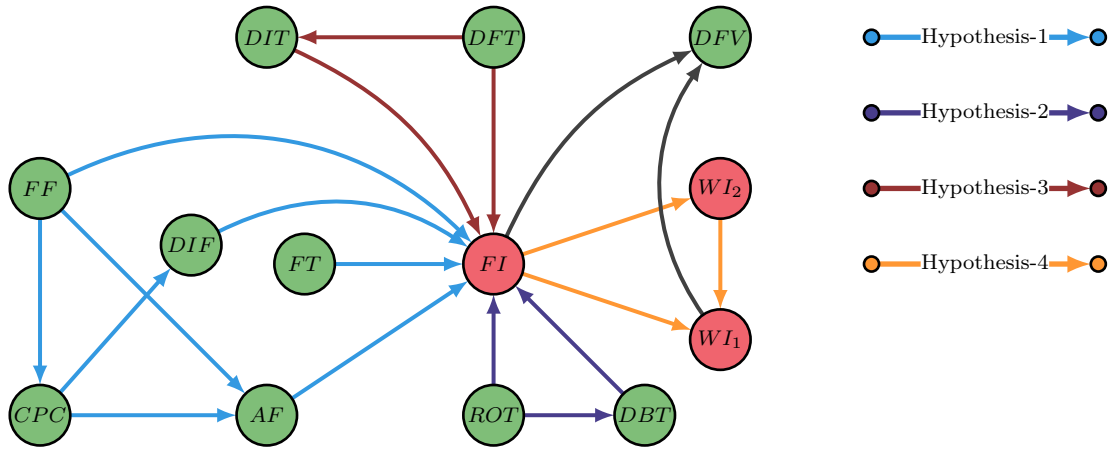

Figure 4.9: Causal Network for Flooding and Weeping

due to the change in the primary causal variables has been indicated through CPC, AF, DIF, DIT and DBT. Individually, change in FF and CPC, causes AF and DIF to change thereby reducing the flow of liquid into the deethanizer. At the same time, change in ROT causes DBT to change thereby increasing the temperature at the bottom section of the deethanizer. Similarly, change in FT and DFT will contribute to the change in temperature inside the deethanizer by increasing the temperature of the feed, which eventually leads to undesired operating condition. Considering the changes in FF and ROT simultaneously along with the changes in FT and DFT, it can be noticed that the outcomes achieved with the proposed method validates the reasons for flooding explained by hypothesis-1, hypothesis-2 and hypothesis-3. Similarly, for weeping, it can be noticed that flooding (FI) causes weeping (WI_1 and WI_2) and among the weeping indicators, WI_2 causes WI_1. In comparison of this outcome with the process knowledge explained in hypothesis-4, it is understood that control of flooding leads to change in conditions inside the deethanizer thereby causing weeping. However, if the control of flooding is performed in a timely manner, with a good flooding predictor, weeping can be avoided. Among the weeping indicators, WI_2 is located closer to FI and WI_1 is measured at the bottom of the deethanizer. Therefore, due to the system delay, WI_2 causes WI_1. Then, at last, effects of flooding and weeping gets encoded in DFV. The end result of causal network estimation using the proposed method helped us to identify the reasons, that are physically interpretable, for the problem of flooding and weeping in the deethanizer.

4.7 Summary

In this chapter, a two-step approach has been proposed for causal analysis. In the first step, a sparse undirected network is reconstructed from sparse inverse covariance matrix with correlation information and in the second step the causal direction is determined using dynamic likelihood score. In the proposed method, a L_0 norm constraint is considered while estimating the sparse inverse covariance matrix and the resultant problem is solved using greedy sparse simplex algorithm. The algorithm is suitably modified by incorporating positive semi-definite constraint on the decision variable. The efficiency of the proposed approach has been demonstrated using a numerical example and an industrial case study. In particular, the main objective of industrial case study is to infer causal relationships in order to address the problem of flooding and weeping in deethanizer unit. From the results, it is observed that the proposed method is able to identify causal connections accurately for both numerical and industrial case studies. From the results of industrial case study, it can be further concluded that the probable reasons for flooding phenomena in a deethanizer unit are the drastic feed change for FCC unit, deethanizer feed temperature and the reboiler temperature of deethanizer. Similarly, flooding is considered to be the probable reason for occurrence of weeping in the deethanizer unit.

Table 4.2: Process variables description

Symbol	Process Variable Description	Symbol	Process Variable Description
ROT	Reboiler Outlet Temperature	WI_1 &WI_2	Weeping Indicator - (1 & 2) (Deeth. Tray Temp.)
FF	Feed for FCC Unit	DIF	Deethanizer Inlet Flow
AF	Feed for Absorber	DBT	Deethanizer Bottom Tray Temperature
FT	Temperature in FCC Unit	DFT	Deethanizer Feed Temperature (From storage tank-2)
DIT	Deethanizer Inlet Flow Temperature	CPC	Wet Gas Compressor Pressure
FI	Flooding Indicator (Flow variable)	DFV	Deethanizer Bottom Flow variable

Table 4.3: Dynamic Likelihood scores for Flooding & Weeping problem

Variable Pairs		$L^d_{x_i \to x_j}$	$L^d_{x_j \to x_i}$	$max(Score)$	Variable Pairs		$L^d_{x_i \to x_j}$	$L^d_{x_j \to x_i}$	$max(Score)$
X_i	X_j				X_i	X_j			
FF	FI	12.76	11.06	12.76	WI_2	FI	10.78	12.96	12.96
FT	FI	13.91	11.50	13.91	FF	CPC	12.64	10.23	12.64
AF	FI	12.67	11.57	12.67	FF	AF	16.35	15.02	16.35
ROT	FI	16.12	12.60	16.12	CPC	AF	12.76	11.56	12.76
DBT	FI	15.88	12.97	15.88	WI_1	WI_2	10.40	16.79	16.79
DIT	FI	16.64	12.48	16.64	DIT	DFT	15.03	16.54	16.54
DFT	FI	14.20	11.33	14.20	DFV	WI_1	14.49	16.45	16.45
DFV	FI	12.22	13.30	13.30	ROT	DBT	21.54	20.09	21.54
WI_1	FI	12.52	14.52	14.52	CPC	DIF	11.44	13.05	13.05
DIF	FI	12.81	11.28	12.81					

Chapter 5

Conclusions & Recommendations

5.1 Conclusions

In this thesis work, we have investigated the problem of data reconciliation and causal inference in the framework of probabilistic graphical models. Key findings of the work are summarized as follows.

- In Chapter 2, we addressed the problem of data reconciliation for linear systems with state uncertainties using Bayesian network framework. In the course of addressing the problem, conditions have been provided to construct the Bayesian network from process network, solution method has been proposed to construct acyclic Bayesian network structure from process network with recycle and this methodology has been extended to address reconciliation in partially measured system. Using the Bayesian network, states are inferred using statistical inference techniques such as maximum likelihood estimation and maximum-a-posteriori estimation. Later, state and measurement noise statistics are estimated simultaneously with the states using the proposed Particle-EM algorithm.

- In the second part of the thesis, we presented a complete data-driven approach and a framework combining the data-driven model with the process knowledge for causal inference using process data. In Chapter 3, a methodology is proposed for the prediction of flooding and weeping using the concept of causality. In the proposed approach, causal network is reconstructed using sparsity con-

strained finite impulse response model coupled with process knowledge such as process connectivity and physics of the process. In the course of addressing the problem, L_0 norm constraint is introduced in the FIR model identification step in order to achieve at most sparse solution and analytical expressions are derived accordingly using the greedy sparse simplex framework. Information obtained in the reconstructed causal network has been used to construct logical monitoring rules for the prediction of flooding and weeping in process operation. The proposed approach has been demonstrated in an industrial application of predicting flooding and weeping in a deethanizer column. Final outcome has been used by the industry to improve the decision making in real-time, which has lead to the prevention of multiple flooding and weeping events during the routine process operation.

- In Chapter 4, a two-step method is proposed for the data-driven approach for causal inference, where in the first step, undirected graph structure is inferred using sparse inverse covariance estimation. Then in the second step, estimated undirected graph is integrated with causality measure to reconstruct the causal network from process data. In sparse inverse covariance estimation, L_0 norm constraint is considered and the resulting non-convex optimization problem is solved in the framework of greedy sparse simplex. The efficacy of the proposed approach is demonstrated in a numerical case study and in an industrial application of flooding and weeping.

5.2 Recommendations

Based on the problems addressed in this thesis, following are some of the recommendations for future work. Since the thesis consists of two different problems, recommendations are presented in two subsections.

5.2.1 Data Reconciliation

1. In the proposed data reconciliation approach, only linear systems with Gaussian uncertainty is considered for the study. This approach can also be extended for non-linear system with non-Gaussian uncertainty.

2. In conventional data reconciliation, it is common to notice that not all the states are measured. In such scenarios, no measurement will be available for certain states. Data reconciliation with non availability of measurements of some particular states can be extended for randomly missing state measurements.

5.2.2 Causal Inference

1. In sparse inverse covariance estimation problem, sample covariance S computed from the data will be accurate if only if the relationship among the random variables are linear. At the same time, inverse covariance estimation problem assumes the random variable to be Gaussian. These assumptions can be relaxed and the proposed method can be extended to network reconstruction for non-Gaussian random variable and possibly for non-linear system.

2. In process industries, it is common to have measurements sampled at different rates thereby making the time scales different from one variable to another. Usually, in time domain causality analysis, data are assumed to be sampled at regular intervals for all the variables. Hence, this problem of causality analysis with multi-rate sampled data can be an interesting one to address.

3. The problem of causal network reconstruction can be formulated in the framework of reinforcement learning, where the RL agent can be utilized to intervene the variables. Based on the reward obtained for particular intervention, edges can be determined among the variables leading to a causal network.

4. From process perspective, flooding and weeping problems are predominant in almost all the process industries dealing with columns for separation. In this context, transfer learning can be integrated with causal analysis, where the causal knowledge obtained from one particular process can be transferred to the process having same issues.

Bibliography

[1] R. S. Mah, G. M. Stanley, and D. M. Downing, "Reconcillation and rectification of process flow and inventory data," *Industrial & Engineering Chemistry Process Design and Development*, vol. 15, no. 1, pp. 175–183, 1976.

[2] Z. Ge, Z. Song, S. X. Ding, and B. Huang, "Data mining and analytics in the process industry: The role of machine learning," *Ieee Access*, vol. 5, pp. 20590–20616, 2017.

[3] S. J. Qin and L. H. Chiang, "Advances and opportunities in machine learning for process data analytics," *Computers & Chemical Engineering*, vol. 126, pp. 465–473, 2019.

[4] S. Sedghi, R. Tan, and B. Huang, "Data analytics approach for online produced fluid flow rate estimation in sagd process," *Computers & Chemical Engineering*, vol. 136, p. 106766, 2020.

[5] Q. Jiang, X. Yan, and B. Huang, "Review and perspectives of data-driven distributed monitoring for industrial plant-wide processes," *Industrial & Engineering Chemistry Research*, vol. 58, no. 29, pp. 12899–12912, 2019.

[6] D. Koller and N. Friedman, *Probabilistic graphical models: principles and techniques*. MIT press, 2009.

[7] R. Raveendran and B. Huang, "Conjugate exponential family graphical models in process monitoring: A tutorial review," *Chemometrics and Intelligent Laboratory Systems*, p. 104095, 2020.

[8] A. Beck and Y. C. Eldar, "Sparsity constrained nonlinear optimization: Optimality conditions and algorithms," *SIAM Journal on Optimization*, vol. 23, no. 3, pp. 1480–1509, 2013.

[9] S. Narasimhan and C. Jordache, *Data reconciliation and gross error detection: An intelligent use of process data*. Elsevier, 1999.

[10] L. P. Johnston and M. A. Kramer, "Maximum likelihood data rectification: Steady-state systems," *AIChE Journal*, vol. 41, no. 11, pp. 2415–2426, 1995.

[11] I. Tjoa and L. T. Biegler, "Simultaneous strategies for data reconciliation and gross error detection of nonlinear systems," *Computers & chemical engineering*, vol. 15, no. 10, pp. 679–690, 1991.

[12] T. Lid and S. Skogestad, "Scaled steady state models for effective on-line applications," *Computers & Chemical Engineering*, vol. 32, no. 4-5, pp. 990–999, 2008.

[13] S. Narasimhan and N. Bhatt, "Deconstructing principal component analysis using a data reconciliation perspective," *Computers & Chemical Engineering*, vol. 77, pp. 74–84, 2015.

[14] K. Marimuthu and S. Narasimhan, "Nonlinear model identification and data reconciliation using kernel principal component regression," *Industrial & Engineering Chemistry Research*, vol. 58, no. 26, pp. 11224–11233, 2019.

[15] Y. Yuan, S. Khatibisepehr, B. Huang, and Z. Li, "B ayesian method for simultaneous gross error detection and data reconciliation," *AIChE Journal*, vol. 61, no. 10, pp. 3232–3248, 2015.

[16] H. Alighardashi, N. M. Jan, and B. Huang, "Expectation maximization approach for simultaneous gross error detection and data reconciliation using gaussian mixture distribution," *Industrial & Engineering Chemistry Research*, vol. 56, no. 49, pp. 14530–14544, 2017.

[17] A. Vasebi, É. Poulin, and D. Hodouin, "Selecting proper uncertainty model for steady-state data reconciliation–application to mineral and metal processing industries," *Minerals Engineering*, vol. 65, pp. 130–144, 2014.

[18] S. Narasimhan and S. Narasimhan, "Data reconciliation using uncertain models," *International Journal of Advances in Engineering Sciences and Applied Mathematics*, vol. 4, no. 1-2, pp. 3–9, 2012.

[19] D. Maquin, O. Adrot, and J. Ragot, "Data reconciliation with uncertain models," *ISA transactions*, vol. 39, no. 1, pp. 35–45, 2000.

[20] S. J. Hashemi, F. Khan, and S. Ahmed, "Multivariate probabilistic safety analysis of process facilities using the copula bayesian network model," *Computers & Chemical Engineering*, vol. 93, pp. 128–142, 2016.

[21] H. Gharahbagheri, S. Imtiaz, and F. Khan, "Root cause diagnosis of process fault using kpca and bayesian network," *Industrial & Engineering Chemistry Research*, vol. 56, no. 8, pp. 2054–2070, 2017.

[22] Q.-X. Zhu, Y. Luo, and Y.-L. He, "Novel multiblock transfer entropy based bayesian network and its application to root cause analysis," *Industrial & Engineering Chemistry Research*, vol. 58, no. 12, pp. 4936–4945, 2019.

[23] J. Mori and V. Mahalec, "Planning and scheduling of steel plates production. part i: Estimation of production times via hybrid bayesian networks for large domain of discrete variables," *Computers & Chemical Engineering*, vol. 79, pp. 113–134, 2015.

[24] M. Sadeghi, D. Hodouin, and C. Bazin, "Mineral processing plant data reconciliation including mineral mass balance constraints," *Minerals Engineering*, vol. 123, pp. 117–127, 2018.

[25] E. C. do Valle, R. de Araújo Kalid, A. R. Secchi, and A. Kiperstok, "Collection of benchmark test problems for data reconciliation and gross error detection and identification," *Computers & Chemical Engineering*, vol. 111, pp. 134–148, 2018.

[26] D. Vogan, "Gauss elimination," *MIT OpenCourseWare*, 2013.

[27] C. Crowe, Y. G. Campos, and A. Hrymak, "Reconciliation of process flow rates by matrix projection. part i: Linear case," *AIChE Journal*, vol. 29, no. 6, pp. 881–888, 1983.

[28] M. Sanchez and J. Romagnoli, "Use of orthogonal transformations in data classification-reconciliation," *Computers & chemical engineering*, vol. 20, no. 5, pp. 483–493, 1996.

[29] J. E. Gentle, *Numerical linear algebra for applications in statistics*. Springer Science & Business Media, 2012.

[30] N. R. Kristensen, H. Madsen, and S. B. Jørgensen, "Parameter estimation in stochastic grey-box models," *Automatica*, vol. 40, no. 2, pp. 225–237, 2004.

[31] J. Valluru, P. Lakhmani, S. C. Patwardhan, and L. T. Biegler, "Development of moving window state and parameter estimators under maximum likelihood and bayesian frameworks," *Journal of Process Control*, vol. 60, pp. 48–67, 2017.

[32] R. C. Neath *et al.*, "On convergence properties of the monte carlo em algorithm," in *Advances in modern statistical theory and applications: a Festschrift in Honor of Morris L. Eaton*, pp. 43–62, Institute of Mathematical Statistics, 2013.

[33] G. C. Wei and M. A. Tanner, "A monte carlo implementation of the em algorithm and the poor man's data augmentation algorithms," *Journal of the American statistical Association*, vol. 85, no. 411, pp. 699–704, 1990.

[34] R. A. Levine and G. Casella, "Implementations of the monte carlo em algorithm," *Journal of Computational and Graphical Statistics*, vol. 10, no. 3, pp. 422–439, 2001.

[35] S. Borman, "The expectation maximization algorithm-a short tutorial," *Submitted for publication*, vol. 41, 2004.

[36] W. M. Bolstad, *Understanding computational Bayesian statistics*, vol. 644. John Wiley & Sons, 2009.

[37] N. P. Lieberman, *Troubleshooting process operations*. PennWell Books, 1991.

[38] T. Barletta, J. Nigg, J. Mayfield, and W. Landry, "Diagnose flooding columns efficiently," *Hydrocarbon Processing*, vol. 80, no. 7, pp. 71–75, 2001.

[39] P. Spirtes and K. Zhang, "Causal discovery and inference: concepts and recent methodological advances," in *Applied informatics*, vol. 3, p. 3, Springer, 2016.

[40] J. Mori, V. Mahalec, and J. Yu, "Identification of probabilistic graphical network model for root-cause diagnosis in industrial processes," *Computers & chemical engineering*, vol. 71, pp. 171–209, 2014.

[41] T. Yuan and S. J. Qin, "Root cause diagnosis of plant-wide oscillations using granger causality," *Journal of Process Control*, vol. 24, no. 2, pp. 450–459, 2014.

[42] L. Barnett and T. Bossomaier, "Transfer entropy as a log-likelihood ratio," *Physical review letters*, vol. 109, no. 13, p. 138105, 2012.

[43] M. Eichler, "Causal inference with multiple time series: principles and problems," *Philosophical Transactions of the Royal Society A: Mathematical, Physical and Engineering Sciences*, vol. 371, no. 1997, p. 20110613, 2013.

[44] C. W. Granger, "Investigating causal relations by econometric models and cross-spectral methods," *Econometrica: journal of the Econometric Society*, pp. 424–438, 1969.

[45] A. Bolstad, B. D. Van Veen, and R. Nowak, "Causal network inference via group sparse regularization," *IEEE transactions on signal processing*, vol. 59, no. 6, pp. 2628–2641, 2011.

[46] X. Han, Z. Shen, W.-X. Wang, and Z. Di, "Robust reconstruction of complex networks from sparse data," *Physical review letters*, vol. 114, no. 2, p. 028701, 2015.

[47] S. Kathari and A. K. Tangirala, "Efficient reconstruction of granger-causal networks in linear multivariable dynamical processes," *Industrial & Engineering Chemistry Research*, vol. 58, no. 26, pp. 11275–11294, 2019.

[48] Z. Zhang, Y. Xu, J. Yang, X. Li, and D. Zhang, "A survey of sparse representation: algorithms and applications," *IEEE access*, vol. 3, pp. 490–530, 2015.

[49] K. Kampa, S. Mehta, C.-A. Chou, W. A. Chaovalitwongse, and T. J. Grabowski, "Sparse optimization in feature selection: application in neuroimaging," *Journal of Global Optimization*, vol. 59, no. 2-3, pp. 439–457, 2014.

[50] A. J. Seneviratne and V. Solo, "On vector l0 penalized multivariate regression," in *2012 IEEE International Conference on Acoustics, Speech and Signal Processing (ICASSP)*, pp. 3613–3616, IEEE, 2012.

[51] R. Tibshirani, "Regression shrinkage and selection via the lasso," *Journal of the Royal Statistical Society: Series B (Methodological)*, vol. 58, no. 1, pp. 267–288, 1996.

[52] H. Zou and T. Hastie, "Regularization and variable selection via the elastic net," *Journal of the royal statistical society: series B (statistical methodology)*, vol. 67, no. 2, pp. 301–320, 2005.

[53] S. Boyd, N. Parikh, E. Chu, B. Peleato, and J. Eckstein, "Distributed optimization and statistical learning via the alternating direction method of multipliers," *Foundations and Trends in Machine Learning*, vol. 3, no. 1, pp. 1–122, 2011.

[54] S.-J. Kim, K. Koh, M. Lustig, S. Boyd, and D. Gorinevsky, "An interior-point method for large-scale l_1-regularized least squares," *IEEE journal of selected topics in signal processing*, vol. 1, no. 4, pp. 606–617, 2007.

[55] J. A. Tropp, "Greed is good: algorithmic results for sparse approximation," *IEEE Transactions on Information Theory*, vol. 50, no. 10, pp. 2231–2242, 2004.

[56] V. S. Pinnamaraju and A. K. Tangirala, "Identification of fir models for lti multiscale systems using sparse optimization techniques," *IFAC-PapersOnLine*, vol. 51, no. 1, pp. 542–547, 2018.

[57] B. S. Dayal and J. F. MacGregor, "Identification of finite impulse response models: methods and robustness issues," *Industrial & engineering chemistry research*, vol. 35, no. 11, pp. 4078–4090, 1996.

[58] C. Glymour, K. Zhang, and P. Spirtes, "Review of causal discovery methods based on graphical models," *Frontiers in genetics*, vol. 10, p. 524, 2019.

[59] J. Runge, S. Bathiany, E. Bollt, G. Camps-Valls, D. Coumou, E. Deyle, C. Glymour, M. Kretschmer, M. D. Mahecha, J. Muñoz-Marí, *et al.*, "Inferring causation from time series in earth system sciences," *Nature communications*, vol. 10, no. 1, pp. 1–13, 2019.

[60] F. Yang, P. Duan, S. L. Shah, and T. Chen, *Capturing connectivity and causality in complex industrial processes*. Springer Science & Business Media, 2014.

[61] M. Kamiński, "Determination of transmission patterns in multichannel data," *Philosophical Transactions of the Royal Society B: Biological Sciences*, vol. 360, no. 1457, pp. 947–952, 2005.

[62] R. Raveendran and B. Huang, "Variational bayesian approach for causality and contemporaneous correlation features inference in industrial process data," *IEEE transactions on cybernetics*, vol. 49, no. 7, pp. 2580–2590, 2018.

[63] M. Kalisch and P. Bühlmann, "Estimating high-dimensional directed acyclic graphs with the pc-algorithm," *Journal of Machine Learning Research*, vol. 8, no. Mar, pp. 613–636, 2007.

[64] J. Peters, D. Janzing, and B. Schölkopf, *Elements of causal inference*. The MIT Press, 2017.

[65] G. Michailidis and F. d'Alché Buc, "Autoregressive models for gene regulatory network inference: Sparsity, stability and causality issues," *Mathematical biosciences*, vol. 246, no. 2, pp. 326–334, 2013.

[66] S. Haufe, K.-R. Müller, G. Nolte, and N. Krämer, "Sparse causal discovery in multivariate time series," in *Causality: Objectives and Assessment*, pp. 97–106, 2010.

[67] K. Kampa, S. Mehta, A. Chou, Chun, W. A. Chaovalitwongse, and T. J. Grabowski, "Sparse optimization in feature selection: application in neuroimaging," *Journal of Global Optimization*, vol. 59, no. 2-3, pp. 439–457, 2014.

[68] Z. Zhang, Y. Xu, J. Yang, X. Li, and D. Zhang, "A survey of sparse representation: algorithms and applications," *IEEE access*, vol. 3, pp. 490–530, 2015.

[69] M. Nagahara, D. Chatterjee, N. Challapalli, and M. Vidyasagar, "Clot norm minimization for continuous hands-off control," *Automatica*, vol. 113, p. 108679, 2020.

[70] G. Marjanovic and A. O. Hero, "$l\_\{0\}$ sparse inverse covariance estimation," *IEEE Transactions on Signal Processing*, vol. 63, no. 12, pp. 3218–3231, 2015.

[71] A. d'Aspremont, O. Banerjee, and L. El Ghaoui, "First-order methods for sparse covariance selection," *SIAM Journal on Matrix Analysis and Applications*, vol. 30, no. 1, pp. 56–66, 2008.

[72] J. Friedman, T. Hastie, and R. Tibshirani, "Sparse inverse covariance estimation with the graphical lasso," *Biostatistics*, vol. 9, no. 3, pp. 432–441, 2008.

[73] K. Scheinberg, S. Ma, and D. Goldfarb, "Sparse inverse covariance selection via alternating linearization methods," in *Advances in neural information processing systems*, pp. 2101–2109, 2010.

[74] J. Fan, Y. Feng, and Y. Wu, "Network exploration via the adaptive lasso and scad penalties," *The annals of applied statistics*, vol. 3, no. 2, p. 521, 2009.

[75] D. Janzing and B. Schölkopf, "Causal inference using the algorithmic markov condition," *IEEE Transactions on Information Theory*, vol. 56, no. 10, pp. 5168–5194, 2010.

[76] L. Qiao, L. Zhang, S. Chen, and D. Shen, "Data-driven graph construction and graph learning: A review," *Neurocomputing*, vol. 312, pp. 336–351, 2018.

[77] S. L. Lauritzen, *Graphical models*, vol. 17. Clarendon Press, 1996.

[78] J. A. Troop, "Greed is good: Algorithmic results for sparse approximation," *IEEE Transactions on Information Theory*, vol. 50, no. 10, pp. 2231–2242, 2004.

[79] J. M. Mooij, J. Peters, D. Janzing, J. Zscheischler, and B. Schölkopf, "Distinguishing cause from effect using observational data: methods and benchmarks," *The Journal of Machine Learning Research*, vol. 17, no. 1, pp. 1103–1204, 2016.

[80] V. Solo, "On causality and mutual information," in *2008 47th IEEE Conference on Decision and Control*, pp. 4939–4944, IEEE, 2008.

[81] S. Kpotufe, E. Sgouritsa, D. Janzing, and B. Schölkopf, "Consistency of causal inference under the additive noise model," in *International Conference on Machine Learning*, pp. 478–486, 2014.

[82] K. S. Miller, "On the inverse of the sum of matrices," *Mathematics Magazine*, vol. 54, no. 2, pp. 67–72, 1981.

[83] V. V. Monov, "A family of symmetric polynomials of the eigenvalues of a matrix," *Linear algebra and its applications*, vol. 429, no. 8-9, pp. 2199–2208, 2008.

[84] Z. Liu, A. Hansson, and L. Vandenberghe, "Nuclear norm system identification with missing inputs and outputs," *Systems & Control Letters*, vol. 62, no. 8, pp. 605–612, 2013.

[85] S. K. Varanasi and P. Jampana, "Nuclear norm subspace identification of continuous time state–space models with missing outputs," *Control Engineering Practice*, vol. 95, p. 104239, 2020.

[86] G. E. Dzyacky, "Distillation column flooding predictor," tech. rep., George E. Dzyacky, Principal Investigator; Seprations Research Program ..., 2010.

[87] T. M. Cover, *Elements of information theory*. John Wiley & Sons, 1999.

Appendices

Appendix A

A.1 Hyper-parameter Selection

Selection of hyper-parameter is important in sparse modelling to obtain optimal model structure. In the present work, both Akaike Information Criteria (AIC) and Bayesian Information Criteria (BIC) are computed and best outcome is used to determine the optimal sparse model structure. Expressions for computing AIC and BIC can be presented as follows.

$$AIC = 2k - 2\ \ln(\hat{L})$$

$$BIC = k\ \ln(n) - 2\ \ln(\hat{L})$$

where, k is the number of model parameters to be estimated, $\hat{L}$ is the maximum likelihood value of the function and n is sample dimension. In order to obtain optimal model structure, both AIC and BIC are computed for the problem presented in Eq. 3.7 for different values of α. Then, optimal hyper-parameter, α_{opt} is selected corresponding to the minimum value of information criterion.

A.2 Zero Norm Constrained Optimization Algorithm: Greedy Methods

In this section, a brief description of L_0 norm minimization problem is discussed by considering a general non-linear function $f(\theta)$. The sparsity constrained optimization

problem can be represented as

$$\min_{\theta} \ f(\theta)$$
$$s.t. \ \|\theta\|_0 \leq s$$

where, the loss function $f(\theta)$ is assumed to be smooth and lower bounded; $\|\theta\|_0$ represents L_0 norm of the parameter vector. s is an integer which controls the level of sparsity. Further, it is also assumed that the loss function can be either convex or non-convex. Based on the assumptions mentioned above, several optimization algorithms are tailored to handle such problems [8]. Some of the algorithms detailed in [8] are guaranteed to converge to a basic feasible (BF) vector and some are guaranteed to converge to a co-ordinate wise minimum (CW-minimum). The definitions of BF-vector and CW-minimum are given in Appendix A.2.1 for the sake of completeness. In the hierarchy of optimal solutions, any optimal point is a CW-minimum and any CW-minimum is a BF-vector. Insights on the optimality conditions and the convergence properties can be obtained from [8]. Therefore, in the current work, the greedy sparse simplex (GSS) algorithm, which is guaranteed to converge to a CW-minimum is used to solve the L_0 norm minimization problem and the algorithmic sequence of GSS approach is detailed in Algorithm 5

In the GSS algorithm, the main idea is to perturb the parameter vector $\theta \in C_s$ sequentially in each direction and the parameters are updated by using Eq. (A.3) & (A.6) based on the optimal δ. This routine is continued until an optimal θ for the specified level of sparsity s is obtained. The sequence of perturbation at every iteration is achieved using the indicator vector e_i, which denotes the vector whose i^{th} element is 1 and rest all zero. An optimal δ in Eq. (A.1) and Eq. (A.4) can be obtained by using first order methods, where the derivatives of the functions in Eqs. (A.1) & (A.4) with respect to δ are equated to zero. Several search based methods such as simplex-method or genetic algorithms can also be incorporated to estimate the optimal δ. However, it is to be noted that, if the objective function is convex, first order methods provide advantage over search based methods in terms of computation time for convergence. Therefore, first order methods are generally preferred for convex objective functions.

A.2.1 Basic feasible vector and CW-Minimum

Letting the set of all vectors with at most s non-zero elements in each vector be denoted as C_s and $I(\theta)$ represents the indices of non-zero elements in the vector θ,

Algorithm 5 Greedy Sparse Simplex Algorithm

- **Initialization:** Choose $\theta_0 \in C_s$ (Set of all vectors with at most s nonzero elements in each vector)
- **General step:** $k = 0, 1, 2, ...Iter$
  - If $\|\theta^k\|_0 < s$, define e_i to be an indicator vector whose i^{th} element is one and rest all zero. Compute for every $i = 1, 2, ...N$

$$\delta_i \in arg\min_{\delta \in \mathbb{R}} f(\theta^k + \delta e_i) \tag{A.1}$$

$$f_i = f(\theta^k + \delta_i e_i) \tag{A.2}$$

    Let $(i_k \in arg\min_{i=1,..N} f_i)$. If $f_{i_k} < f(\theta^k)$, then set

$$\theta^{k+1} = \theta^k + \delta_{i_k} e_{i_k} \tag{A.3}$$

    Otherwise, STOP.
  - If $\|\theta^k\|_0 = s$, define $I_1(\theta)$ to be the set of all non-zero indices of θ and e_i, e_j to be indicator vectors whose i^{th} and j^{th} elements are one and rest all zeros respectively. For every $i \in I_1(\theta^k)$ and $j = 1, ...N$ compute

$$\delta_i^j \in arg\min_{\delta \in \mathbb{R}} f(\theta^k - \theta_i^k e_i + \delta e_j) \tag{A.4}$$

$$f_i^j = f(\theta^k - \theta_i^k e_i + \delta_i^j e_j) \tag{A.5}$$

    Let $(i_k, j_k) \in arg\min\{f_i^j : i \in I_1(\theta_k), j = 1, ...N\}$. If $f_{i_k}^{j_k} < f(\theta^k)$, then set

$$\theta^{k+1} = \theta^k - \theta_{i_k}^k e_{i_k} + \delta_{i_k}^{j_k} e_{j_k} \tag{A.6}$$

    Otherwise, STOP.

---

the following definitions are given considering the minimization problem $\min_{||\theta||_0 \leq s} f(\theta)$ where $f : \mathbb{R}^n \to \mathbb{R}$.

Basic Feasible Vector: A vector, $\theta^* \in C_s$ is called a *basic feasible* vector to the above problem, if

1. $||\theta^*||_0 < s \implies \bigtriangledown f(\theta^*) = 0$

2. $||\theta^*||_0 = s \implies \bigtriangledown_i f(\theta^*) = 0 \; \forall \; i \in I(\theta^*)$

Coordinate-wise Minimum: Letting θ^* be a feasible solution of the optimization problem, then it is called a *Coordinate-wise Minimum* if

1. $\|\theta^*\|_0 < s \implies f(\theta^*) = \min_{\delta \in \mathbb{R}} f(\theta^* + \delta e_i) \; \forall \; i = 1, 2, \ldots, n$

2. $\|\theta^*\|_0 = s \implies f(\theta^*) \leq \min_{\delta \in \mathbb{R}} f(\theta^* - \theta_i^* e_i + \delta e_j) \; \forall \; i \in I(\theta^*), j = 1, 2, \ldots, n$

A.3 FIR Model Identification using Greedy Sparse Simplex

In the method for causal network reconstruction presented in Chapter 3, FIR model is identified with sparsity constraint on the parameter. In the course of addressing the problem of causal network reconstruction, in order to recover the most sparse parameter vector, L_0 norm is preferred over L_1 norm. Hence the optimization problem presented in Eq. 3.6 is considered. Among different methods to solve L_0 constrained problem, greedy sparse simplex approach presented in Algorithm 5 is considered and analytical expressions are derived accordingly for FIR model to achieve near global optimal solution. Detailed derivation is presented below.

For $\|\theta^k\|_0 < s$, Eq. 3.4 is considered and perturbed by optimal δ and the indicator vector e_i. Expression for optimal δ can be derived by following the steps given below.

Consider the function in Eq. 3.6 and express it as minimization problem given in Eq. A.1.

$$\begin{aligned}
\delta_i &= arg\min_{\delta \in \mathbb{R}} f(\theta^k + \delta e_i) \\
&= arg\min_{\delta \in \mathbb{R}} \left(Y^T Y - 2(\theta^k + \delta e_i)^T X^T Y + (\theta^k + \delta e_i)^T X^T X (\theta^k + \delta e_i) \right)
\end{aligned}$$

$$\begin{aligned}
= arg\min_{\delta \in \mathbb{R}} \; & Y^T Y - 2(X\theta^k)^T Y - 2\delta (Xe_i)^T Y + (X\theta^k)^T (X\theta^k) + \\
& 2\delta (Xe_i)^T (X\theta^k) + \delta^2 (Xe_i)^T (Xe_i)
\end{aligned} \tag{A.7}$$

where, $i = 1, 2, ...M(t-p)$ and e_i is an indicator vector with dimension same as θ which takes 1 in the i^{th} position and 0 in rest of the position. Then, optimal expression for δ is obtained by taking derivative for Eq. A.7 and equating it to zero. After algebraic rearrangement, final expression for optimal δ can be obtained as

$$\frac{df(\theta^k + \delta e_i)}{d\delta} = 0 \Rightarrow -2(Xe_i)^T Y + 2(Xe_i)^T (X\theta) + 2\delta (Xe_i)^T (Xe_i) = 0$$

$$\Rightarrow \delta = \left((Xe_i)^T (Xe_i)\right)^{-1} (Xe_i)^T (Y - X\theta^k) \tag{A.8}$$

Expression of optimal δ, given in Eq. A.8, is substituted in $f(\theta^k + \delta e_i)$ and minimum value of the function along with its index is computed. Upon obtaining the index of minimum function value, parameter of that particular index is updated as

$$\theta^{k+1} = \theta^k + \left[\left((Xe_i)^T (Xe_i)\right)^{-1} (Xe_i)^T (Y - X\theta^k)\right]_k e_{i_k} \tag{A.9}$$

For $\|\theta^k\|_0 = s$, support set $I_1(\theta^k)$ is constructed with the indices of non-zero elements from θ^k. Then, the function in Eq. 3.6 is expressed as minimization problem given in Eq. A.4,

$$\delta_i^j = arg\min_{\delta \in \mathbb{R}} f(\theta^k - \theta_i^k e_i + \delta e_j)$$

$$= arg\min_{\delta \in \mathbb{R}} Y^T Y - 2(\theta^k - \theta_i^k e_i + \delta e_j)^T X^T Y + \tag{A.10}$$
$$(\theta^k - \theta_i^k e_i + \delta e_j)^T X^T X (\theta^k - \theta_i^k e_i + \delta e_j)$$

In the above equation, on taking derivative of the function with respect to δ and equating it to zero, an expression for the optimal value of δ is obtained.

$$\frac{df(\theta^k - \theta_i^k e_i + \delta e_j)}{d\delta} = 0 \Rightarrow -2(Xe_j)^T Y + (Xe_j)^T X\theta^k - (Xe_j)^T (X\theta_i^k) e_i +$$
$$(X\theta^k)^T (Xe_j) - (X\theta_i^k)^T (Xe_j) + 2\delta (Xe_j)^T (Xe_j) = 0$$

$$\Rightarrow \delta_i^j = \left((Xe_j)^T (Xe_j)\right)^{-1} (Xe_j)^T \left(Y - X(\theta^k - \theta_i^k e_i)\right) \tag{A.11}$$

On obtaining the optimal value of δ, function $f(\theta^k - \theta_i^k e_i + \delta e_j)$ is evaluated at the optimal value and the parameter is updated when the function is minimum at $(i \in I_1)$ and j as the following.

$$\theta^{k+1} = \theta^k - \theta_{i_k}^k e_{i_k} + \left[\left((Xe_j)^T (Xe_j)\right)^{-1} (Xe_j)^T \left(Y - X(\theta^k - \theta_i^k e_i)\right)\right]_k \tag{A.12}$$

Aforementioned steps are solved iteratively to obtain the sparse estimate of the parameters.

A.4 Proof for Mutual Information is Non-negative and its relationship in Causal structure identification

The proof presented here is derived based on the understanding acquired from the book "Elements of information theory" written by Cover. [87]. In the first place, we begin with the discussion of non-negative property of mutual information. Secondly, we extend the discussion to its relation with causal structure identification problem.

Consider two random variables x_i and x_j which are $i.i.d$ multivariate Gaussian, the Mutual information of which can be defined as

$$I(x_i, x_j) = \mathbb{E}\left[\ln\ \left(\frac{P(x_i, x_j)}{P(x_i)P(x_j)}\right)\right]$$

By Jensen's inequality, for any convex function $f(\cdot)$,

$$\mathbb{E}\left[f(\cdot)\right] \geq f\left(\mathbb{E}[\cdot]\right)$$

Therefore, the mutual information can be written as

$$\begin{aligned}
\mathbb{E}\left[\ln\ \left(\frac{P(x_i, x_j)}{P(x_i)P(x_j)}\right)\right] &\geq \ln\left(\mathbb{E}\left[\frac{P(x_i, x_j)}{P(x_i)P(x_j)}\right]\right) \\
&\geq \ln\ \left(\int_{x_i}\int_{x_j} P(x_i)P(x_j)\frac{P(x_i, x_j)}{P(x_i)P(x_j)}dx_i dx_j\right) \\
&\geq \ln\left(\int_{x_i}\int_{x_j} P(x_i, x_j)dx_i dx_j\right) \\
I(x_i, x_j) &\geq 0
\end{aligned}$$

When the random variables are independent, from the definition of mutual information, $I(\cdot, \cdot) = 0$ and when the random variables are not independent, $I(\cdot, \cdot) > 0$.

Now, consider the case of pairwise causal structure identification problem. Given the variables x_i and x_j, we want to determine the relationship among them, which is assumed to be either $x_i \to x_j$ or $x_j \to x_i$ but not both, under certain assumptions. In such a case, it is further assumed that the underlying causal model is additive noise model of the form $x_j = f(x_i) + \eta$ for the causal structure $x_i \to x_j$. On interpreting the graphical structure for additive noise model, it can be understood that model input

(x_i) is independent of noise (η). Due to the independence between input and noise, from the definition of mutual information, $I(x_i, \hat{\eta}) = 0$. In the case when additive noise model is interpreted as $x_j \to x_i$ i.e., the dotted path in the graphical model, the input is no longer independent of additive noise and instead is affected by it i.e., x_j is affected by η. Since, the mutual information between two dependent random variables is non-negative, the mutual information between x_j and η is positive i.e,, $I(x_j, \hat{\eta}) > 0$.

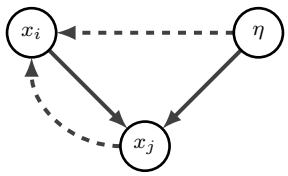

Figure A.1: Additive noise model graph structure for $x_i \to x_j$ (solid edge) along with anti-causal interpretation $x_j \to x_i$ (dashed edge)